



**Defense Nuclear Agency
Alexandria, VA 22310-3398**



DNA-TR-94-184

Next Generation Ultra-Wideband (UWB) Intrusion Detection Radar

**Gerald F. Ross, et al.
ANRO Engineering Inc.
Electronics Division
450 Bedford Street
Lexington, MA 02173**

March 1996

Technical Report

CONTRACT No. DNA 001-92-C-0157

Approved for public release;
distribution is unlimited.

19960322 018

Destroy this report when it is no longer needed. Do not return to sender.

**PLEASE NOTIFY THE DEFENSE NUCLEAR AGENCY,
ATTN: CSTI, 6801 TELEGRAPH ROAD, ALEXANDRIA, VA
22310-3398, IF YOUR ADDRESS IS INCORRECT, IF YOU
WISH IT DELETED FROM THE DISTRIBUTION LIST, OR
IF THE ADDRESSEE IS NO LONGER EMPLOYED BY YOUR
ORGANIZATION.**



DISTRIBUTION LIST UPDATE

This mailer is provided to enable DNA to maintain current distribution lists for reports. (We would appreciate your providing the requested information.)

- Add the individual listed to your distribution list.
- Delete the cited organization/individual.
- Change of address.

NOTE:

Please return the mailing label from the document so that any additions, changes, corrections or deletions can be made easily. For distribution cancellation or more information call DNA/IMAS (703) 325-1036.

NAME: _____

ORGANIZATION: _____

OLD ADDRESS

CURRENT ADDRESS

TELEPHONE NUMBER: () _____

DNA PUBLICATION NUMBER/TITLE

CHANGES/DELETIONS/ADDITIONS, etc.)
(Attach Sheet if more Space is Required)

DNA OR OTHER GOVERNMENT CONTRACT NUMBER: _____

CERTIFICATION OF NEED-TO-KNOW BY GOVERNMENT SPONSOR (if other than DNA):

SPONSORING ORGANIZATION: _____

CONTRACTING OFFICER OR REPRESENTATIVE: _____

SIGNATURE: _____

CUT HERE AND RETURN



REPORT DOCUMENTATION PAGE

Form Approved

OMB No. 0704-0188

Public reporting burden for this collection of information is estimated to average 1 hour per response including the time for reviewing instructions, searching existing data sources, gathering and maintaining the data needed, and completing and reviewing the collection of information. Send comments regarding this burden estimate or any other aspect of this collection of information, including suggestions for reducing this burden, to Washington Headquarters Services, Directorate for Information Operations and Reports, 1215 Jefferson Davis Highway, Suite 1204, Arlington, VA 22202-4302, and to the Office of Management and Budget, Paperwork Reduction Project (0704-0188), Washington, DC 20503.

1. AGENCY USE ONLY (Leave blank)		2. REPORT DATE 960301	3. REPORT TYPE AND DATES COVERED Technical 920916 - 950715	
4. TITLE AND SUBTITLE Next Generation Ultra-Wideband (UWB) Intrusion Detection Radar			5. FUNDING NUMBERS C - DNA 001-92-C-0157 PE - 62715H PR - PF TA - FE WU - DH327740	
6. AUTHOR(S) Gerald F. Ross, Joseph D. DeLorenzo, Lee R. Cain and Peter Mitchell				
7. PERFORMING ORGANIZATION NAME(S) AND ADDRESS(ES) ANRO Engineering Inc. Electronics Division 450 Bedford Street Lexington, MA 02173			8. PERFORMING ORGANIZATION REPORT NUMBER	
9. SPONSORING/MONITORING AGENCY NAME(S) AND ADDRESS(ES) Defense Nuclear Agency 6801 Telegraph Road Alexandria, VA 22310-3398 NOSA/Witter			10. SPONSORING/MONITORING AGENCY REPORT NUMBER DNA-TR-94-184	
11. SUPPLEMENTARY NOTES This work was sponsored by the Defense Nuclear Agency under RDT&E RMC Code B4662D RF FE 00003 7010A 25904D.				
12a. DISTRIBUTION/AVAILABILITY STATEMENT Approved for public release; distribution is unlimited.			12b. DISTRIBUTION CODE	
13. ABSTRACT (Maximum 200 words) This report describes the theory and development of an ultra-wideband (UWB) electronic scanning radar (ESR) using a linear array of 10 microwave sources for intrusion detection application. Each source produces a 1 kW peak S-band pulse having a duration of 1 ns. At boresight, the array produces an effective radiated power (erp) of 100 kW because the voltages of the individual sources add coherently in the far field. In addition to the ESR feature, a new algorithm was developed having the constant false alarm rate (CFAR) tunnel diode receiver threshold on noise and ground clutter. To reduce false alarms and improve detection and identification of crawlers, walkers, runners, and animal and vehicle targets, a new signal processing scheme employing a leading edge filter (LEF), in combination with neural network processing concepts, have been successfully developed. And by training neural networks to recognize these signatures, the results show promise for future use in other UWB systems. A primary advantage of the UWB ESR radar is low cost. It is estimated that the cost of this type of system is less than 1/10 of comparable conventional radar ESR systems. Efforts to commercially exploit this technique are in progress.				
14. SUBJECT TERMS Linear Array Radar Low Cost Ultra-Wideband Radar Neural Network Electronic Scanning Radar Intrusion Detection Leading Edge Filter			15. NUMBER OF PAGES 100	
			16. PRICE CODE	
17. SECURITY CLASSIFICATION OF REPORT UNCLASSIFIED	18. SECURITY CLASSIFICATION OF THIS PAGE UNCLASSIFIED	19. SECURITY CLASSIFICATION OF ABSTRACT UNCLASSIFIED	20. LIMITATION OF ABSTRACT SAR	

UNCLASSIFIED

SECURITY CLASSIFICATION OF THIS PAGE

CLASSIFIED BY:

N/A since Unclassified.

DECLASSIFY ON:

N/A since Unclassified.

SECURITY CLASSIFICATION OF THIS PAGE

UNCLASSIFIED

SUMMARY

This report describes an advanced type radar system, particularly useful for detecting human targets at ranges up to 1 mile, over wide angles, and in mildly-cluttered environments such as airfields. This new radar exploits so-called ultra-wideband (UWB) technology developed for DNA over a ten-year period on related intrusion detection programs. UWB technology, which provides 1 foot or less resolution, is much less expensive than conventional radar technology, which in today's budget conscious environment makes it a very attractive candidate to protect, for example, against hang glider attacks.

A UWB signal is one whose signal bandwidth is very wide; the fractional bandwidth is greater than 25%. This system employs a signal whose apparent spectral centroid is in the low microwave band (i.e., 2.5 GHz), with a bandwidth of 1 GHz. These signals are generated very inexpensively, and by new ideas developed on this program, can be used to form narrow effective radar beams in space. These beams can be electronically scanned by an ordinary computer; there are no expensive digital phase shifters or delay lines required. The transmitter array developed on this program uses ten active elements. Each element radiates a 1 kW peak power, 1 nanosecond duration, 2.5 GHz signal. The waveforms radiated into free space contain only several rf cycles and are synchronized by a computer in such a manner that they are coherent in time. The coherent pulsed transmitter produces a peak radiated power of 100 kW. The cost of the transmitter for each element is on the order of \$100 in small quantities. We believe this to be the first truly low-cost UWB electronic scanning radar (ESR) array.

The main attribute of an UWB ESR array is its ability to achieve high range and angle resolution, simultaneously, at low cost. The array developed on this program scans ± 30 degrees in 21 different beam positions with a range resolution of less than a foot; a newly designed circuit was developed to extend this angular coverage to ± 45 degrees, but was not integrated into the radar because of program time constraints.

The UWB ESR developed on this program employs three "fences". Typically, a near fence set at 300 feet, a mid fence at 1000 feet and a far fence set at 4000 feet. The fences can be moved to any desired range. Each fence contains 12 contiguous 10-foot range gates, spanning a 120-foot width in range. The cluster of ten range gates moves sequentially from the near to mid to far fence positions and then repeats this sequence in the next beam position. Thus, the system creates 252 range-azimuth cells within each of the fences.

The system dwells for 32 pulse periods in each range gate position and the system prf is 10 kHz (a 100 μ s period). Thus, the total time to search and scan the entire protected area is:

$$12 \text{ gates} \times \frac{3.2\text{ms}}{\text{gate}} \times 3 \text{ fences} \times 21 \text{ beam positions} \sim 2.4 \text{ seconds.}$$

The receiver developed for this program incorporates several unique features. A constant false alarm rate (CFAR) tunnel diode receiver is used to detect the very short duration signals. The CFAR detector is range-gated by a 20 ns window representing 10 feet in space. A new superhetrodyne detector is employed to increase the sensitivity. Unlike previous UWB systems, the sensitivity here is adjusted on the basis of noise and ground clutter instead of noise alone. The processor senses the change in the noise plus the clutter level due to the presence of an object in a range-azimuth cell. If the signal is detected in two contiguous range cells in one or more beam positions, then the signal is fed to a so-called leading edge filter (LEF) which, with the aid of a trained neural network, determines with a high degree of certainty, whether the intruder is a crawling, walking, running person, or an animal.

The LEF is another innovation developed for DNA. It was determined that the short pulse return from a human target is very complex. Scattering occurs from primarily the head, the arms, the legs and the torso, the so-called scattering centers. In addition to the direct returns from the scattering centers, there are the ground bounce returns. The result is a complex return which varies significantly by constructive and destructive interference with only small movements of the body. The result is that the sensitive tunnel diode threshold detector changes states over about a two nanosecond variation depending upon slight movements of the target; the apparent leading edge to the target changes. This change in distance is converted to a slowly varying voltage which is analyzed by the trained neural network. Extensive field tests were performed on numerous human targets using an impulse transmitter source in conjunction with a tapped delay line high speed comparator forming the LEF. The results of these tests are impressive and are reported herein.

The extended range intrusion detection UWB ESR array developed on this program was tested both in the laboratory and in the field. The individual subsystems such as the ESR transmitter array, the LEF, the superhetrodyne tunnel diode CFAR receiver, etc., were developed and successfully tested on the bench. The radar was then assembled and tested as a system at Hanscom Field, Bedford, MA.

The radar system, including the transmitter receiver and processor developed on this program are very sophisticated. It is estimated that an additional 12 months is required to introduce additional improvements and to fully integrate and test the present and new components into a prototype system. It is strongly recommended that this work be continued, because of its obvious cost-effectiveness for intrusion detection. Specifically, in the

- **Transmitter Antenna Array:** The circuitry to increase the scan angle from ± 30 to ± 45 degrees should be integrated into the radar.
- **Receiving Antenna:** A receive antenna array should be designed and integrated into the transmit array (e.g., every other element). A means to electronically steer the receive antenna pattern would considerably increase the range of the radar. Currently, a single wideband receive element is used to cover the required scan volume.
- **Software:** The detection and processing software should be evaluated by a concerted series of field tests and revised as necessary for system optimization. A reduction in the time required to scan the coverage area may be desirable. It is suggested that the software be modified to tailor the coverage area to selected range-azimuth cells, e.g., to follow the contour of a wall or road. The computer display should also be improved to enhance operation interaction.
- **LEF:** The LEF must be integrated into the contiguous range gate processor circuit above to test target responses for reduced false alarms and finally:
- **ANRO** should team with an experienced radar manufacturer to make preproduction models of this radar in Phase III. During Phase II, ANRO has conducted preliminary talks with Lockheed-Martin, Syracuse, N.Y., to serve as a potential Phase III partner. Their experienced radar system engineers were very impressed with the simplicity of the hardware and the potential cost reductions possible with this technology. They attended the final ANRO/DNA demonstration on June 29, 1995, and business discussions with them are continuing.

This system also provides low-cost, effective coverage for airfields, prison yards, storage areas and other such expanses in the presence of mild clutter; the capability to recognize human targets greatly reduces the false alarm rate. Enhancements visualized provide expanded coverage of areas up to one square mile and a capability to tailor the coverage to individual deployments.

CONVERSION TABLE

Conversion factors for U.S. Customary to metric (SI) units of measurement.

MULTIPLY $\xrightarrow{\hspace{10em}}$ BY $\xrightarrow{\hspace{10em}}$ TO GET
 TO GET $\xleftarrow{\hspace{10em}}$ BY $\xleftarrow{\hspace{10em}}$ DIVIDE

angstrom	1.000 000 X E -10	meters (m)
atmosphere (normal)	1.013 25 X E +2	kilo pascal (kPa)
bar	1.000 000 X E +2	kilo pascal (kPa)
barn	1.000 000 X E -28	meter ² (m ²)
British thermal unit (thermochemical)	1.054 350 X E +3	joule (J)
calorie (thermochemical)	4.184 000	joule (J)
cal (thermochemical/cm ²)	4.184 000 X E -2	mega joule/m ² (MJ/m ²)
curie	3.700 000 X E +1	*giga becquerel (GBq)
degree (angle)	1.745 329 X E -2	radian (rad)
degree Fahrenheit	$t_k = (t^{\circ}f + 459.67)/1.8$	degree kelvin (K)
electron volt	1.602 19 X E -19	joule (J)
erg	1.000 000 X E -7	joule (J)
erg/second	1.000 000 X E -7	watt (W)
foot	3.048 000 X E -1	meter (m)
foot-pound-force	1.355 818	joule (J)
gallon (U.S. liquid)	3.785 412 X E -3	meter ³ (m ³)
inch	2.540 000 X E -2	meter (m)
jerk	1.000 000 X E +9	joule (J)
joule/kilogram (J/kg) radiation dose absorbed	1.000 000	Gray (Gy)
kilotons	4.183	terajoules
kip (1000 lbf)	4.448 222 X E +3	newton (N)
kip/inch ² (ksi)	6.894 757 X E +3	kilo pascal (kPa)
ktap	1.000 000 X E +2	newton-second/m ² (N-s/m ²)
micron	1.000 000 X E -6	meter (m)
mil	2.540 000 X E -5	meter (m)
mile (international)	1.609 344 X E +3	meter (m)
ounce	2.834 952 X E -2	kilogram (kg)
pound-force (lbs avoirdupois)	4.448 222	newton (N)
pound-force inch	1.129 848 X E -1	newton-meter (N·m)
pound-force/inch	1.751 268 X E +2	newton/meter (N/m)
pound-force/foot ²	4.788 026 X E -2	kilo pascal (kPa)
pound-force/inch ² (psi)	6.894 757	kilo pascal (kPa)
pound-mass (lbm avoirdupois)	4.535 924 X E -1	kilogram (kg)
pound-mass-foot ² (moment of inertia)	4.214 011 X E -2	kilogram-meter ² (kg·m ²)
pound-mass/foot ³	1.601 846 X E +1	kilogram/meter ³ (kg/m ³)
rad (radiation dose absorbed)	1.000 000 X E -2	**Gray (Gy)
roentgen	2.579 760 X E -4	coulomb/kilogram (C/kg)
shake	1.000 000 X E -8	second (s)
slug	1.459 390 X E +1	kilogram (kg)
torr (mm Hg, 0° C)	1.333 22 X E -1	kilo pascal (kPa)

*The becquerel (Bq) is the SI unit of radioactivity; 1 Bq = 1 event/s.

**The Gray (Gy) is the SI unit of absorbed radiation.

TABLE OF CONTENTS

Section	Page
SUMMARY	iii
CONVERSION TABLE	vii
FIGURES	x
1 INTRODUCTION	1
1.1 GENERAL	1
1.2 BACKGROUND	3
2 THE ARRAY CONCEPT AND THE ELEMENT SOURCES	6
2.1 INTRODUCTION	6
2.2 ARRAY CONCEPT	6
2.3 THE ELEMENT SOURCE	7
3 SYNCHRONIZATION OF A TEN-ELEMENT ARRAY	11
3.1 INTRODUCTION	11
3.2 THE INITIAL SYNCHRONIZATION APPROACH	11
3.3 A LOW-COST DIGITAL TECHNIQUE TO AFFECT SYNCHRONIZATION DEVELOPED ON THIS PROGRAM	16
3.4 THE CALIBRATION TECHNIQUE REQUIRED FOR UWB BEAM STEERING	18
3.5 THE DESIGN OF THE TEN-ELEMENT ARRAY	20
3.5.1 Design Considerations for the 10-Element Array	20
3.5.2 Space-Time Array Analytical Study Results	26
3.5.3 Time Domain Array Performance Relative to Equivalent CW Array Performance	35
4 THE LEADING EDGE FILTER	41
4.1 INTRODUCTION	41
4.2 LEF FUNCTIONAL DESCRIPTION	41
4.3 LEF OUTPUT VOLTAGE DESCRIPTION	43
4.4 AN INTRODUCTION TO ARTIFICIAL NEURAL NETWORKS	48
4.5 A NEURAL NET WITH LEF VOLTAGE WAVEFORMS AS INPUTS	50
4.6 THE USE OF THE LEADING EDGE FILTER TO IDENTIFY INTRUDERS	52

TABLE OF CONTENTS (Continued)

Section		Page
4.7	EXPERIMENTAL VERIFICATION OF CLASSIFICATION CONCEPTS	54
4.8	SUMMARY OF RESULTS AND SUGGESTIONS FOR FUTURE WORK	56
5	THE GATED CFAR RECEIVER AND BEAM STEERING STRATEGY	58
5.1	BACKGROUND	58
5.2	THE RECEIVER SEARCH STRATEGY	62
	5.2.1 Range and Bias Adjustment	63
	5.2.2 Threshold Criterion	64
	5.2.3 Activity Required each 100 μ secs., i.e., PRF Interval	65
6	THE DNA UWB INTRUSION DETECTION ARRAY RADAR SYSTEM OPERATIONS AND TESTING	66
6.1	INTRODUCTION	66
6.2	THE EFFECT OF WEATHER CONDITIONS ON UWB TRANSMISSIONS	66
6.3	UWB SIGNALS AND INTERFERENCE	66
6.4	POSSIBLE DELETERIOUS EFFECTS OF UWB RADIATION ON HUMANS	69
6.5	TESTING OF THE UWB RADAR	70
	6.5.1 The Transmitter	70
	6.5.2 The Receiver and Display	71
7	REFERENCES	76
Appendix		
A -	GLOSSARY OF TERMS	A-1
B -	TESTING AND TRAINING A NEURAL NET FOR INTRUSION DETECTION	B-1

FIGURES

Figure		Page
2-1	Linear array concept.	7
2-2	ANRO's patented Marx generator.	8
3-1	Radiated-received waveform from ANRO S-band source.	12
3-2	Basic synchronization scheme to accommodate long term drift.	13
3-3	Time delay vs. V_{be} for ganging application (1 ps/mv).	14
3-4	Equivalent circuit of the synchronization loop.	15
3-5	Digital synchronization.	17
3-6	Frequency domain measurement of line delay.	18
3-7	Bias (mV) vs. time (ns); transmitter calibration characteristics.	19
3-8	Perspective view of the 10-element transmitter array.	20
3-9	Parabolic cylindrical reflector - cross section view.	22
3-10	Parabolic reflector radiation.	22
3-11	Parabolic reflector antenna with directive feed element.	23
3-12	Three dB beamwidth vs. element spacing for a ten-element S-band array.	24
3-13	Approximate overall array dimensions.	24
3-14	Trough reflector configuration design.	25
3-15	Linear array with corporate feed receive elements.	26
3-16	Ten element array geometry.	27
3-17	System waveform.	27
3-18	Beam width with 0.7 foot spacing.	28
3-19	Beam width with 1.0 foot spacing.	28
3-20	Beam width with 1.5 foot spacing.	29

FIGURES (Continued)

Figure		Page
3-21	Beam width with 2.0 foot spacing.	29
3-22	3 dB width vs. element spacing for a ten element array.	30
3-23	Grating lobe and sidelobe level with 0.7 foot spacing.	31
3-24	Grating lobe and sidelobe level with 1.0 foot spacing.	31
3-25	Grating lobe and sidelobe level with 1.5 foot spacing.	32
3-26	Grating lobe and sidelobe level with 2.0 foot spacing.	32
3-27	On boresight field structure with 0.7 foot spacing.	33
3-28	On-boresight field structure with 1.3 foot spacing.	33
3-29	On-boresight field structure with 2.0 foot spacing.	34
3-30	Field structure at $\pi/4$ pointing angle with 0.7 foot spacing.	34
3-31	Power level at $\pi/4$ pointing angle with 0.7 foot spacing.	35
3-32	CW grating lobes with 0.7 foot element spacing.	36
3-33	CW grating lobes with 1.0 foot element spacing.	36
3-34	CW grating lobes with 1.5 foot element spacing.	37
3-35	CW grating lobes with 2.0 foot element spacing.	37
3-36	Power level vs. angle for 0.7 foot element spacing.	38
3-37	Power level vs. angle for 1.0 foot element spacing.	38
3-38	Power level vs. angle for 1.5 foot element spacing.	39
3-39	Power level vs. angle for 2.0 foot element spacing.	39
3-40	Comparison of beamwidth with short pulses vs. CW array.	40
4-1	Leading edge filter.	43
4-2	LEF output waveform for human running out.	44
4-3	LEF output waveform for human walking out.	45
4-4	LEF output waveform for human crawling out.	46

FIGURES (Continued)

Figure		Page
4-5	A typical neuron.	48
4-6	Feed-forward artificial neural network.	49
4-7	Wide bandwidth LEF waveform.	52
4-8	Narrow bandwidth LEF waveform.	52
5-1	Range azimuth cells.	60
5-2	Range gated variable threshold tunnel diode detector receiver.	60
5-3	Envelope detector concept.	61
5-4	Range and bias adjustments.	64
6-1	Beam scan positions in field of view and range cell.	73
6-2	Beam and range cell display	74
6-3	Nearest neighbor cell confirmation of target activity in next scan.	75

SECTION 1

INTRODUCTION

1.1 GENERAL.

This final report describes the results of work performed by ANRO Engineering, Inc. (ANRO) under a Phase II, Defense Nuclear Agency contract, No. DNA001-92-C-0157. The purpose of this program was to develop a new class of electronic scanning radar system (ESR) for particular application to intrusion detection. This ESR differs from conventional systems by its transmitted signal. It generates very short microwave pulses (e.g., 1 nanosecond @ 2.5 GHz) having fractional bandwidths of 40% or greater. These signals are termed ultra-wideband (UWB) transmissions.

There are several advantages of using UWB signals in conjunction with the antenna array developed on this program for intrusion detection. These advantages are:

1. The extension of the maximum range against human targets to one mile.
2. The ability to resolve intruder "target" properties and, thus, reduce false alarms.
3. The means to reduce ground clutter by range gating and beam narrowing techniques.
4. The performance of 1 and 2 above, with very low-cost hardware implementation; a factor of 10 times less than conventional ESR techniques.
5. The difficulty of an intruder detecting the presence of the transmitted signal. UWB signals have, inherently, a low probability of intercept (LPI) and detection (LPD).

The UWB ESR array, based on a concept suggested by Drs. Ross and Susman in 1973,[1] was reduced to practice by Drs. Ross and Nicolson, and Mr. Mitchell on this program; ANRO intends to file a U.S. patent application on the new scanning hardware technique.

Another technique concerning the use of a "leading edge filter" (LEF) to decrease false alarms was also suggested by Dr. Ross on an earlier DNA effort. It was combined here with neural network processing concepts developed by Dr. DeLorenzo and experimentally reduced to practice on this program through field experiments. A U.S. patent application will also be filed describing this new concept.

Operating any radar where targets (intruders) are sought over shallow elevation angles represents a major clutter-return problem. Even seeking walkers or crawlers over a relatively open area such as an airfield still results in a significant clutter return. Dr. Nicolson, inventor of the original short pulse UWB constant false alarm rate (CFAR) receiver, developed an algorithm on this program for finding intruders in clutter and motion. After determining the possible presence and velocity of a target, the LEF can be used as an adjunct check to make a final identification and determination.

The second section of this report describes background information on UWB technology and its application to ESR radar. It includes a description of ANRO's patented S-band generator, which drives each array radiating element; also, the predicted peak power generated by each source. The predicted range of the array is calculated to be one mile on a walking target.

In Section 3, the novel antenna array synchronization technique is described. Included in this section are the design of the linear array and the effective antenna beam narrowing performance curves as a function of element spacing. The beam narrowing, accomplished here by the use of a ten-element array, provides for a narrow two-dimensional detection cell. This narrow range-azimuth cell is not usually available on UWB radar systems.

The LEF concept is described in Section 4. This work includes extensive field data proving the efficacy of the technique.

The CFAR receiver processing scheme, combined with the array scanning algorithm, is described in Section 5. A discussion of receiver threshold criteria, as well as a background discussion tracing the history of the tunnel diode CFAR detector is presented.

The final section contains the results of the tests completed in the laboratory and in the field, and effects of weather conditions on UWB transmissions, and its possible harmful effects on humans. A discussion on the problems of obtaining FCC licensing of UWB is also offered. A glossary of terms is included in Appendix A to aid the reader in understanding some of the terminology associated with UWB radar. A description of the procedures used to train and test the neural network is presented in Appendix B.

1.2 BACKGROUND.

In 1984, ANRO developed, under a Phase I and Phase II, an impulse radar or time domain reflectometer using a 40 watt peak source designed to protect missile sites against walking and crawling human intruders. The range of this bistatic sensor was 50-150 feet; the transmitter and the receiver were separated by about three feet. This earlier program used many of the techniques developed by Dr. Gerald F. Ross, Principal Investigator, beginning in 1965 and placed them in a cost-effective package. A license for this technology was sold to Sperry Marine, Inc., Charlottesville, VA, which marketed the product to law enforcement agencies. The Small Business Administration, in their 5th Annual report to Congress, listed this project as one of their most successful DoD sponsored SBIR programs in 1988.

In May 1991, the U.S. Air Force Ballistic Missile organization awarded ANRO a Phase I SBIR to develop an extended range covert UWB radar for use as a base security sensor for mobile missile applications. In that program, ANRO developed four 1 kW S-band sources having a root means square (rms) pulse width of 1 ns and synchronized them to produce a 16 kW peak signal. In addition, low-cost techniques for electronically scanning a UWB beam in space were formulated and experimentally evaluated for two elements. A desktop computer steered the beam by changing only dc voltages, without the use of expensive microwave switching components.

The Phase II effort was then proposed and sponsored by DNA when the Air Force mobile missile program was canceled. ANRO proposed to extend the successful 4-element array developed under Phase II to ten. Ten synchronized sources would theoretically radiate a peak power of 100 kW, because the individual sources would be synchronized. Once again, only a computer was to be used to scan the beam in space. This is the basis of the program just completed for DNA.

Specifically, the objective of the program, as given in the Statement of Work (SOW), was to develop a next generation UWB extended range intrusion detection radar sensor for the protection of nuclear and conventional facilities. The range of the system was to be one mile or greater for a walking intruder with a significant reduction in false alarms in mildly cluttered areas using special system enhancements. The new extended range system would consist of three key elements: an electronically scanned array of 10 low-cost, synchronized sources of S-band energy, 1 ns in duration, to produce a 100 kW peak signal; a new superhetrodyne tunnel diode receiver with a 8.5 dB improvement in sensitivity; and a LEF for target discrimination and false alarm reduction.

The program was completed in June 1995 having met all the stated objectives with one possible exception. Specifically, the SOW described an ESR transmitter array in Task 1 containing 10 elements that could be scanned in space up to 32 different beam positions. We accomplished 21 beam positions in the field, but developed the component necessary to achieve 32 positions; the circuitry was not installed into the system because of time constraints.

Task 2 describes a 4-element receive array where the output from each element is summed by a corporate feed network. This was accomplished and used in the field test. There was no need for a duplexer since the array was sufficiently separated from the transmitting array to prevent receiver damage (e.g., 2 feet).

Task 3 dealt with the receiver design. A superhetrodyne front-end was added to a tunnel diode (TD) range gated receiver. Although not described in the SOW, considerable effort was spent in developing the new concept of biasing or establishing the threshold of the TD receiver by clutter and noise. Here, the presence of a signal would change the 1, 0 pattern at the output of the receiver and indicate the possible presence of a target. Software was developed to test the output of contiguous range gates in angle and range. Software was also developed to scan the array, and display the receiver output.

Task 4 was concerned with the development and evaluation of the LEF. We established a comprehensive set of human intrusion motions and then used a UWB source to test the responses. Engineers-in-training at Rochester Institute of Technology were used to execute the required motions and serve as the intruding targets. These tests were taken in Rochester, N.Y. and were directed by Dr. DeLorenzo, a well known expert in time domain target scattering. Four different UWB generators operating at different nominal operating frequencies were constructed. Tests were made at L and S-band. Extensive waveforms regarding targets and their motions were recorded. Specific details on target profile, size, and speed is found in Section 4. Neural networks, although not included in the SOW, were found to be ideal in processing the huge amount of field data taken. The results, described in Section 4, show that these networks can be trained to perform recognition and do it well.

Task 5, involving system control and display, involved beam steering control and the scanning function and integration with the receiver as described in Task 3. A desktop computer with a color display is used to display the range gate and beam position locations, as well as target detections.

The final task in the SOW (Task 6) required system integration and test. ANRO constructed a proof-of-principle system model which indicated performance both in the laboratory and the field.

All parts of the SOW were successfully completed or exceeded. The next step is to develop the system into an operational UWB ESR in a Phase III program directed at a specific government application. It is estimated that a prototype radar can be constructed and developed within a 12-month period given the work already performed under Phase II.

SECTION 2

THE ARRAY CONCEPT AND THE ELEMENT SOURCES

2.1 INTRODUCTION.

Generally, when an antenna is very wideband it also has a very broad effective beamwidth. This follows, generally, from Fourier transform considerations. This means that if an antenna supports the propagation of UWB signals one, generally, expects a wide antenna coverage angle. On this program where an area protection radar is required, this is desirable. But in other cases where, for example, one would want to restrict police radar coverage to a single lane on a highway, UWB signals may not be the proper choice.

It is interesting to note that there are techniques that can be used to circumvent the general relationship between bandwidths and beamwidths. The use of an array of wide angle UWB sources is an excellent example of how one can narrow the beam of a radar using electronic scanning techniques and still cover the required scanning area. On this program, we have developed such an array of UWB array elements and sources to provide for narrowing the effective antenna beam pattern while covering the required angular sector. The basic concept of using an array for UWB beam pattern formation, developed earlier by Ross and Susman, is described next. The patented Marx generator source used to drive each element which radiates somewhat greater than a kilowatt is described in Section 2.3.

2.2 ARRAY CONCEPT.

Consider the linear array of N elements shown in Figure 2-1. These elements are equally spaced and extend over a distance, L . Now, if an omni-directional element located at each point in Figure 2-1 is excited by an impulsive source, $\delta(t)$, then an observer located at distance D from the array, where $D \gg L$, would measure an intensity $N\delta(t)$. However, at some angle, θ , the observer would note a train of N pulses each spaced $\frac{l}{c}\sin\theta$ seconds apart, where c is the speed of light. To ensure that all the impulses would coalesce at the angle θ , it is necessary to place an incremental time delay between elements of

$$\frac{l\sin\theta}{c} \text{ sec,}$$

where l is the element spacing.

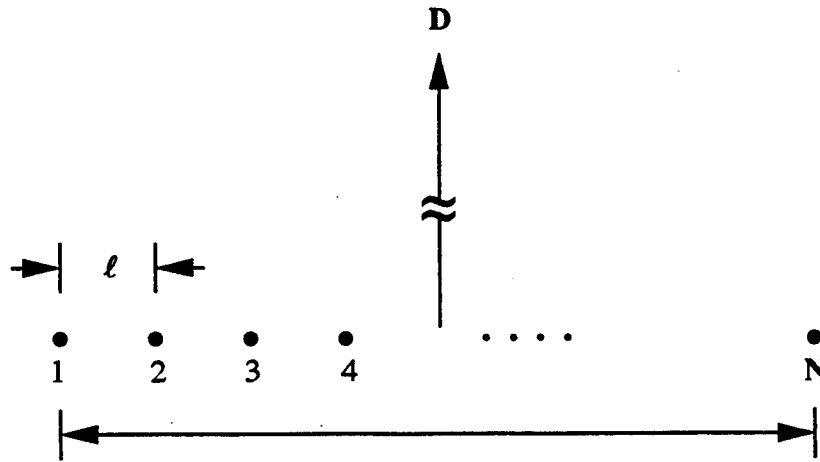


Figure 2-1. Linear array concept.

Since real radiating elements are not omni-directional and have their own intrinsic bandwidths, one cannot radiate an impulse even if it could be generated. Section 3 of this report describes the response of the array to a Gaussian pulse excitation assuming perfect radiating elements. The antenna element and reflector design further disperses or distorts the transmission, especially for off angle signals.

The function of the array is to add signals (voltages), coherently, in the far field at a given angle in space. This means, because of coherence, that if one drives each element with a 1 kW source, the effective radiated power (erp), as measured in the far field, is not 10 kW, but rather 100 kW; that is, we gain N^2 times the power radiated by a single element.

2.3 THE ELEMENT SOURCE.

The large impulse-like voltage used to drive each antenna radiating element is accomplished by use of the Marx generator in conjunction with an avalanche diode shown in Figure 2-2. A Marx generator resembles a simple photo flash unit in a camera. It produces a very short sudden high intensity peak power signal using very little energy.

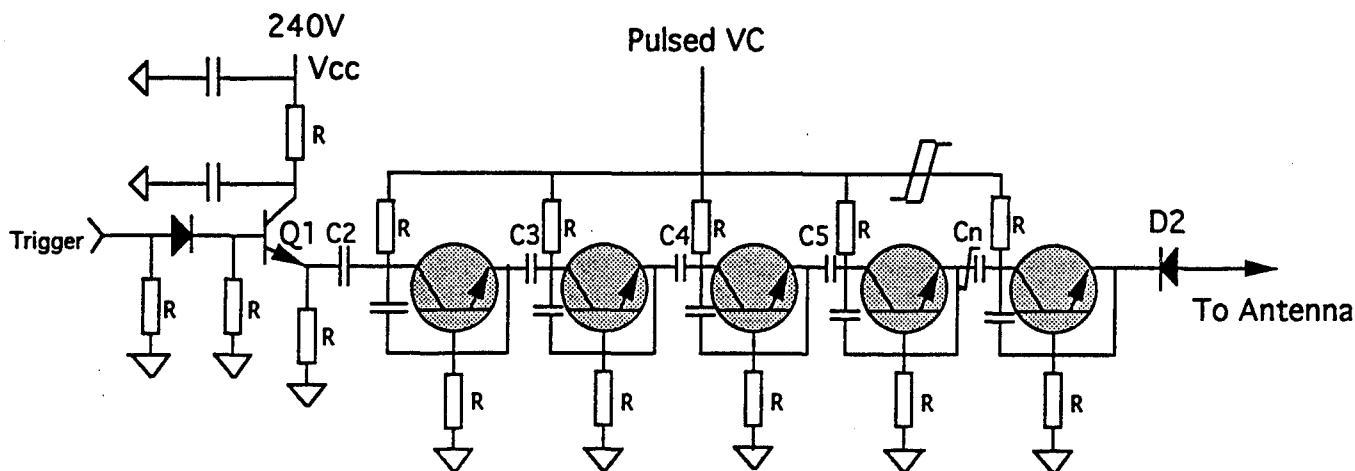


Figure 2-2. ANRO's patented Marx generator.

The Marx generator consists, essentially, of a bank of a number of capacitors C2, C3, C4,... and Cn. These capacitors are charged in *parallel* at a low voltage, but upon triggering, discharge in *series*. The result is that very high voltages (kv) can be achieved over short time durations (ns). And all this can be done very economically, because the parts cost of the Marx generator are very inexpensive.

A diagram of ANRO's patented Marx generator is shown in Figure 2-2. Capacitors C2 through Cn are charged to V_{cc} before a trigger is applied. The video trigger fires Q1 which starts the avalanche breakdown of the chain producing a 1400 volt, nanosecond rise-time pulse incident on reversed biased avalanche diode D2: At some point this high voltage causes D2 to avalanche, resulting in about a 1000 volt, 100 ps or less, rapidly changing leading edge. It is this rapidly changing voltage which excites the antenna causing radiation; the antenna radiates, essentially, its impulse response. V_{cc} is appropriately gated off just before capacitors C₂ through C_N discharge. This is necessary to reduce the average current drain from the supply as well as reducing the avalanche transistor dissipation.

To measure the erp of the source, the peak voltage was measured one meter from its source by the same type of receiving element; the V_{pp} voltage was 10 volts. Therefore, the peak power received at a 50 ohm receive antenna load is given by

$$P_p = \frac{E^2}{50} = \frac{\left(\frac{5}{\sqrt{2}}\right)^2}{50} = \frac{1}{4} \text{ watt,} \quad (2.1)$$

where $\frac{5}{\sqrt{2}}$ is assumed to be the rms voltage.

The effective power density radiated over a sphere by the transmitter is given by

$$\frac{P \cdot G_T}{4\pi R^2}, \quad (2.2)$$

where G_T is the gain of the dipole radiating element. The power received by the receiving dipole antenna, having a gain of G_R , is obtained by multiplying 2.2 by the effective area of the antenna, viz:

$$A_{\text{eff}} = \frac{\lambda_0^2 G_R}{4\pi}, \quad (2.3)$$

so that the equation for determining peak power is given by:

$$\frac{P \cdot G_T}{4\pi R^2} \cdot \frac{\lambda_0^2 G_R}{4\pi} = P_p = \frac{1}{4} \text{ watt.} \quad (2.4)$$

Solving for the effective radiated power (erp) = $P \cdot G_T$, we have

$$\text{erp} = P \cdot G_T = \frac{P_p (4\pi)^2 R^2}{\lambda_0^2 G_R}. \quad (2.5)$$

And, for a 1 meter distance,

$$R^2 = 1;$$

$$P_p = 1/4 \text{ W from 2.1;}$$

$$\lambda_0^2 = 1.33 \times 10^{-2} \text{ m}^2 \text{ for } f_0 = 2.6 \text{ GHz;}$$

$$G_R = 2 \text{ for a dipole in a corner reflector.}$$

Substituting, we have

$$\text{erp} = \frac{\frac{1}{4} (4\pi)^2}{1.33 \times 10^{-2} \cdot 2} = 1.48 \text{ kW.} \quad (2.6)$$

Note: To determine the peak power at the load we assumed $\frac{5}{\sqrt{2}}$ was the rms voltage; that is, the pulse was fully present for all three cycles. In fact, this should be derated by determining the rms value of the transmitted waveform. The answer appears to be closer to $\frac{(5\sqrt{3})^2}{50}$. This reduces 2.6 by a factor of $1.48 \times 3/4 = 1.11$ kW, which we approximate by specifying the source output as 1 kw. At a pulse rate of 10 kHz, the average power is given by:

$$\text{Average Power} = 1.11 \cdot 10^3 \cdot \frac{\text{pulse duration}}{\text{pulse repetition period}} \sim \frac{10^{-9}}{100 \times 10^{-6}} \sim 10^{-2} \text{ watts.} \quad (2.7)$$

SECTION 3

SYNCHRONIZATION OF A TEN-ELEMENT ARRAY

3.1 INTRODUCTION.

The importance of developing an array of UWB radiators is twofold. First, it permits one to significantly narrow the effective beamwidth of an antenna as described in the original Ross, Susman patent.[1] This permits the radar engineer to form a narrow, two-dimensional range/azimuth cell; the fine range resolution afforded by the bandwidth of signal and the narrow beam width which becomes more effective as the number of elements, N , increases. The second significant factor is the increase in peak power incident on the target. If the signals radiated from each source can be synchronized so that at a given point in the far field they add coherently, then one obtains an effective peak power equal to N^2 times the erp of a single source; that is, for a 1 kW peak source present at each radiating element, an array of ten elements radiates an erp of 100 kW.

Once synchronization is achieved by the technique developed on this program, it can be shown that there is an inexpensive way to place an incremental time delay taper on the elements necessary to steer the peak of the beam in space. In addition, at close-in ranges, the timing of the individual sources is controlled to focus the energy in the desired range cell. This is usually accomplished in conventional ESR systems by computer controlled digital phase shifters which tends to make the radar very expensive. A unique digital feedback scheme was developed on this program to affect synchronization. Beam steering is accomplished by opening the loop and then injecting a dc voltage into a step recovery diode (SRD) delay network; calibration for all the elements is accomplished by comparing the delay caused by the SRD network to a standard length of coaxial cable.

In this section, we present earlier attempts at synchronization, the technique developed on this program, beam steering, a description of the key calibration technique and the antenna patterns achieved with the ten element UWB array.

3.2 THE INITIAL SYNCHRONIZATION APPROACH.

It is advantageous to gang or synchronize lower power sources in an array for the generation of UWB energy for the reasons described in 3.1. To affect synchronization and electronic scanning, the problem of both short term jitter and long term thermal drift must be solved. Of the

two problems, short term jitter is, generally, the easier of the two to cure. Overtriggering has been found to reduce short term jitter to less than 20 ps, at least with the avalanche transistor devices used in the sources. And for sources below 2.5 GHz, where the rf period is 400 ps or greater, this is sufficient. Thermal drift, however, requires considerable attention.

To quantify the problem, consider the transmitted waveform shown in Figure 3-1 from ANRO's 13 stage Marx generator source used to drive each antenna element in the array.[2] Since there are only 3 cycles present in the S-band ($f_0 \approx 2.6$ GHz) waveform with a corresponding period of about 400 ps, it is difficult to imagine how one would synchronize an array of these sources given the thermal drift of the sources (e.g., 1 ns/s). To maintain a peak power within 1 dB of the theoretical maximum for a 10-element array, a differential time delay of less than 20 ps would have to be maintained in spite of thermal drift and the variability of components. To accomplish synchronization, an analog closed loop scheme was first used. The synchronization of sources was later improved using digital closed loop techniques as described in the next section. The following is a description of the analog scheme used to synchronize the earlier array of S-band sources.[3]

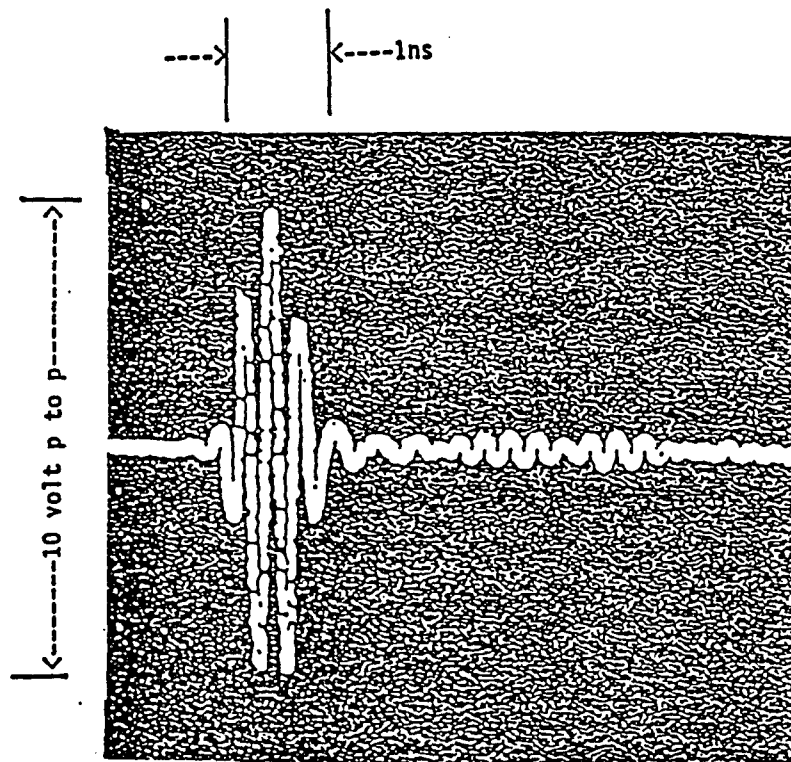


Figure 3-1. Radiated-received waveform from ANRO S-band source.

Consider the circuit employing an avalanche transistor source (Marx generator) shown in Figure 3-2. This is one of ten such elements used in the DNA array for this program. An S-band CW 2.3 GHz oscillator is used as the common synchronizing clock for all ten elements.

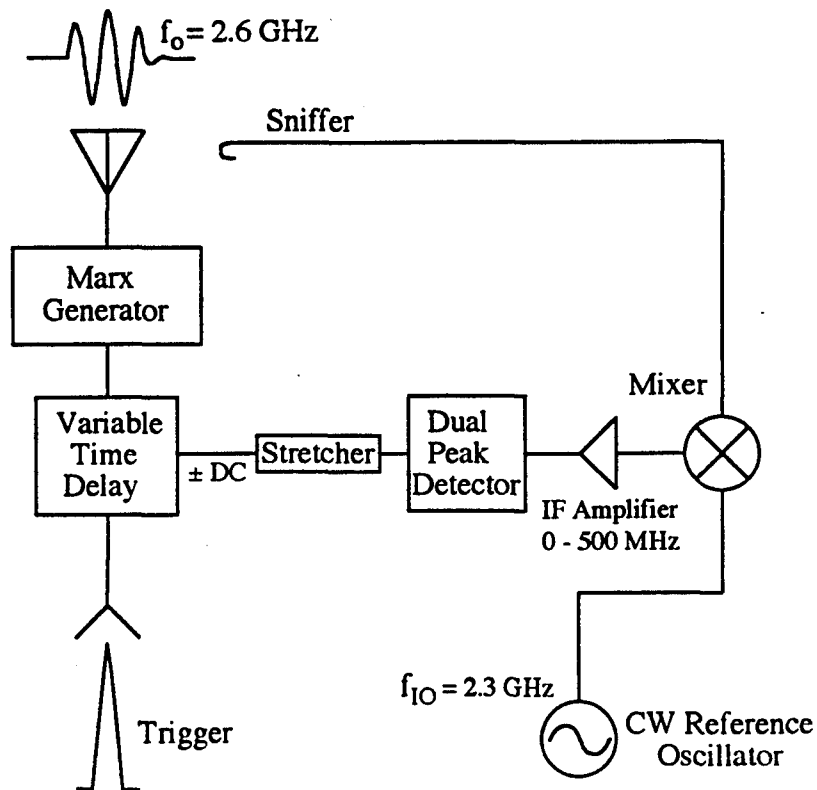


Figure 3-2. Basic synchronization scheme to accommodate long term drift.

A small part of the transmitter signal is sampled by a "sniffer" or probe at each element and mixed with the CW microwave reference signal. A bandpass filter (BPF) is used to select only the lower sideband signal. The resulting beat signal, because of the duration of the transmission and the judicious choice of the local oscillator frequency, is approximately a plus or minus half-cycle of rf energy or a baseband pulse depending upon the phase difference between the CW oscillator and the transmitter output. The baseband pulse (plus or minus) is peak detected and stretched. This dc voltage is then used to control the delay of the avalanche transistor output with respect to the trigger pulse. A functional relationship of the dc voltage between base and emitter of the avalanche transistor and the time delay of the output pulse is shown in Figure 3-3.

When the loop is closed, the gain in the loop (for example, about 30 for the array application) locks the phase of the pulsed transmitter output to that of the CW S-band reference. Although the gain in the loop can be increased to make the long term drift arbitrarily small, the time constant of the loop must be made long to prevent oscillation (e.g., 100 milliseconds, and depends upon anticipated thermal drift). As indicated earlier, short term drift is reduced to less than 20 ps by overtriggering the Marx generator. This can readily be seen and quantitatively measured by viewing a sampling oscilloscope.

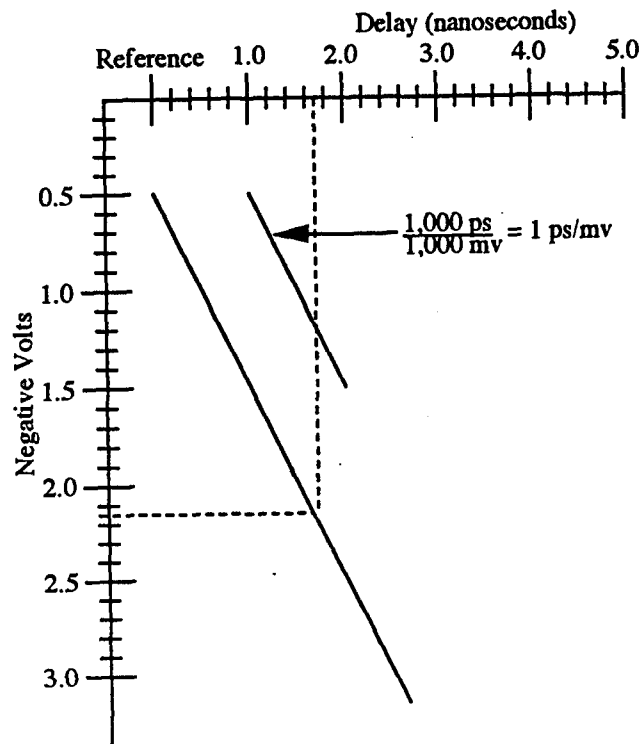


Figure 3-3. Time delay vs. V_{be} for ganging application (1 ps/mv).

The feedback loop created for temperature stabilization can be mathematically modeled. Consider the electrical equivalent circuit of the loop as shown in Figure 3-4.

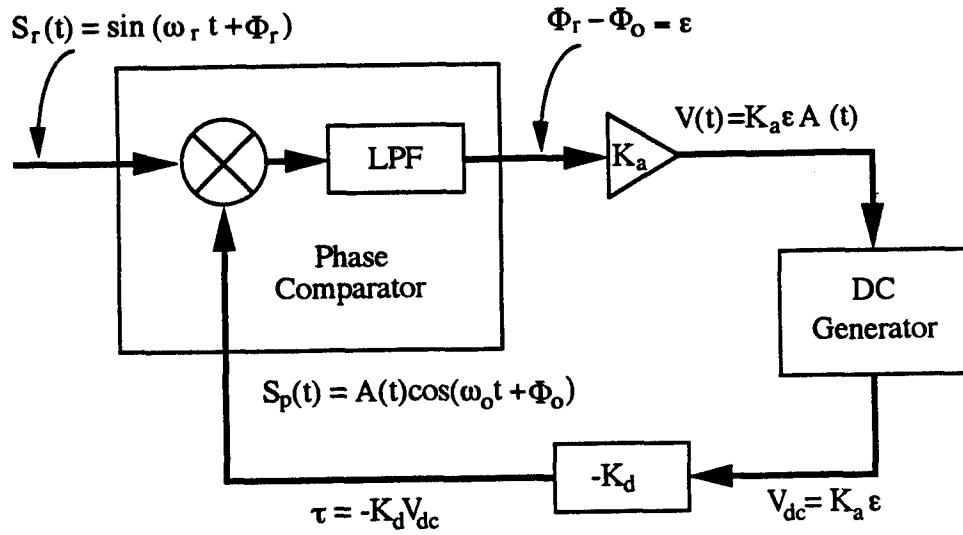


Figure 3-4. Equivalent circuit of the synchronization loop.

If the CW reference signal is expressed as

$$S_r(t) = \sin(\omega_r t + \Phi_r), \quad (3.1)$$

then the element waveform is given by

$$S_p(t) = A(t)\cos(\omega_o t + \Phi_o), \quad (3.2)$$

where $A(t)$ is the pulse shape and $\Phi_o = \omega\tau$.

The output of the phase comparator is given by

$$\Phi_r - \Phi_o = \epsilon. \quad (3.3)$$

The output of the comparator is amplified to produce a baseband voltage waveform of the form

$$V(t) = K_a \epsilon A(t), \quad (3.4)$$

which is the peak detected and stretched to produce the DC voltage

$$V_{dc} = K_a \epsilon. \quad (3.5)$$

The DC voltage is applied to the emitter base junction of the avalanche transistor to implement a transmitted pulse delay given by

$$\tau = -K_d V_{dc}, \quad (3.6)$$

where

$$\Phi_o = \omega_o \tau.$$

The closed loop equations are obtained by substitution as follows

$$\Phi_o = \omega_o \tau = -\omega_o [-K_d K_a \epsilon] = \omega_o K_d K_a [\Phi_r - \Phi_o]. \quad (3.7)$$

Let

$$\omega_o K_d K_a = G, \text{ then} \quad (3.8)$$

$$\Phi_o = G\Phi_r - G\Phi_o \text{ or rewriting } \Phi_o[1+G] = G\Phi_r, \text{ and}$$

$$\Phi_o = \frac{G}{[1+G]}\Phi_r, \text{ and } \Phi_r - \Phi_o = \epsilon = \Phi_r \left[1 - \frac{G}{[1+G]} \right]$$

which shows, as expected, that the phase error decreases as the loop gain, G, increases (e.g., $\epsilon \rightarrow 0$ as $G \rightarrow \infty$).

3.3 A LOW-COST DIGITAL TECHNIQUE TO AFFECT SYNCHRONIZATION DEVELOPED ON THIS PROGRAM.

An improved low-cost digital closed loop approach to synchronization and electronic steering was developed on this program to replace the analog scheme described in 3.2: many of the costly microwave components have been eliminated. The modified approach is shown in Figure 3-5. A crystal controlled source (e.g., 10 kHz) excites a single avalanche transistor trigger baseband source which produces a 100+ volt, 5 ns pulse. This pulse is fed to a "star" power divider which produces $n + 1$ pulses each having about a 10 volt amplitude. These are the trigger pulses which excite each Marx generator.

In place of the base-to-emitter voltage vs. time delay transducer, described in section 3.2, a SRD circuit is used where the snap time of the diode and hence the leading edge of the pulse is a function of a dc current applied by the computer. It is the leading edge of this pulse that triggers each transmitter. The $n + 1$ output port of the star power divider feeds a separate Marx generator, identical to the other n . This generator serves as a reference and replaces the costly CW microwave oscillator used earlier. This reference source feeds a n -port star power divider which produces about 10 volt very short duration (e.g., 100 ps) baseband pulses that occur when its avalanche diode transitions. Each of these signals are compared with similar sampled signals

obtained from the antenna radiating element sources in a high speed comparator. When the very narrow reference pulse coalesces with a similar short pulse signal from each of the element sources in the high speed comparator, a stretched signal is sent to the computer. These pulses are forced to coalesce by the computer continuously feeding an appropriate formatted search current to the SRD. Thus, a closed loop is formed by the computer always locking each source to the short pulse clock reference generator. The software for assuring synchronization and beam steering has been developed for the ten-element *linear* array. New software for a 25-element *planar* array is now being written for an Air Force program to detect buried bunkers. This planar array should radiate almost 1 MW erp. A patent disclosure describing this new synchronization technique is in preparation.

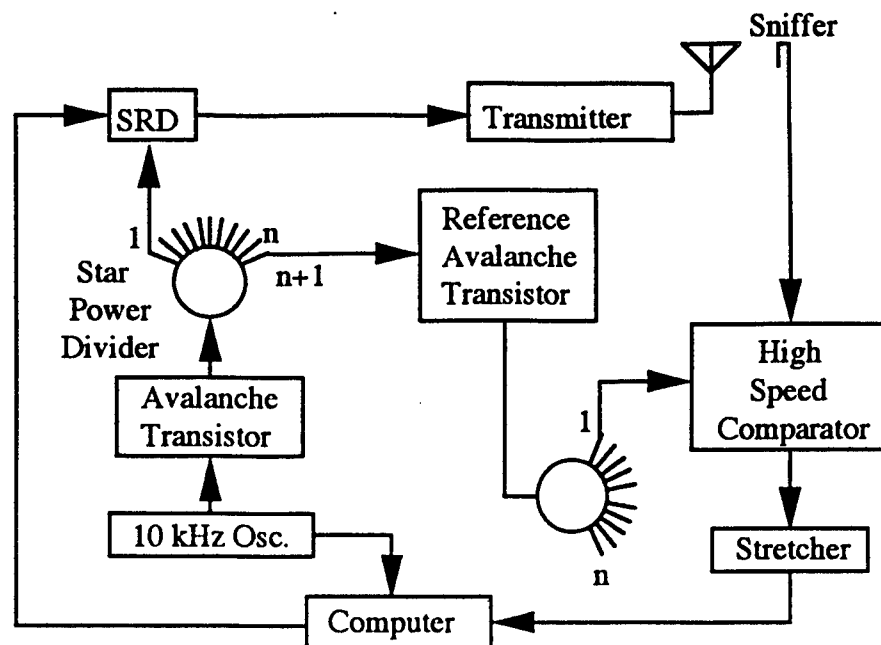


Figure 3-5. Digital synchronization.

To accomplish electronic scanning, the computer assigns a prescribed incremental current to each SRD circuit on alternate pulses; the synchronization function is accomplished on the other part of the cycle. The beam steering angle is selected from a look-up-table in the computer. Depending on the spacing of the elements in the array and the position, for example, of an approaching intruder, the required time delay taper is placed at the elements; the time delay taper

is not likely to be linear but rather parabolic. The computer assigns the precise time delay required at each element for the signals to coalesce at a particular angle and range. The calibration procedure is described in 3.4.

3.4 THE CALIBRATION TECHNIQUE REQUIRED FOR UWB BEAM STEERING.

Calibration of the trigger reference using (three) delay lines is a crucial part of accomplishing UWB beam steering. To have satisfactory coherent adding and subtracting of the wave amplitude from each element, the beam must be positioned to within 1/8th wavelength, or 1/2 inch. This translates into realizing differential time delays at each element to within 50 ps or better.

Three line delays were cut to exact lengths of 6 ns, 7 ns, and 8 ns. This provides calibration delays of ± 1 ns either side of the 7 ns line.

The correct line lengths were confirmed with a frequency domain measurement. Since frequency can be counted, it lends itself to very accurate measurement. The calibration procedure is illustrated in Figure 3-6.

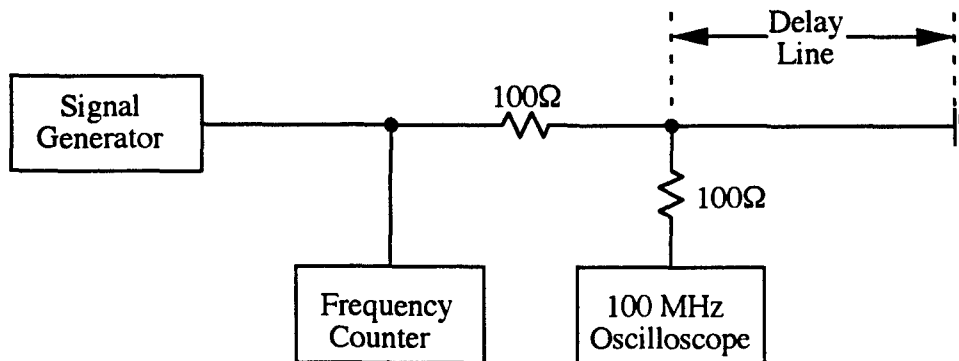


Figure 3-6. Frequency domain measurement of line delay.

The delay line under test is short circuited at the end, and connected to a stripline T junction through surface mount 100 ohm resistors to give some isolation to the resonant element. There is an anti-resonant null in the oscilloscope signal at two times the transmit time in the delay cable. The null is sharp, but not sharp enough to judge the line length to better than 100 ps. The numbers confirmed the line lengths, but accuracy was not good enough for the frequency domain results to become the primary standard of measurement.

The delays that are read into the computer to which the transmitters are locked, are in the trigger reference "STAR" generator. The STAR generator is so called because ten simultaneous reference signals emanate from it. The generator has its own delay from the time it is triggered through the delay lines, to the time it fires. It is not adequate just to know the delay line lengths from measurement on the bench; they should be measured 'in situ' on the pulse emerging from the STAR generator, with all connections made through the contacts of mercury wetted reed relays which exhibit precise and repeatable characteristics.

Mercury reed switches were used to introduce standard delays of -1.5 ns, -0.75 ns, 0 ns, +0.75 ns, and +1.5 ns into the timing of one of the transmitters. The computer was programmed to accumulate measurements on the three calibration points for each firing time of the transmitter. This way it is possible to obtain a family of three curves, showing bias (mV) as a function of firing time at each calibration point. See Figure 3-7.

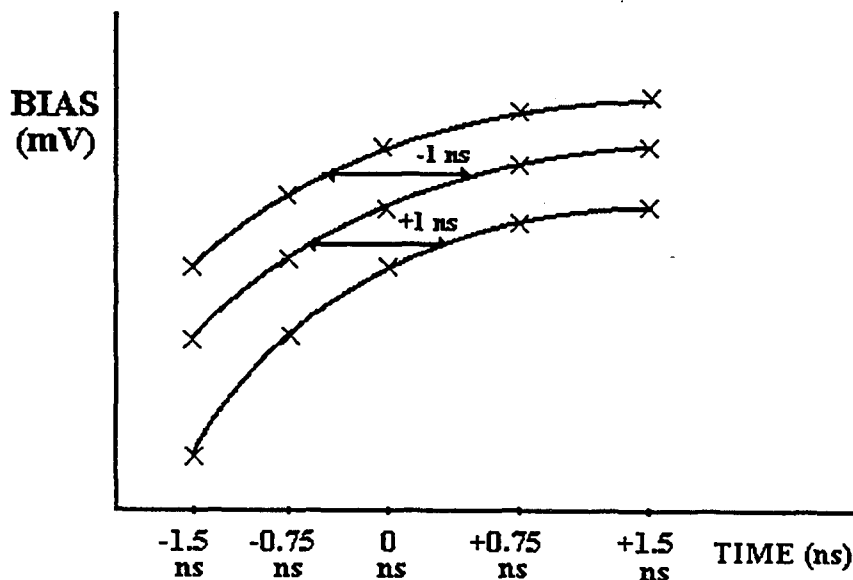


Figure 3-7. Bias (mV) vs. time (ns); transmitter calibration characteristics.

The horizontal separation between the curves is the calibration line length, which can be read directly from the graph. The calibration numbers resulting from measurement of the span at five places is:

$$-(1.016 \pm 0.11) \text{ ns}, + (1.035 \pm 0.11) \text{ ns}.$$

The bias (mV) vs. time (ns) curves are not straight lines. This means the slope (mV/ps) is not constant, but it is a function of bias. Having three calibration points means it is possible to make a first order match to the curvature, analytically equivalent to drawing a parabola through the three points rather than a straight line. This is what was done, and it makes interpolation of the bias for steering very faithful to the actual bias curve.

The work in the calibration technique, as well as the programming of the beam steering technique was the contribution of Mr. Peter Mitchell.

Software has been written and implemented to permit electronic scanning of the beam over an angle of ± 30 degrees; this will be extended to ± 45 degrees at the next stage of development. The time delay settings for the different beam positions include corrections for range focusing.

3.5 THE DESIGN OF THE TEN-ELEMENT LINEAR ARRAY.

3.5.1 Design Considerations for the 10-Element Array.

The SOW requires the construction of a 10-element linear array of 1 kW s-band (2.5 GHz) UWB sources. By the addition of coherent voltages, a total erp of 100 kW is achieved in the far field. The Phase I effort used four individual transmitter elements in a linear array configuration. The initial analysis indicated that the transmitted beam could be narrowed in the vertical plane (the plane of expected targets) by mounting the elements in a parabolic cylindrical reflector. A vertical beamwidth of 30° appeared to be appropriate for a preliminary design goal for this application. Figure 3-8 shows a perspective view of the original antenna array.

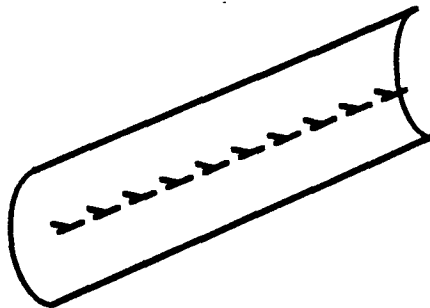


Figure 3-8. Perspective view of the 10-element transmitter array.

The dimensions of a beam produced by a generalized linear array are controlled primarily by the spacing of the elements and the dimensions of the physical structure, with the principal dimensions of a rectangular array are defined as the height (h) and the width (w). For uniform illumination of the structure, the beamwidth can be estimated by[4]

$$\begin{aligned}\sin\theta_x \approx \theta_x &= 0.886\lambda/w \\ \sin\theta_y \approx \theta_y &= 0.886\lambda/h.\end{aligned}$$

For the DNA S-band array, the wavelength is assumed to be 12 cm. To achieve a 30° vertical beamwidth, assuming a planar array, the required height of the array is 0.212 m (8.4 in) using the above criteria.

The preliminary design for the antenna system employed a parabolic cylinder reflector to decrease the beamwidth in the plane normal to the array axis (x). Figure 3-9 illustrates a cross section view of the initial design concept for the parabolic cylinder reflector and the dipole feed elements. The coordinates of the point p can be found by[5]

$$p = F \sec^2 \varphi/2$$

where φ = the angle drawn from the focal point towards the parabolic arc and F is the focal length.

The dimension d, height of the parabolic cylinder, is a principal factor in determining the transmitted beamwidth. Again using a uniformly illuminated parabola aperture, the beamwidth can be estimated by[6]

$$\theta = 58\lambda/d.$$

When the focal length is assumed to be $\lambda/2$, or 6 cm., and a desired beamwidth in the y plane of 30°, requires a dimension d of 0.232 m (9.13 in.). Various other estimation tools[7],[8] yield dimensions of between 0.2 to 0.25 m (7.8 to 9.8 in.). Thus, an array height (height of the cylindrical parabolic aperture) of about 0.213 m appeared to be a valid first order estimation.

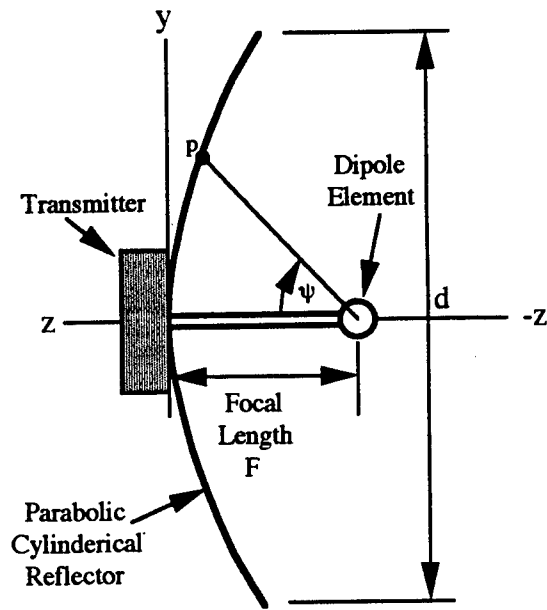


Figure 3-9. Parabolic cylindrical reflector - cross section view.

A parabolic reflector is typically used to achieve beam focusing and gain above an isotropic radiator. Figure 3-10 below depicts the theoretical radiation paths from an isotropic radiator located at the focal point of a parabola. The reflected rays form a plane wave front which propagates along the axis of the array.

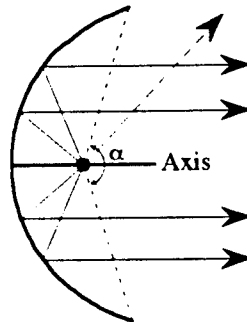


Figure 3-10. Parabolic reflector radiation.

All radiation that strikes the parabolic reflector surface is reflected in phase, producing a narrowed beam shape and the attendant gain. However, any radiation from the primary source or feed antenna at the focus of the parabola which is not directed into the parabola (the solid angle area α in Figure 3-10) is not collimated, but is radiated by direct paths over the solid angle area

not included in the reflector area. This is not only inefficient, but the distributed radiation degrades the pattern of the plane wave formed by the parabola. Therefore, parabolic reflector antenna systems usually include some form of "splash plate" or reflector element to direct more of the energy into the parabolic reflector. This may take the form of a flat plate placed behind the driven element, or a reflective element, such as a 0.6λ dipole, as shown in Figure 3-11. A directive horn or a corner reflector can also be used as a directive feed element.

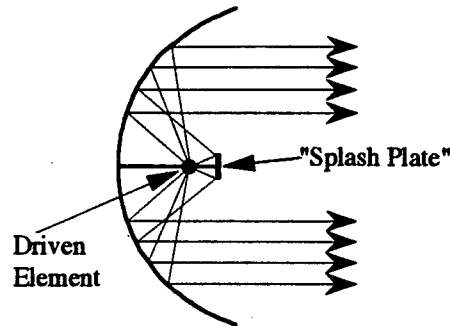


Figure 3-11. Parabolic reflector antenna with directive feed element.

The analysis of the anticipated beamwidth of a 10-element S-band array as a function of element spacing[9] calculated by Dr. DeLorenzo is presented in 3.5.2. Figure 3-12 shows the predicted 3 dB beamwidth for element spacings of 0.7 feet to 2 feet. This analysis indicates that an element spacing of about 0.6 feet (7 in., or 17.8 cm) will produce a beamwidth of about 1.6° . This was the spacing for the array on this program.

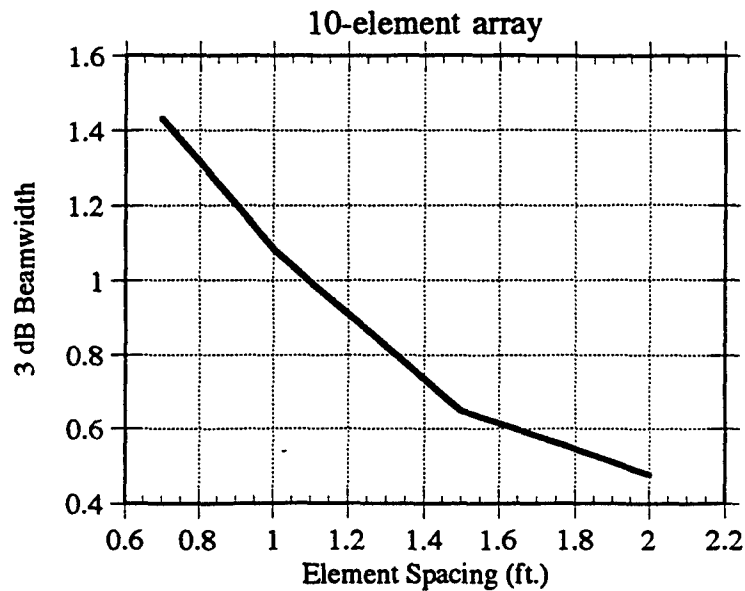


Figure 3-12. Three dB beamwidth vs. element spacing for a ten-element S-band array.

An element spacing of 0.6 foot between elements requires a transmitter array approximately 6 feet in length. The approximate overall dimensions for the 10-element S-band array are shown in Figure 3-13.

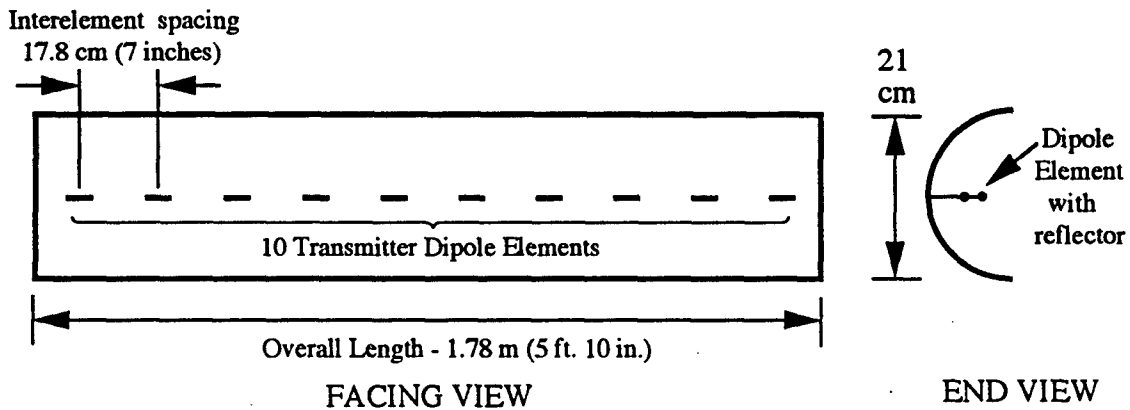


Figure 3-13. Approximate overall array dimensions.

Given that the dimensions derived above are approximately correct, consideration was then given to the physical construction of the array. Since it is necessary to transport the array for outdoor tests, it became clear that some changes to the reflector design were desirable.

Consideration was given to building the array so that it can be easily disassembled for shipment and handling, and should resist bending and twisting when suspended in air. For this reason, a variant of the corner reflector known as a trough reflector was substituted for the perfect parabolic surface described above. The trough reflector has a flat rear section in the apex region where the transmitter module can be conveniently mounted. To determine the appropriate reflector dimensions, a single corner reflector was designed with variable hinges to find the best angle for maximum amplitude and minimum dispersion. The result showed that 110° was optimum. The final design for the reflecting surface is shown in Figure 3-14.

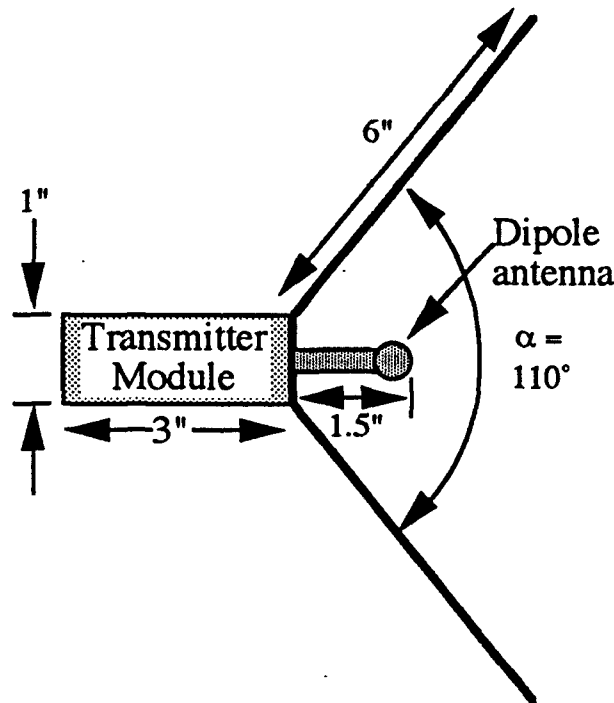


Figure 3-14. Trough reflector configuration design.

To simplify array construction, a slot was placed through the apex of the trough reflector so that the dipole radiating elements can pass through the reflector. Conducting tape was then used to close the gap. In this way, the ten transmitter modules did not have to be disassembled from the antennas before mounting.

For the receive antenna it was decided to use two receive elements located in the center of the array placed above and below the trough array as shown in Figure 3-15. The signals from these elements are summed in a simple T connector. If more directivity is required in the vertical

plane, two more elements will be added and two other T connectors will be used to sum the signals in a corporate feed. One possibility is to develop a UWB duplexer and use the current antenna elements together with appropriate delays in each receiver line. But this is an elaborate change requiring a new development program. A stack of four receive elements, having the same polarizations, but placed in the center of the linear array was used as a compromise.

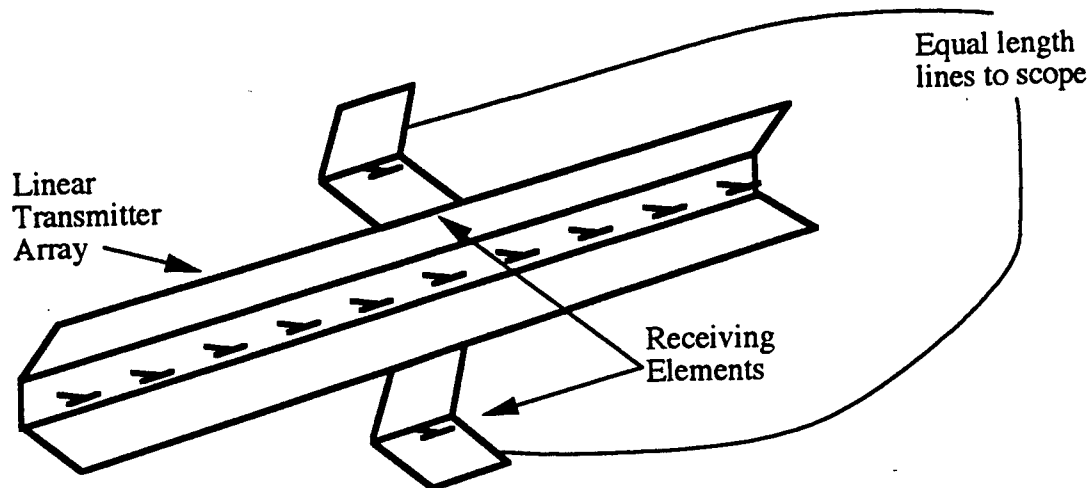


Figure 3-15. Linear array with corporate feed receive elements.

3.5.2 Space Time Array Analytical Study Results.

To determine the effect of element spacing for a short pulse array, the ten element array geometry, shown in Figure 3-16 was analyzed. The beam direction angle is denoted as

$$\Phi = \Phi_o = \pi/2.$$

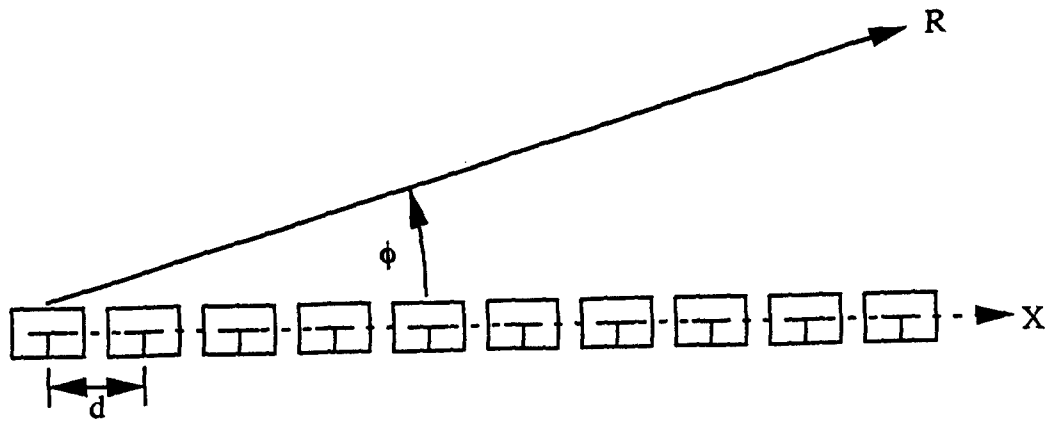


Figure 3-16. Ten element array geometry.

Figure 3-17 shows the system waveform, obtained as the coherent sum of the radiation from all 10 radiating elements in the broadside direction.

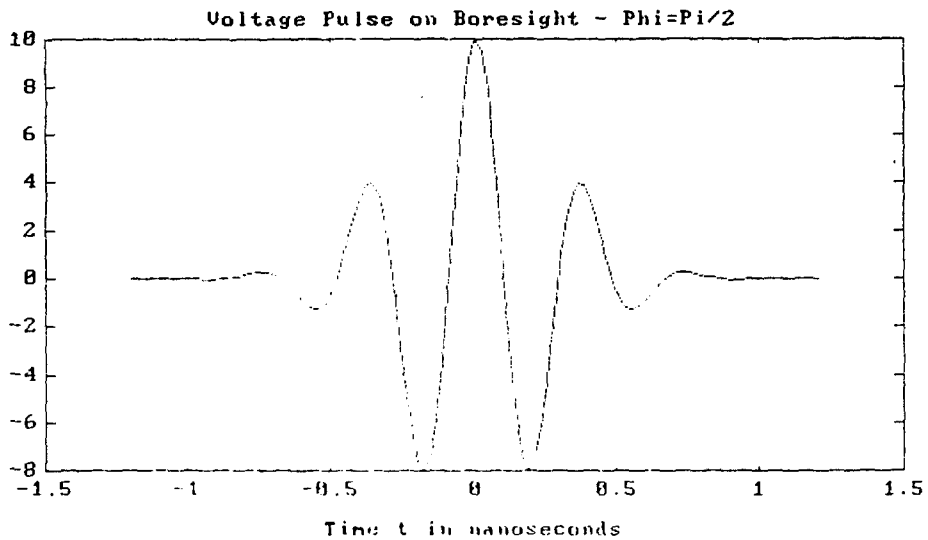


Figure 3-17. System waveform.

The plot of power as a function of angle along the $t = 0$ axis defines the shape of the main beam. The beam width is measured between the half power points, along the $t = 0$ axis, as shown in

Figures 3-18 - 3-21. As the element spacing increases, the length of the array increases and the beam width decreases. This expected result is shown quantitatively in Figure 3-23 (as measured from the curves in Figures 3-18 - 3-21).

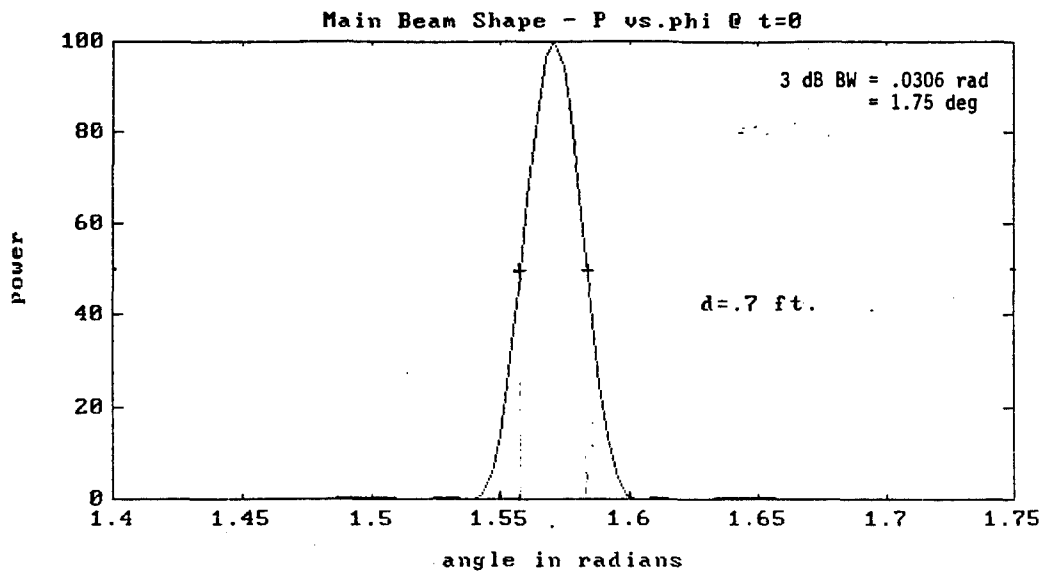


Figure 3-18. Beam width with 0.7 foot spacing.

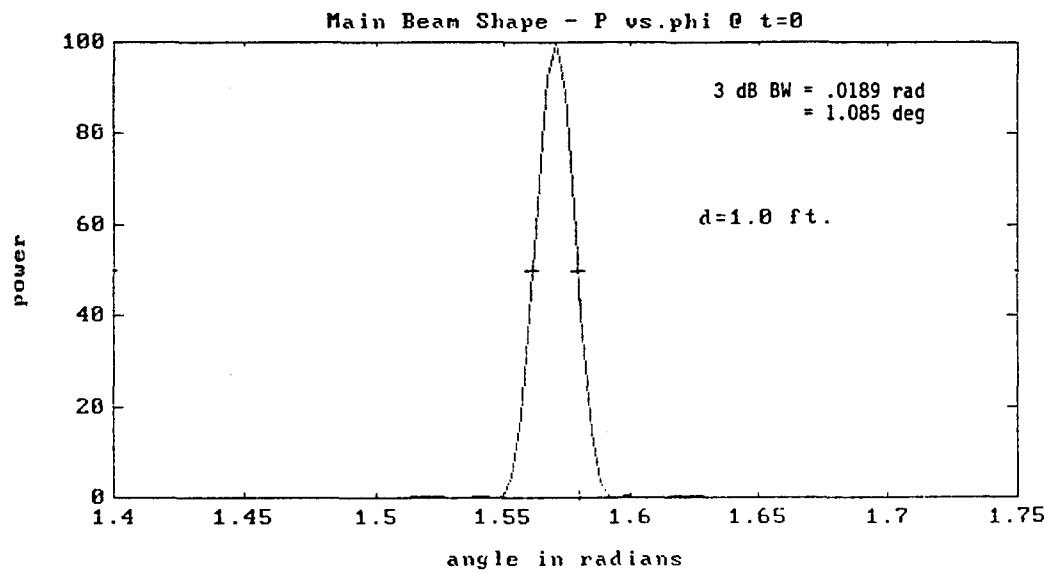


Figure 3-19. Beam width with 1.0 foot spacing.

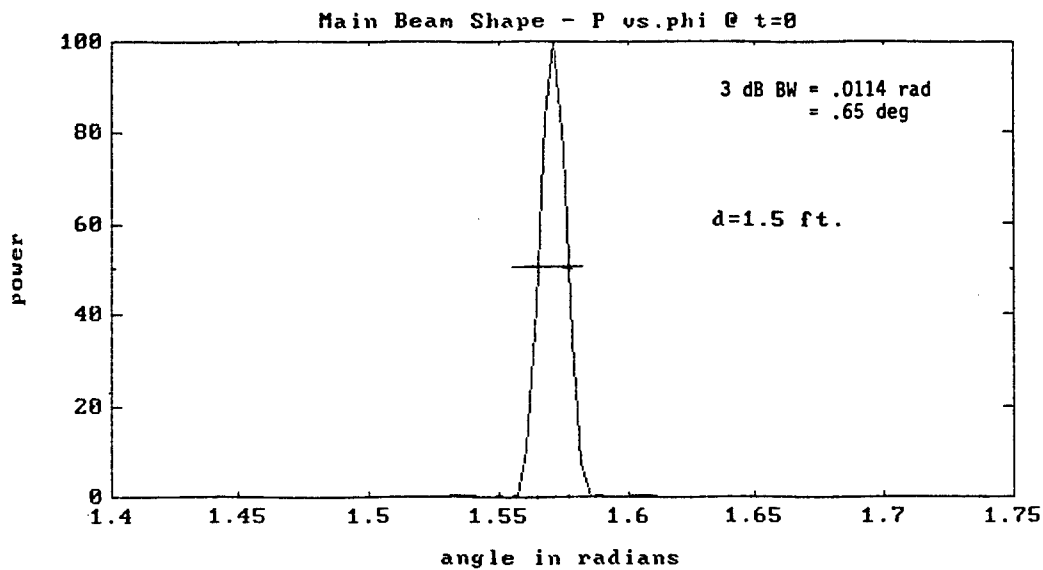


Figure 3-20. Beam width with 1.5 foot spacing.

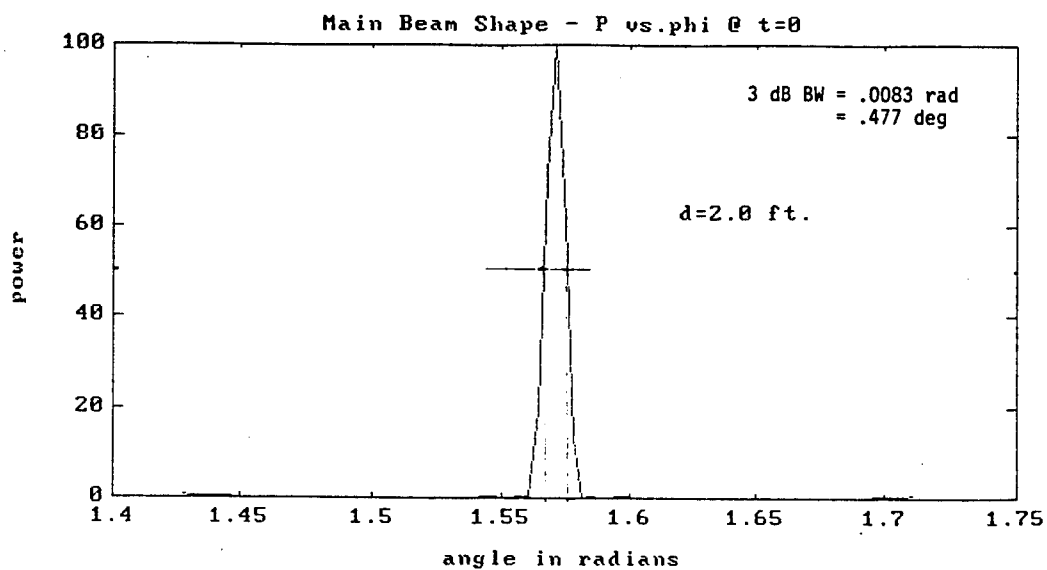


Figure 3-21. Beam width with 2.0 foot spacing.

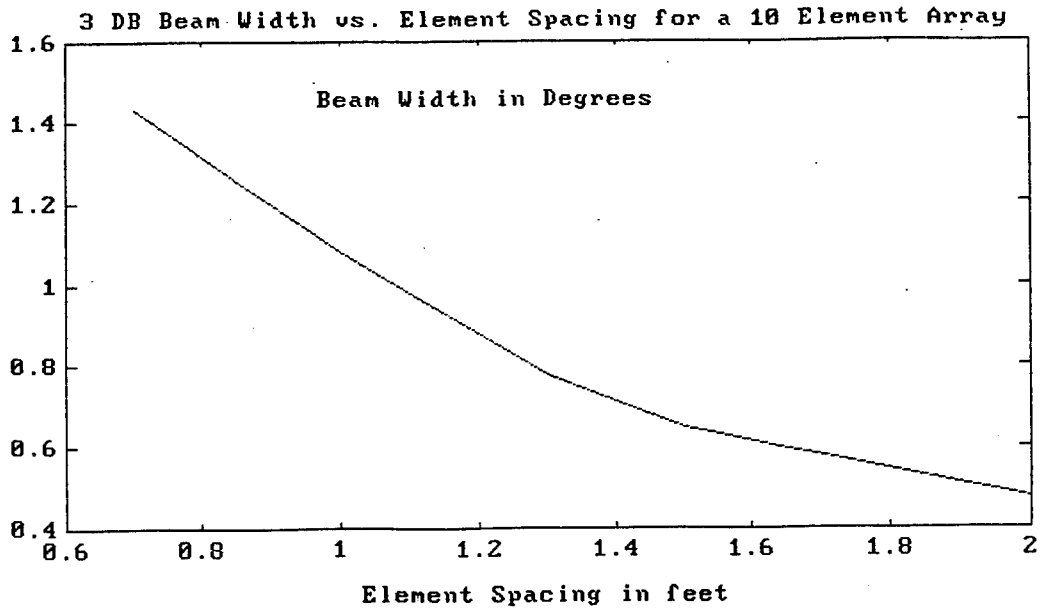


Figure 3-22. 3 dB beam width vs. element spacing for a ten element array.

The wavelength of the pulse center frequency (2.6 GHz) is 0.115 meters. Since the closest element spacing of 0.7 feet = 0.2134 meters is larger than the wavelength, grating lobes are anticipated. The radiated pulses are, however, short enough to reduce the grating lobe structure to levels comparable to ordinary sidelobes. The grating lobes and the asymptotic sidelobe levels of unity in the equivalent voltage field pattern of the beam are illustrated in Figures 3-23 - 3-26.

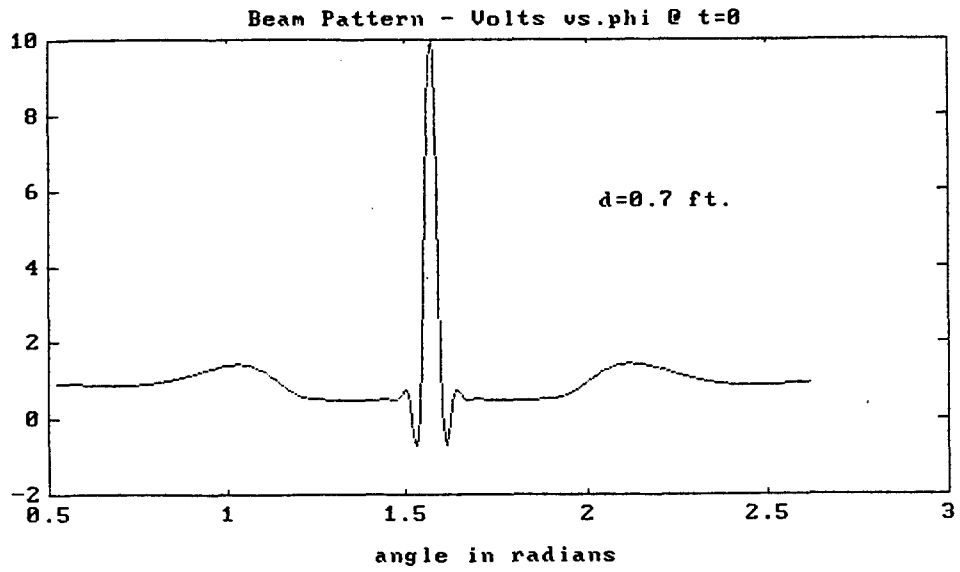


Figure 3-23. Grating lobe and sidelobe level with 0.7 foot spacing.

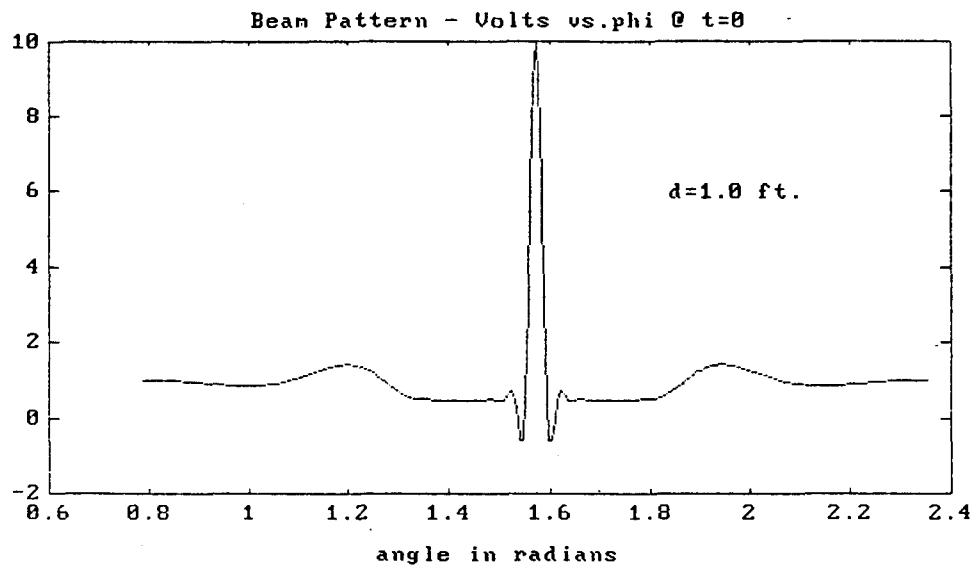


Figure 3-24. Grating lobe and sidelobe level with 1.0 foot spacing.

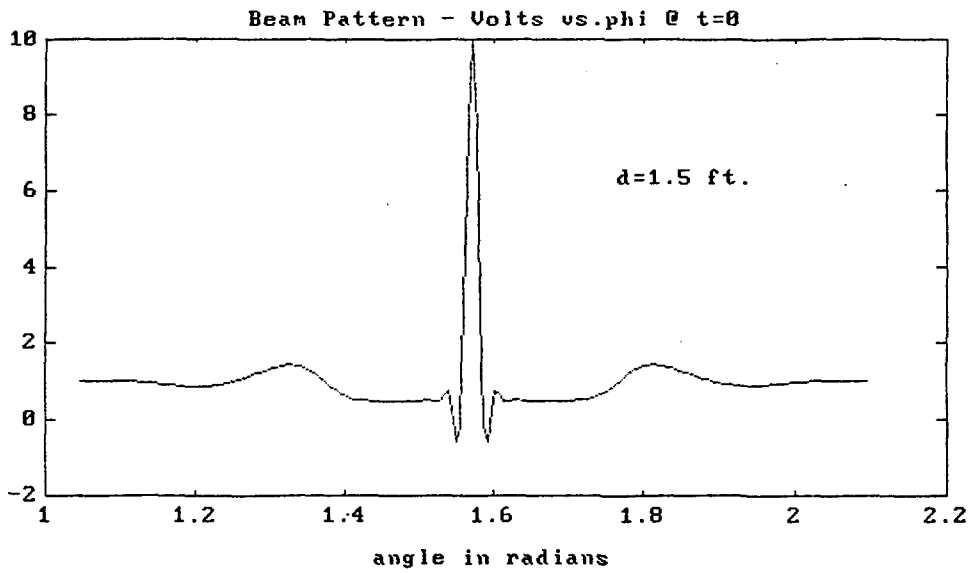


Figure 3-25. Grating lobe and sidelobe level with 1.5 foot spacing.

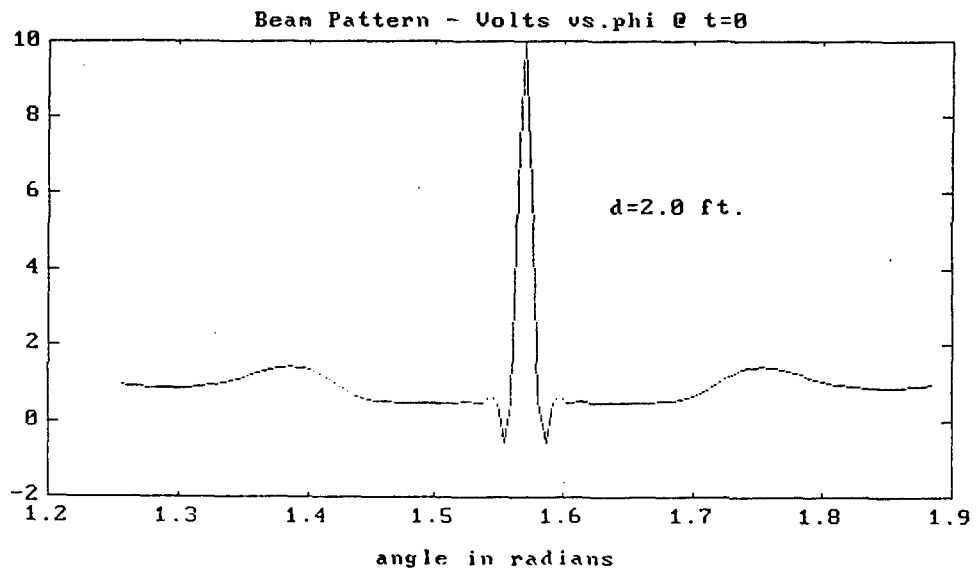


Figure 3-26. Grating lobe and sidelobe level with 2.0 foot spacing.

Figures 3-27 - 3-29 show the three dimensional structure of the field for three different element spacings and a broadside beam direction.

Field vs. Time and Angle
Element Spacing, $d=0.7$ feet

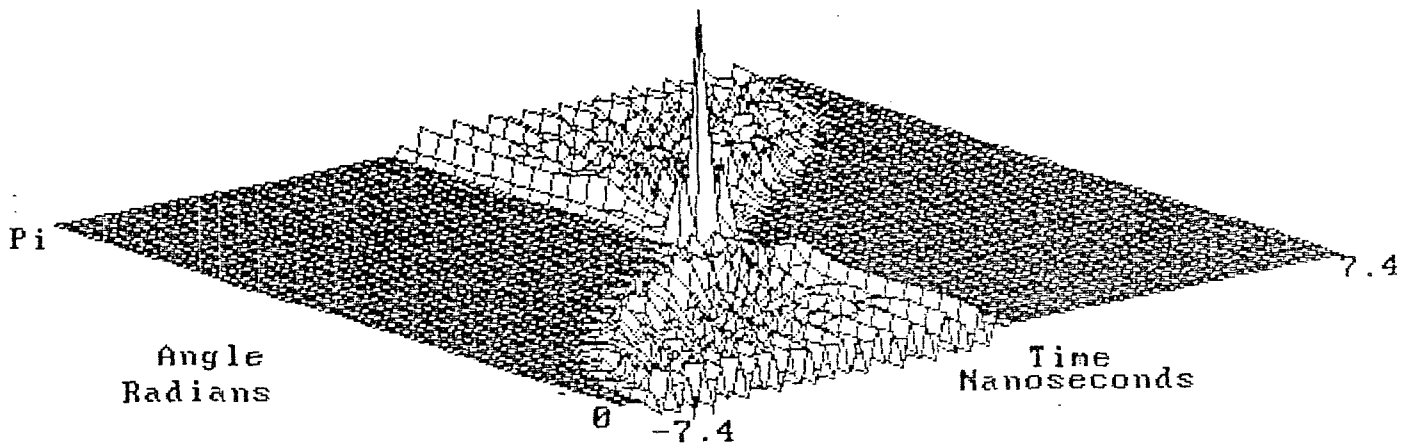


Figure 3-27. On-boresight field structure with 0.7 foot spacing.

Field vs. Time and Angle
Element Spacing, $d=1.3$ feet

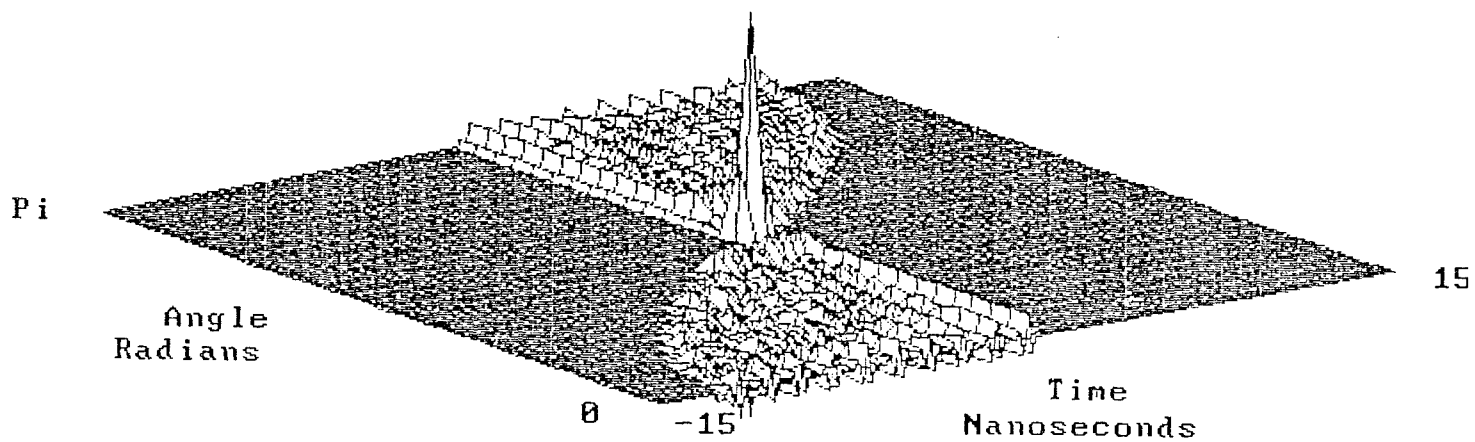


Figure 3-28. On-boresight field structure with 1.3 foot spacing.

Field vs. Time and Angle
 Element Spacing, $d=2.0$ feet

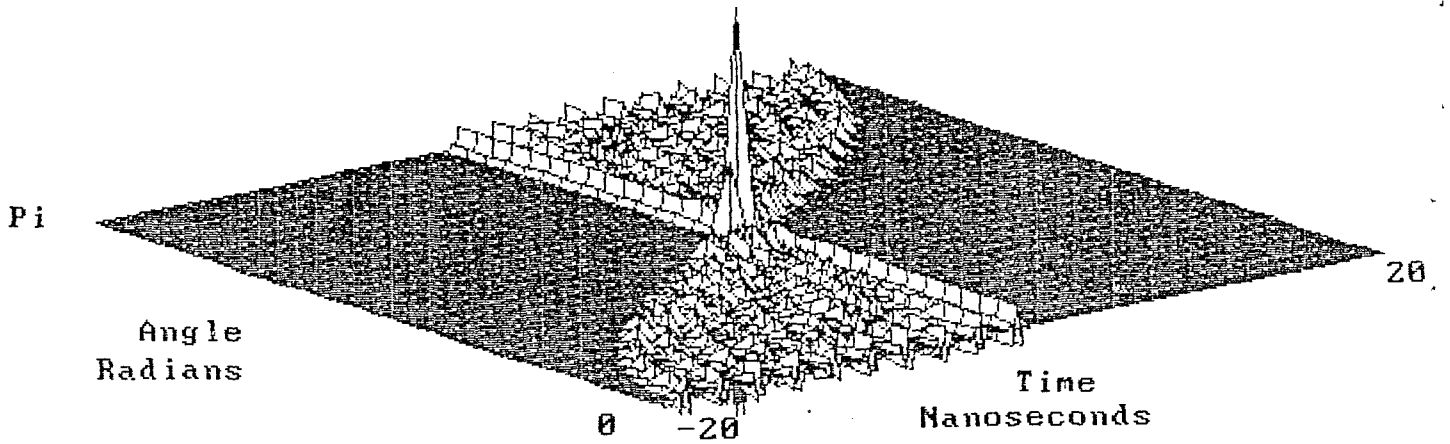


Figure 3-29. On-boresight field structure with 2.0 foot spacing.

Figure 3-30 shows the three dimensional field for the .7 foot spacing with a beam pointing angle of $\pi/4$ radians. Figure 3-31 shows the 3-D power pattern for the same case.

Field vs. Time and Angle
 Element Spacing, $d=.7$ feet
 $\pi/4$ Pointing Angle

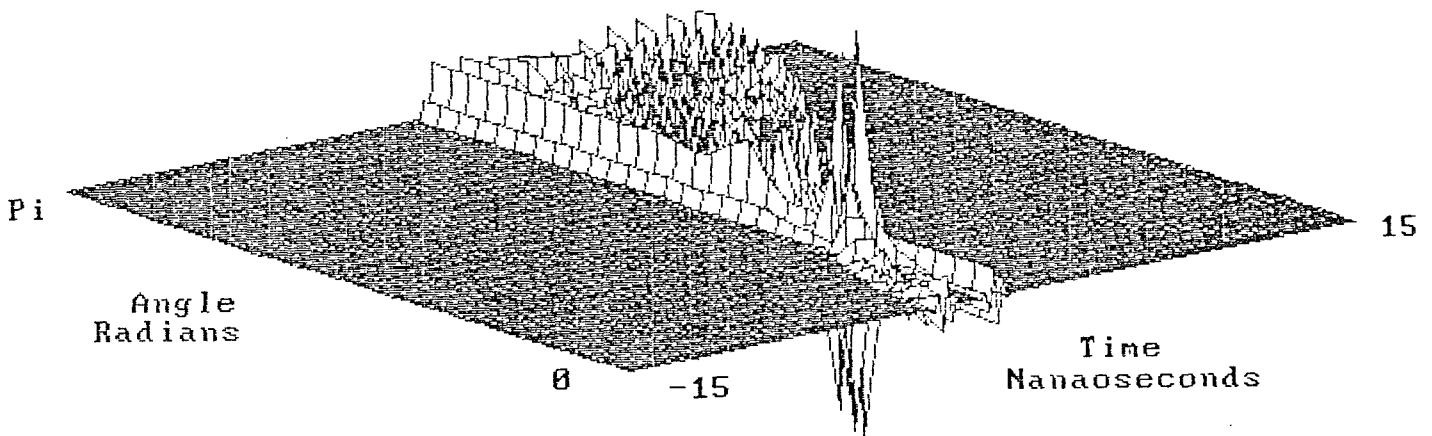


Figure 3-30. Field structure at $\pi/4$ pointing angle with 0.7 foot spacing.

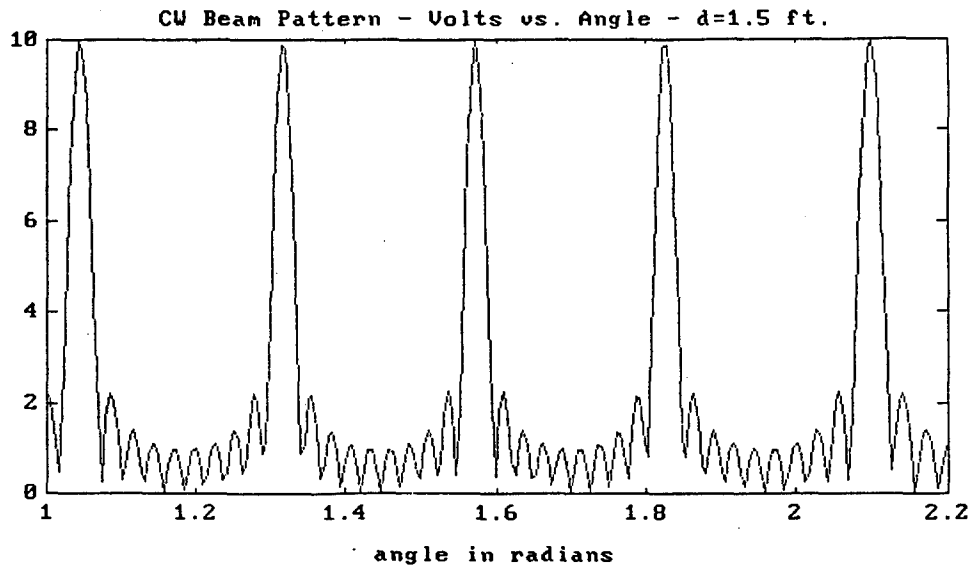


Figure 3-34. CW grating lobes with 1.5 foot element spacing.

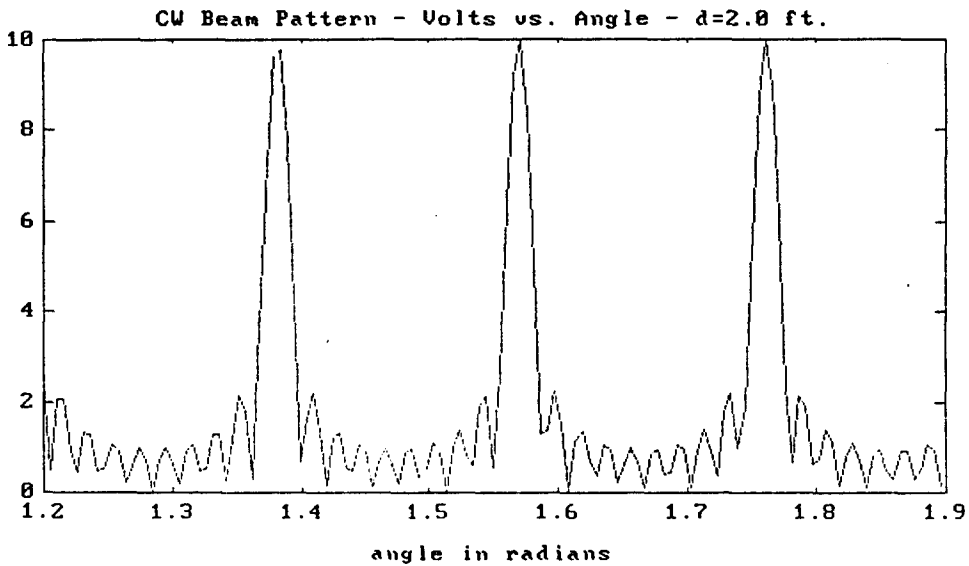


Figure 3-35. CW grating lobes with 2.0 foot element spacing.

These patterns, when compared with the short pulse patterns in Figures 3-23 - 3-26, show a marked reduction (nearly elimination) of the grating lobes. *This provides the basis for still another major performance advantage of the short pulse array; namely, a beam width reduction of almost a factor of two over the CW case.*

The plots of power versus angle for the CW cases are shown in Figures 3-36 - 3-39. The beam widths are measured between the half power points of the main beam and are noted on the figures.

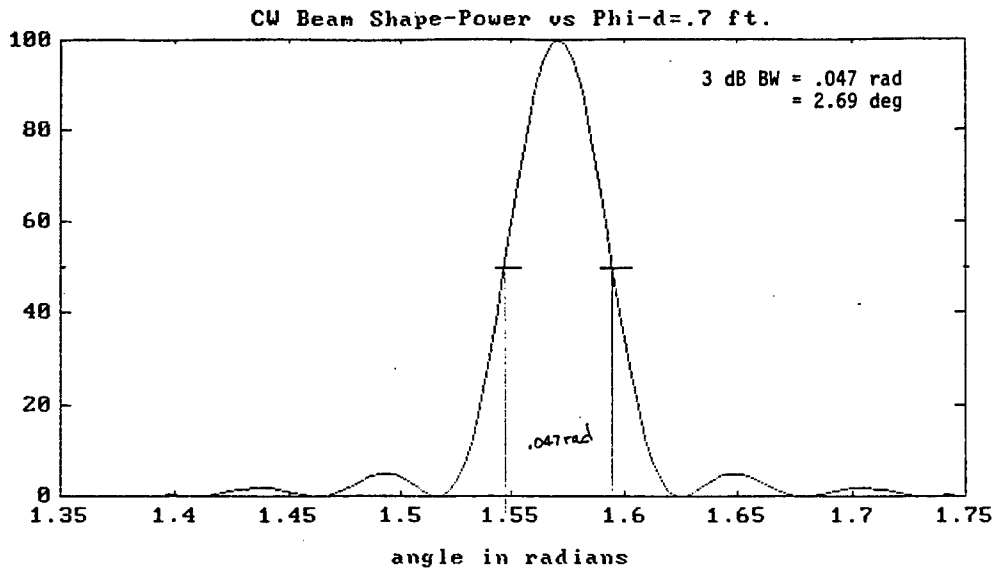


Figure 3-36. Power level vs. angle for 0.7 foot element spacing.

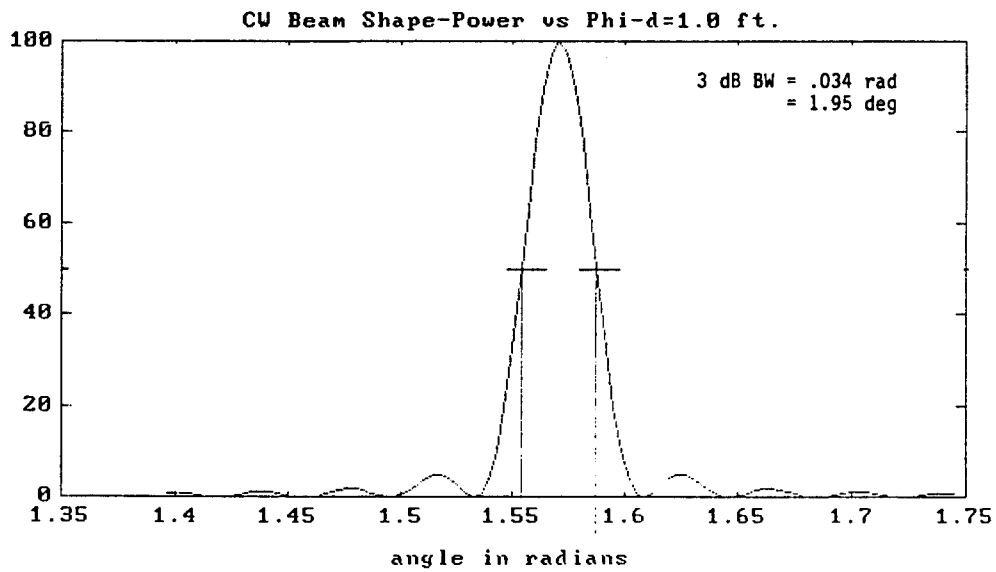


Figure 3-37. Power level vs. angle for 1.0 foot element spacing.

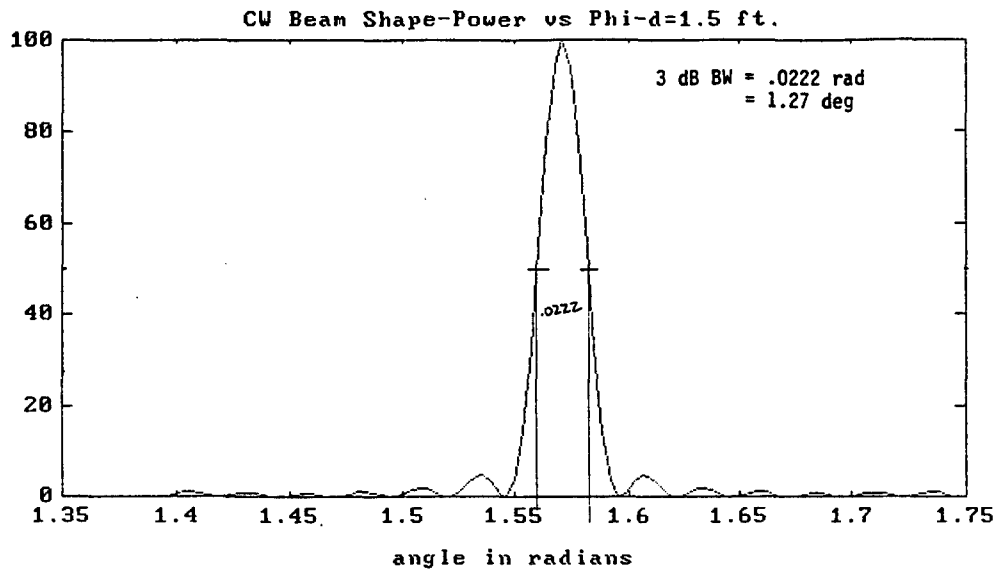


Figure 3-38. Power level vs. angle for 1.5 foot element spacing.

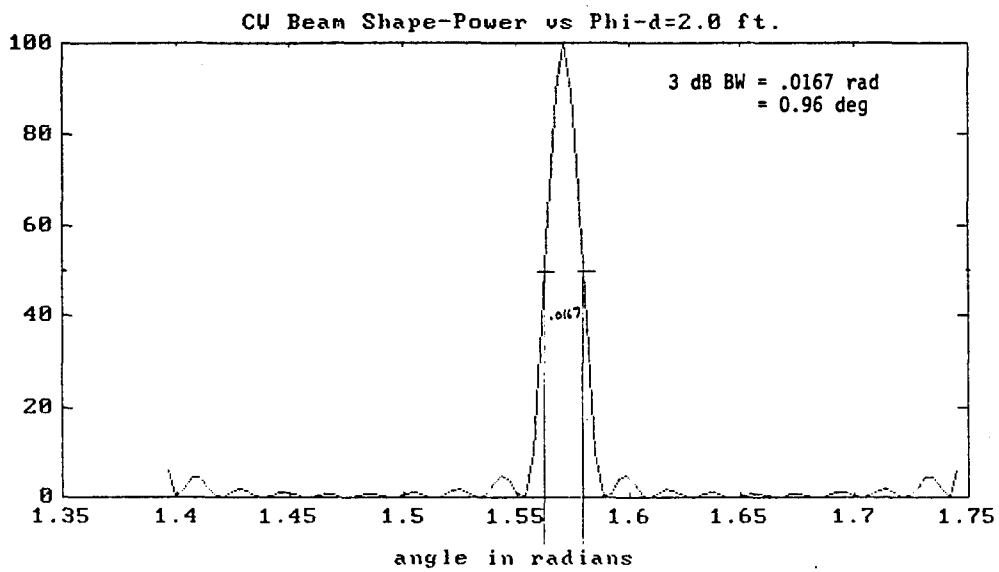


Figure 3-39. Power level vs. angle for 2.0 foot element spacing.

Figure 3-40 compares the beamwidths of the CW arrays with those obtained using short pulse excitation of the array with the same element spacings. Clearly, there is nearly a factor of two reduction of the beam width when short pulse excitation is used.

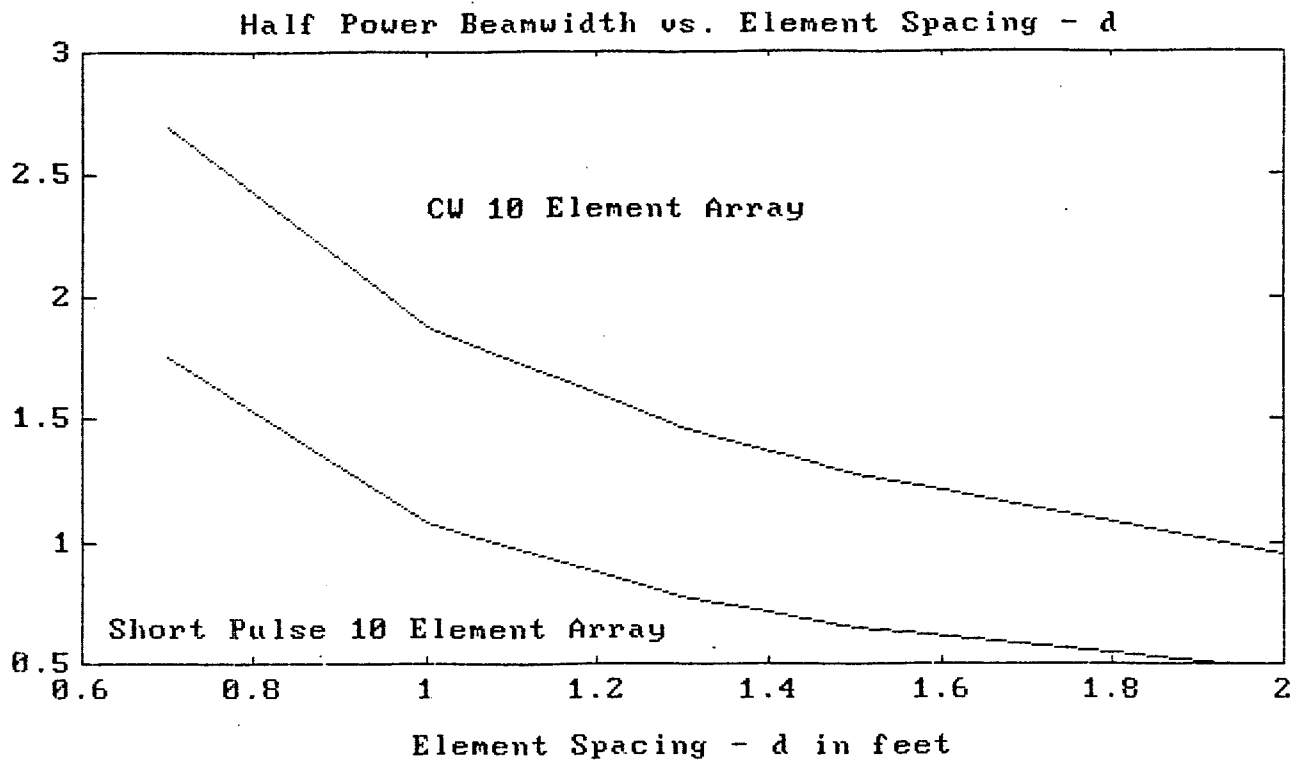


Figure 3-40. Comparison of beamwidth with short pulse vs. CW array.

SECTION 4

THE LEADING EDGE FILTER

4.1 INTRODUCTION.

The leading edge filter (LEF) was implemented during the Phase I study. Its purpose in this network is to use the fluctuations of the leading edge of UWB radar returns from moving targets to reduce nuisance alarms caused by, for example, fast moving animals. However, the analysis of Phase I test results showed that the LEF was significantly more robust as a target identifier than its name might suggest. In particular, it was noted that the LEF output waveforms contained range information that was not used during the Phase I tests. This observation led to the inclusion of Phase II tasks to investigate the use of both range and range rate information to improve the ability of UWB intrusion detectors to reduce nuisance alarms. The results of these Phase II studies are presented in the following sections.

Section 4.2 presents a functional description of the LEF and describes the modifications that were made to obtain range information. A description of the LEF output voltage waveforms is contained in section 4.3. Section 4.4 introduces neural network classification techniques; while Section 4.5 describes how a neural network would work with LEF output voltage waveforms to classify target trajectories. Section 4.6 presents the use of the LEF to identify intruders and reduce false alarms. Section 4.7 describes the experimental effort that was implemented to demonstrate the classification concepts described in Section 4.5. Section 4.8 outlines work that should be done to further develop the trajectory classification concept and to see if the LEF robustness can be increased still further by implementing scattering center neural network analysis.

4.2 LEF FUNCTIONAL DESCRIPTION.

The LEF described and discussed in the Phase I report and the Phase II proposal is basically the same design used in the experiments described here. The main difference between the system described previously and that used to furnish the experimental data used in this study, is the output filter is now a DC coupled low pass filter cutting off at 4 kHz as opposed to a band pass filter between 1 and 8 Hz.

To understand the operation of the LEF consider the functional block diagram in Figure 4-1. A sample of the transmitted pulse is used to generate a delayed pulse denoted as $P(t)$ at node X. The pulse is 1.5 ns wide and is delayed by a range gate generator by an amount that corresponds to the beginning of the range segment being monitored. $P(t)$ is applied to one end of a tapped delay line. The taps are spaced apart by a distance that corresponds to one foot increments in free space. A received pulse arriving during the monitored range segment is detected by the tunnel diode (TD) and subsequently triggers a 1.5 ns rectangular pulse denoted by $P'(t)$ at node Y. $P'(t)$ is applied to the other end of the tapped delay line. Avalanche transistor threshold circuits placed at each of the taps are designed to trigger only when $P(t)$ and $P'(t)$ coalesce and the pulses are shaped so that only one tap at a time can be activated. The trigger voltage at the activated tap sets a flip-flop which holds its voltage until the next transmission cycle. A target closest to the system activates the first tap and sets the flip-flop. The voltage is held for the entire inter-pulse interval and is then reset before the next pulse transmission. The result is that a target present in the first range cell produce a pulse stretched to 100 microseconds at the output of the tap circuit. Voltages at the other taps are zero. A target positioned one foot beyond the location of the beginning of the range segment being monitored will produce a 100 microsecond voltage pulse at the second tap output. All other taps are inactive.

Clearly the LEF, up to this point, is providing target range measurement with range resolution of one foot. LED's (one for each tap) mounted on the front panel of the receiver indicates the location of the target in one foot increments. A target moving through the monitored range segment will activate each of the taps in sequence. Watching the LED's is equivalent to tracking the target in real time. The final step in the process is to combine the individual tap voltages to create a voltage versus time waveform that contains the inherent information in each of the tap voltages. In the present unit, this is accomplished in a resistor summing network which provides maximum voltage for activation of the closest range cell and minimum voltage for a target at the most distant range cell. The net result is to produce a voltage waveform that has its amplitude proportional to range location and its rate of change proportional to its speed. One voltage versus time waveform contains complete information about the target trajectory through the monitored range segment. The output of this "OR" gate is passed through a DC coupled low pass filter. In the present hardware, this filter cuts off at about 4 kHz.

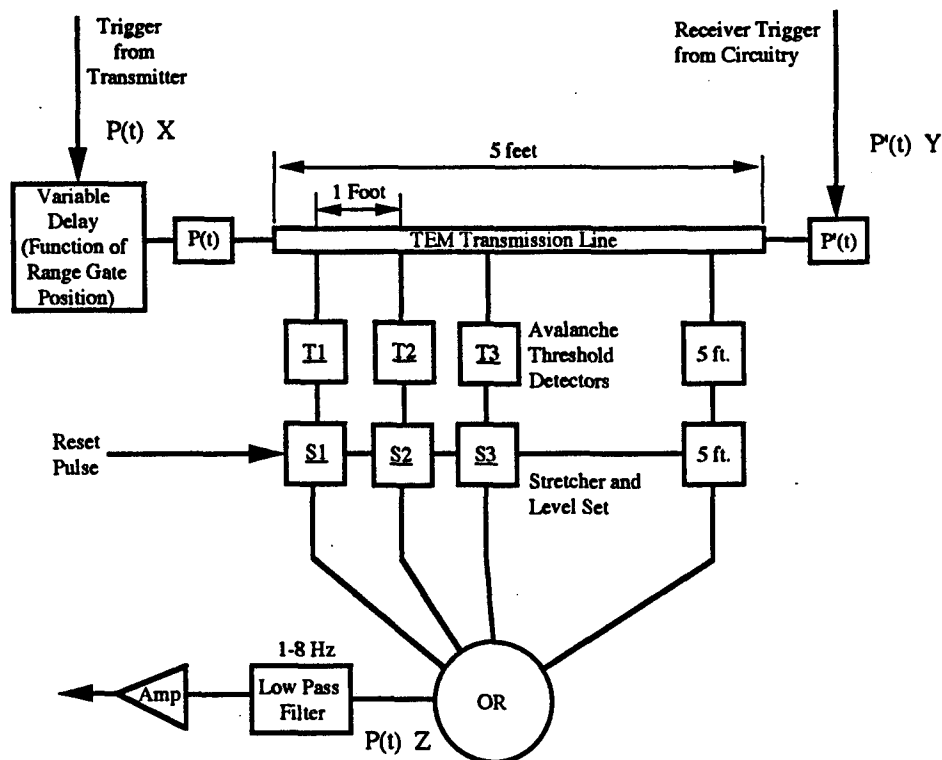


Figure 4-1. Leading edge filter.

4.3 LEF OUTPUT VOLTAGE DESCRIPTION.

The LEF, in reality, is a pulse position (range) amplitude modulator. The resulting waveform contains both range and range rate information. The voltage levels of the pulses corresponding to each of the five range positions vary from .23 volts to 1.11 volts in equal steps of .23 volts. A human being moving away from the system through the one foot range increments produces a sequence of pulses with amplitudes varying from 1.11 volts down to .23 volts (super imposed on a small DC level of about .04 volts). Examples of the waveforms actually measured during the program as a human being ran, walked and crawled away from the system through the monitored range segments are shown in Figures 4-2, 4-3 and 4-4. Each of the five voltage levels are clearly present in all cases. The variable rates of change between running, walking and crawling are also obvious. The macro characteristics of the waveforms are exactly as predicted by analysis of the hardware. The high frequency modulation of the pulse amplitudes was not predicted and is believed to be caused by the relative motion of the scattering centers of the target with respect to each other and the ground as the target moves through the range intervals.

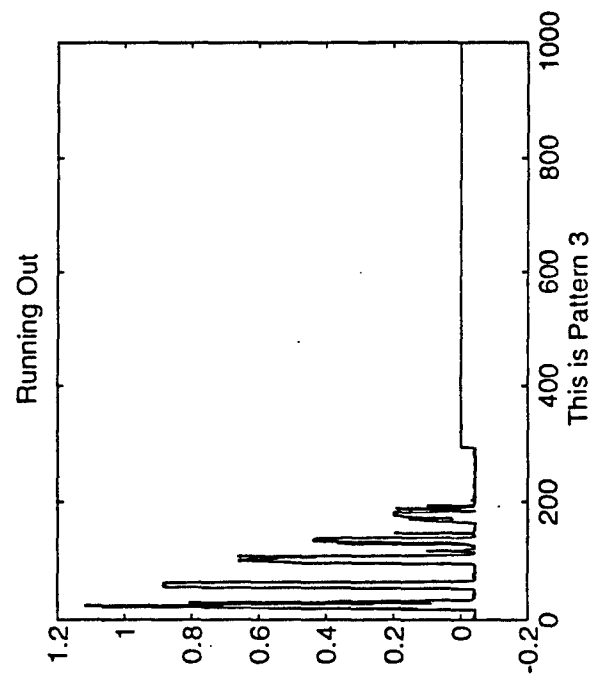
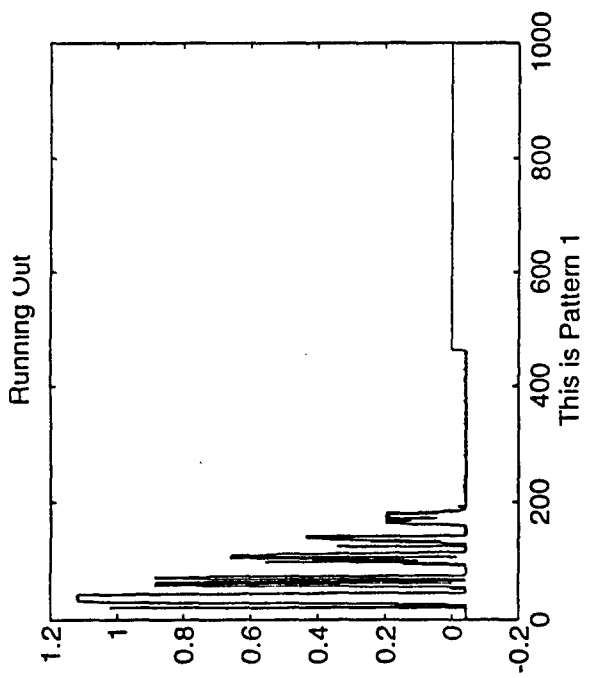
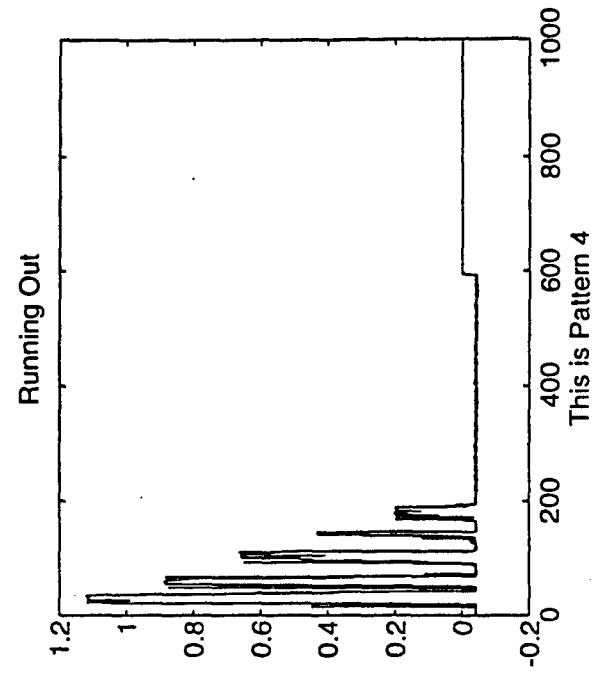
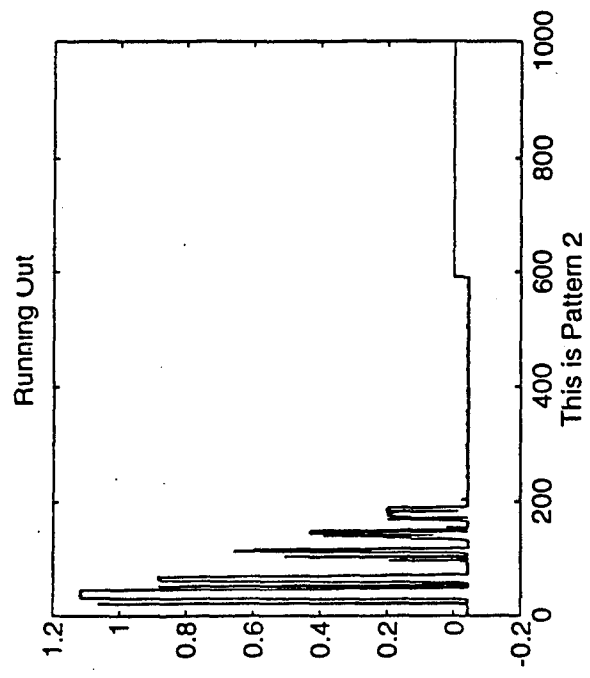


Figure 4-2. LEF output waveform for human running out.

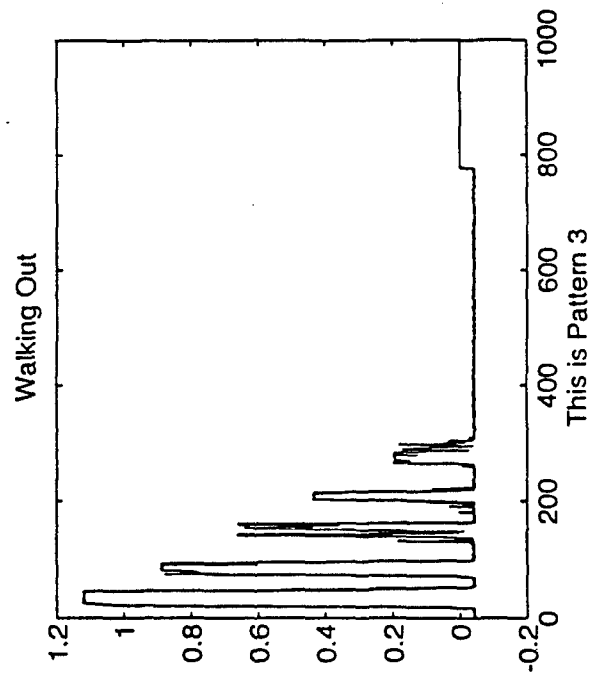
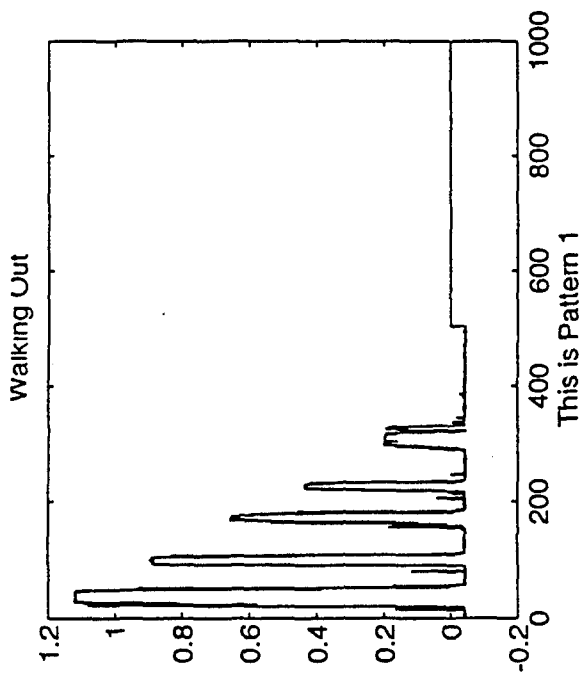
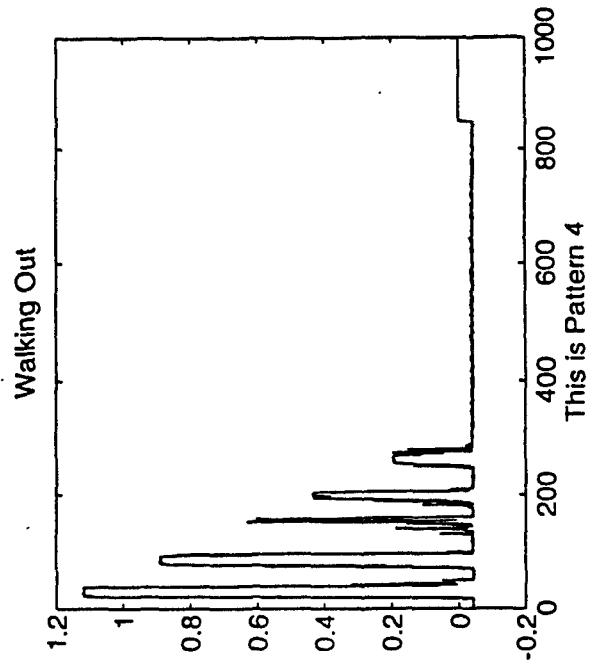
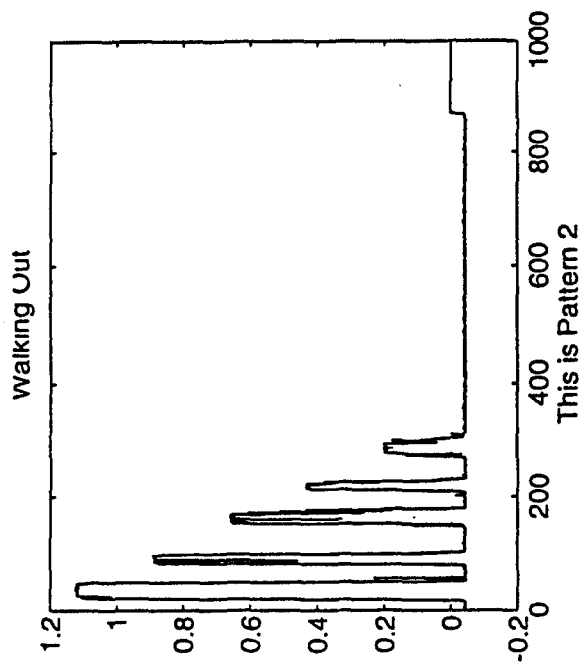


Figure 4-3. LEF output waveform for human walking out.

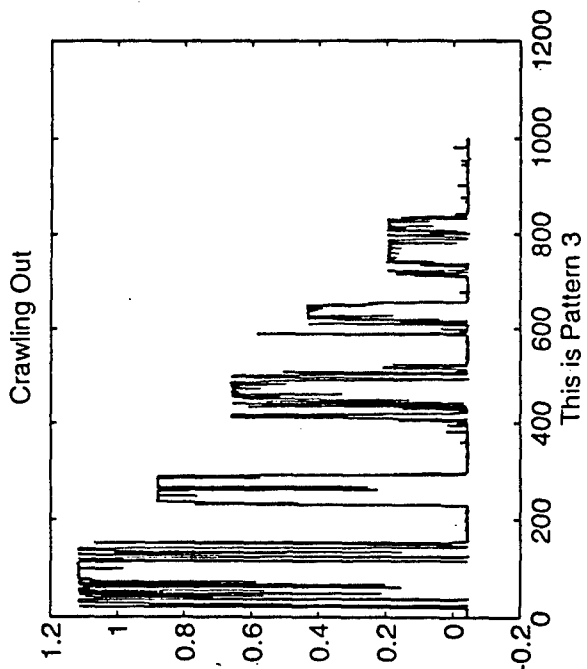
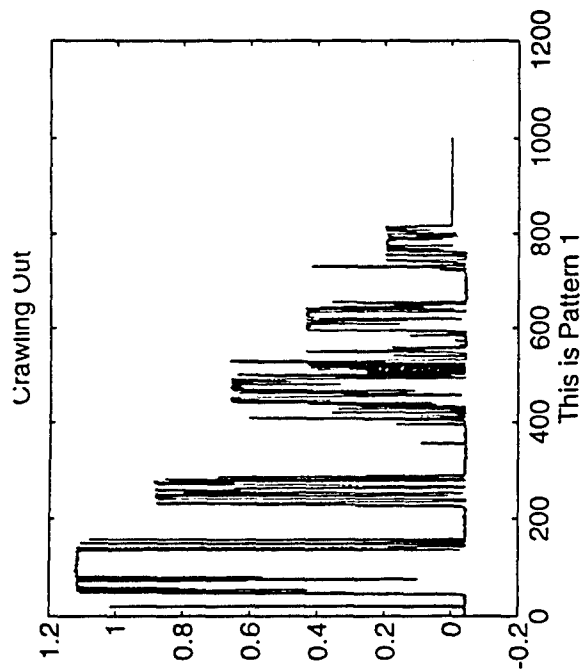
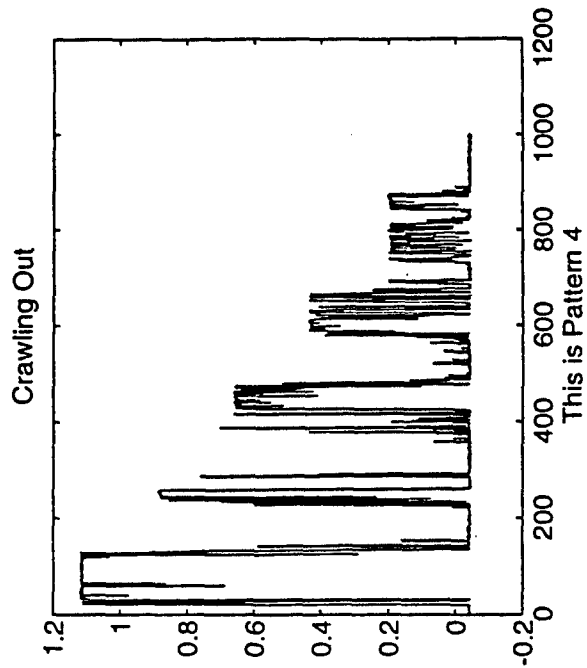
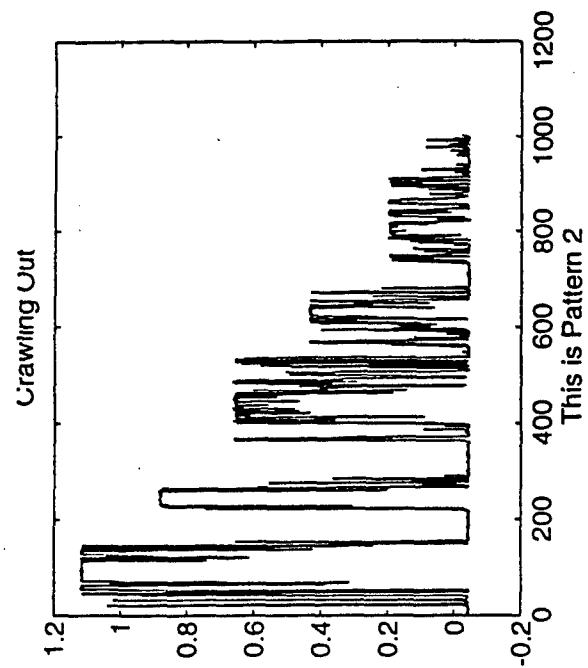


Figure 4-4. LEF output waveform for human crawling out.

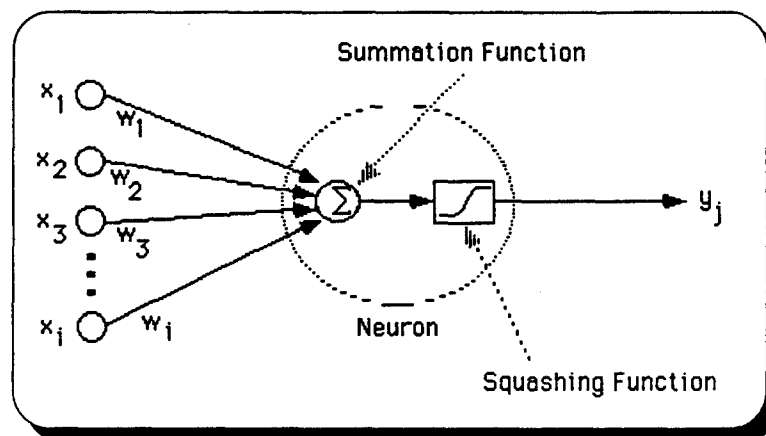
In summary, each waveform consists of two distinctly different sets of feature discriminants. The first, and more easily used, is the pulse amplitude modulated (PAM) signal that is produced by the LEF as a target moves through the range segments produced by the tapped delay line processor in the LEF. A target moving through the beam produces a PAM signal that is directly related to the specific trajectory the target follows as well as how fast it is moving. Fine structure (high frequency modulation) in the PAM signal currently is not used and target classification is accomplished by associating a threat with a particular type of trajectory. An animal that is meandering through the area being protected will not produce a trajectory that closes in on the protected site. An intruder, however, will produce a waveform that shows closure on the protected facility. The second set of feature discriminants is contained in the high frequency modulation of the trajectory PAM signal. If it can be proved that these high frequency modulation components are caused by the relative motion of scattering centers, then the fine structure produced by animals of different sizes and shapes as well as human beings will have unique fine structure patterns. If this is shown to be the case, then LEF classification will be even more robust. The data gathered during this study had some fine structure; however, based on the understanding of the LEF operation, it is obvious that the output amplifier bandwidth is still not wide enough to capture all of the fine structure. In addition, the taps on the delay line are spaced too far apart to capture all of the scattering center characteristics. Considering these limitations in the existing hardware led to the decision to employ the lower bandwidth trajectory waveforms for classification and postpone classification studies based on scattering center motion to a future program.

When the Phase II proposal was written, target classification was anticipated to be carried out by matched filtering or correlation detection. Since that time, significant advances in the state of the art of neural network classification techniques have been made. Neural networks have significant advantages over matched filters or correlation detectors in as much as the neural network, during its training operation, highlights the features in the waveform that provide the essential discriminants and it diminishes those waveform inputs that are not significant. In most cases, the neural net classifier is a better classifier than the matched filter. A second advantage is that the network is self taught. The waveform characteristics do not have to be defined a priori for the system to work. All matched filter or correlator inputs must be known and programmed before the quality of the classification scheme can be determined. These reasons led to the decision to employ a neural network to classify targets based on the LEF target trajectory waveforms.

4.4 AN INTRODUCTION TO ARTIFICIAL NEURAL NETWORKS.

To classify LEF outputs of UWB radar returns with an artificial neural networks (net), one must understand what a net is and how it works. For the purpose of LEF classification, the standard backward-error-propagation or backprop net will be introduced and discussed in this section.

An artificial neural network is a system modeled after the human brain. It consists of neurons, which are summing points for the system, much like the neurons in the brain. A single neuron with i inputs is shown in Figure 4-5. Each of the input elements, x_i are weighted by the elements w_i and input to a summing junction. The output of the neuron is a nonlinearly compressed ("squashed") sum of all the weighted inputs. The weights are simply just multiplication factors. The squashing function is a log-sigmoid or a tan-sigmoid function. It can be any non-linearity, but these are convenient because they keep the output of each neuron in a fixed range and they are easily differentiated. Differentiability is an essential feature of these non-linear transfer functions.



$$y_j = f(x_1 + x_2 + \dots + x_i)$$

Figure 4-5. A typical neuron.

This basic structure is repeated over and over and is totally inter-connected very similar to the way it is in a human brain. This elaborate architecture provides a vast amount of computing capability. A typical configuration is shown in Figure 4-6.

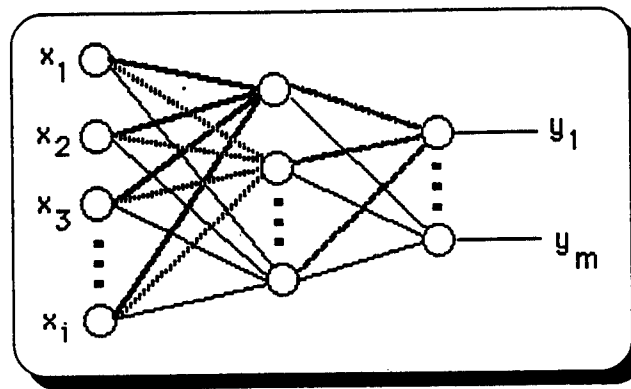


Figure 4-6. Feed-forward artificial neural network.

The power of this architecture is not obvious unless it is realized that with the proper weights and a large enough network, this system can perform almost any decision making task. The elegance of a net accrues from the fact that the weights do not need to be known a priori and can be "learned" by implementing appropriate procedures. Clearly then, success depends on the development of methods for determining the appropriate weights to use for a given problem. At this stage of neural network research and development, many learning algorithms exist. They automatically adjust the weights so that when a particular pattern in a set of patterns is presented to the net, it is able to indicate which pattern is present. The process is conceptually simple; however, the learning process may actually execute thousands of steps and take many hours on a 486-based computer to fully train a net.

Basically, the net is trained by presenting an input pattern to the input nodes. These are the x_1 , x_2 , ..., x_i nodes shown in Figure 4-6. Each of the inputs are split to provide weighted inputs into each of the next set of nodes. Each node sums all its weighted inputs and applies an appropriate compression function. The next layer of nodes accepts the outputs from the first layer and repeats the process. This is done for every nodal layer including the output. Since the input patterns during training are known, the desirable output pattern for every input pattern is also known. Since the initial set of weights are set randomly the first set of outputs cannot possibly be correct. What is done is to establish the desirable output pattern as a target output and compare the output from the first iteration to the target output pattern. An error vector with each output element, y_j , having an error associated with it, is generated for this pattern. This is done for every other input pattern. All the errors for each output are summed together. Using a routine called backward-error-propagation, the error for each output is fed back through the net and the weights are changed such that the error for each output decreases in a negative gradient descent. The net

actually calculates how much each weight contributes to the error at the output. It then makes the largest change to those weights that contributed most to the output error. Since the net is being trained for all of the patterns and the weights are adjusted for all the patterns, it eventually converges on a set of weights that perform the needed operation. *The neural network is essentially a massively parallel information processing structure that can be trained to solve a problem.*

4.5 A NEURAL NET WITH LEF VOLTAGE WAVEFORMS AS INPUTS.

To demonstrate that the net can be trained to classify different trajectories of a target moving through a range segment monitored by a UWB radar with a LEF, the LEF output voltage waveforms are used as inputs to the net. Consider the LEF output voltage waveforms generated by a human walking, running, and crawling away from the system along the radar boresight as previously shown in Figures 4-2, 4-3 and 4-4. The network is to be trained to classify the motion of a human when presented with an LEF waveform that it has not been trained with. The 4 KHz bandwidth waveforms were narrow band filtered and resampled so that 100 samples rather than 2000 samples represented the LEF output voltages. All the fine structure in the voltage waveforms are removed by this operation. The high and low bandwidth LEF waveform representations are shown for comparison in Figures 4-7 and 4-8.

With 100 samples per waveform, 100 input nodes are required. It is well known that a two-layer net can solve any non-linear problem given that it has a sufficient number of nodes; therefore two layers will be used as depicted in Figure 4-6. A two-layer net has three sets of nodes, namely; the input layer of nodes, the hidden layer and the output layer. In this problem, there are three output classes that all waveforms must fall into; therefore, there will be three output layer nodes; each should only be "on" or a "1" if the input pattern is of that class. Although it has not been proved, it is commonly held that the number of hidden nodes should be twice the number of output nodes. Following common practice then, the LEF net will consist of 100 input nodes, six hidden nodes, and three output nodes.

Initially all the weights will be small random values. Assume that the first pattern applied to the net is a walking pattern. The output for each layer is calculated using the outputs from the previous layer. Since all the weights are random, the output will be random as well. This output is compared to the target output, which would have only the walking output on. Therefore, the target output vector for this pattern would be 1 0 0. An error vector would be calculated for the current output. This would be repeated with all the patterns for walking, running, and crawling. The backpropagation learning rule is used to adjust the weights of the network to minimize the

sum-squared error of the network. This is accomplished by continually changing the values of the weights in the direction of steepest decent with respect to the error. Derivatives of error (called delta vectors) are calculated for the networks output layer and then backpropagated through the network until delta vectors are available for each hidden layer. After the first weight changes are made, one Epoch is said to have taken place. This process is repeated until the net reaches a predetermined error goal. This error-goal is chosen so that the net properly provides an output for every pattern which is acceptably close to the desired output. At this point the net is said to have been trained.

Once the net has been trained to classify all the patterns in the training set, it is necessary to determine how good the net is at classifying similar patterns that it has not seen. To test the net once the training error goal has been reached, new data is incorporated into a test pattern set and applied to the network input nodes. When the net classifies the test pattern set properly, the net is ready for use.

Nets are evaluated with their Sum-Squared-Error (SSE). The SSE is calculated by determining the error for each of the outputs for each pattern; squaring them, then adding them together to get a SSE for each pattern. The pattern SSE's are summed to get the total SSE. The lower the total SSE the better the net has trained.

Typically, though, the net is better analyzed by looking at the SSE for each pattern. As long as the SSE for each pattern is low, say under 0.05 or so, then a threshold for each output may be used to provide binary decisions.

Once the net meets the established performance specification with a good set of test patterns, implementation of an artificial neural net provides many benefits. Since the net uses only multiplication and addition operations, it is incredibly fast. Further, there are chips available which may be programmed with the correct weights. These chips are completely parallel systems. All the multiplications occur simultaneously at MHz rates. For low speed systems, a computer may be programmed to monitor the inputs, compute the outputs of the net, and use these outputs to perform any desired actions. The net architecture provides classification without having to write a classification algorithm. Implementation is relatively inexpensive without the need for elaborate hardware.

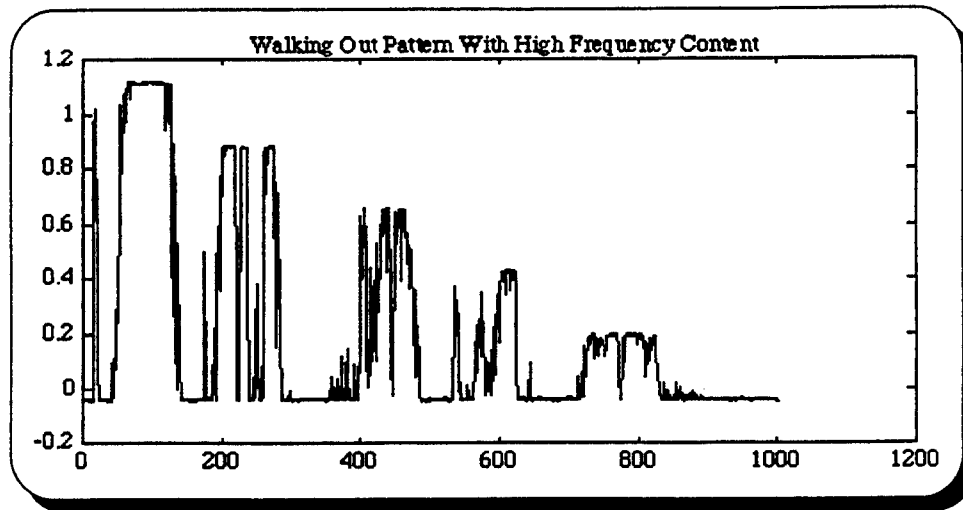


Figure 4-7. Wide bandwidth LEF waveform.

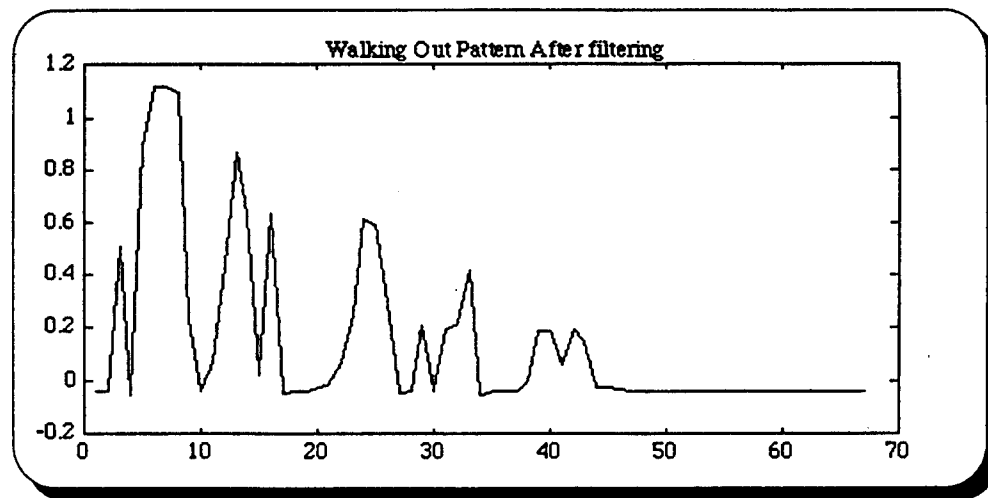


Figure 4-8. Narrow bandwidth LEF waveform.

4.6 THE USE OF THE LEADING EDGE FILTER TO IDENTIFY INTRUDERS.

The reduction of false alarms from fixed objects in a beam and objects moving randomly through the beams is not a simple task. If, however, a human observer was presented with a real-time display of objects moving through an area surrounding a protected site, it is reasonable to assume that the human being would be able to determine, with a reasonably high probability of being correct, which objects would present a threat to the site and which ones would not. The work described in the report addresses the sorting problem in two separate steps. The first step is the use of adjacent range and angle cells to determine whether a received pulse is from a moving or

fixed object, and uses logic to eliminate returns from fixed objects or clutter. The second sorting technique, namely the LEF, coupled with a neural net, is intended to further reduce nuisance alarms caused by targets in a range and angle bin that has passed the moving target logic test. The LEF-neural net processor can be considered to be working on the fine structure as opposed to the more coarse adjacent cell processor. When we look at the overall problem, namely the sorting of targets based on the type of motion (or absence of motion) through an area surrounding a protected site, these two separate processing steps appear to offer a new and powerful approach to develop an appropriate signal processing technique to automate an intruder sorting process and minimize false alarms.

From a systems perspective, there are two distinct functions to be implemented; namely, to 1) detect objects in the area and 2) determine if the objects are a threat to the site. The hardware and software to scan the area and detect objects has been built and successfully demonstrated. Separately, the hardware and software that can assist in the classification of detected objects also has been built and tested; however, in view of the insight gained on the program, the processing activity should be considered to be still in the exploratory analytical phase. Unfortunately, there was insufficient time to evaluate both steps together.

It is important to realize that the hardware technology and software tools to complete intruder sorting is now available. What is required is to integrate both the bin sorting and neural net fine tuning into a system. Since the data rates of information concerned with human intrusion are so low, there appears to be a real opportunity to implement an integrated real-time target identification processor completely in software. A human being moving at a rate of 9 meters per second (a 3 minute mile) moves less than a millimeter in the 0.1 millisecond interval between transmitted pulses. The motion is negligible in radar time. With desktop computers now running at a 100 MHz and high speed graphics cards becoming more prevalent for addressing commercial real-time video markets, it is reasonable to expect (although the study has not been done) that a computer can be used to present an operator with an area display (similar to a plan position indicator) and that neural network software (or hardware if necessary) can be implemented in real-time to automate the process of target classification. This concept of displaying all detected objects on a Range-Angle Map as they move with time and then determining whether the motion in radar coordinates is that of a true or false target is known as "retrospective processing". It is a concept that is extremely difficult to implement in many radar environments; but in the intrusion detection situation (with targets moving so slowly), the problem appears to be tractable. Additional work is required to complete the definition of a more robust processing concept that leads to the design of a real-time system.

4.7 EXPERIMENTAL VERIFICATION OF CLASSIFICATION CONCEPTS.

As discussed previously, targets moving through the beam will generate LEF output waveforms that are directly related to the trajectory the target takes. To demonstrate that a neural network can be trained to classify trajectories using LEF waveforms as inputs, three classes of patterns were generated; these were a human being walking out, running out, and crawling out. This set was named RAD808 data. Sixty waveforms for each of the three classes were generated by humans actually walking, running and crawling away from the system along boresight. The LEF waveforms were applied to the input port of a data acquisition board which sampled, quantified, and binary encoded the data. It then passed the data to a data processing software package which generated ASCII data files. Header information introduced by the Snapmaster software package had to be removed before the data files could be processed by appropriate Matlab programs. Every single data file from this set was consistent and every pattern had the proper five levels for the range gates. As described previously, the waveforms were filtered (using Matlab algorithms) to remove high frequency information, then sampled at a rate to produce 100 samples per waveform. The net was now trained with 40 of the 60 patterns from each case, i.e. walking out, running out, and crawling out. The remaining twenty were used to test the net. This gave outstanding results (sum square errors $(SSE)_{\text{training}} = 0.0676$ and $SSE_{\text{test}} = 0.0671$). This set trained in only three epoches! This was run several times. About half of the time the net did not classify well but the other half classified with excellent results. The results are shown in Table 4-1.

Table 4-1. Summary of the final training sessions.

Test Run Number	SEE _{training}	SSE _{test}	SEE _{test} per pattern
1	0.07	0.07	0.559 x 10⁻³
2	0.47	2.43	20.3 x 10⁻³
3	0.2	1.9	15.8 x 10⁻³
4	0.08	10.4	86.6 x 10 ⁻³
5	0.84	4.89	40.8 x 10⁻³
6	0.17	0.3	2.53 x 10 ⁻³
7	0.28	0.29	2.44 x 10⁻³
8	0.11	1.05	8.75 x 10⁻³
9	0.12	7.64	63.7 x 10 ⁻³
10	0.46	8.73	72.8 x 10 ⁻³
11	0.25	3.37	28.1 x 10⁻³
12	0.85	15.2	127 x 10 ⁻³

Note: The test SSE shown in bold are considered good training results.

The notation that only runs with SSE's per test pattern less than .05 per pattern are good results is somewhat arbitrary; but it is reasonable. Consider an SSE per pattern of .05. This value implies an error of .224 at each output node on the average. This means that a target node value of "1" would be selected if the actual test node value was .775 or greater. For an output node target value of "0" the actual value could be .224 or less. In other words the last step in classification of a pattern is the actual selection rule used. A possible selection rule for SSE's of .05 would be to select a pattern if the output node value is greater than .775, otherwise reject. Clearly, more experience with patterns generated in a practical application would be important input to the process of selecting a final decision rule.

In the twelve runs outlined above, the weights determined for the best test run (run #1) would be recorded and permanently set at each node. A new pattern introduced into the net should function within the SSE guideline determine by the test run. For run #1, SSE=.00056 which indicates a difference of .024 between a target node value and an actual test value. This yields essentially errorless pattern selection.

A detailed outline of the procedure actually followed to train and test the net is presented in Appendix B.

4.8 SUMMARY OF RESULTS AND SUGGESTIONS FOR FUTURE WORK.

We have shown that an UWB radar system with a LEF can be used to correctly identify particular motions of a human being through a radar field. This is based on the system being trained to identify the motions of walking, running, and crawling out through the radar beam. This classification was performed with an artificial neural network which was trained with 40 returns from each of these three cases. The system was tested with 20 returns which were completely independent of those it was trained with. The net was shown to be able to classify these 60 test returns with an average per pattern sum-squared error of 0.559×10^{-3} . A hard limiting threshold layer could be added to obtain near perfect classification of these responses.

We believe, based on this preliminary testing, that this system could be developed to very accurately classify many types of human motion. More importantly, this work extends to the possibility of developing a system to identify human responses among various non-human motions; and to subsequently use the net to reject alarms caused by animals and other non-threatening intrusions.

The following tasks should be implemented to achieve nuisance alarm reduction in UWB systems:

- 1) Develop sets of nominal waveforms that would be generated by targets moving through the beam in all reasonable possible paths. These analytically determined paths can be used to establish a range of paths and associated waveforms that would be classified as a threat. Set up an experimental site protection scenario, generate and collect an all inclusive set of data to be used to train a net. Design and implement a data collection system that can automatically be activated when an animal enters the beam. Collect as much animal training data as necessary to fully train the net to recognize threats based on trajectory information.
- 2) Redesign the LEF to bring the range gates close enough together so that the motions of arms and legs relative to the torso will generate much higher frequency patterns that will carry information about the scattering center structure of the target moving through the gates. If this can be achieved, then targets can be classified based on their physical structure and variations during motion through the beam. These classification schemes will be

largely independent of trajectory and depend mostly on the physical characteristics of the target. It is believed that this system (if it works as anticipated) would be more robust than a trajectory based system.

SECTION 5

THE GATED CFAR RECEIVER AND BEAM STEERING STRATEGY

5.1 BACKGROUND.

Some years ago, ANRO engineers developed a technique for setting the threshold sensitivity of a tunnel diode detector for a short pulse radar system. The radar was simple and inexpensive; it had no beam forming or range gating, and the purpose of the CFAR circuit was to set the detector sensitivity close to the noise level when the transmitter was not radiating. The idea was to increase the threshold of a tunnel diode detector until it fired very occasionally on noise; this was done by entering the ones and zeroes representing hits and no-hits into a shift register, and summing the contents. The sum was used to adjust the threshold to get perhaps 1 or 2 hits randomly in every 32 tries. On alternate pulse repetition frequencies this measurement was made with the transmitter off. A separate or target register was then employed when the transmitter was on. Sudden presence of a target would produce a string of ones from the detector, it being statistically highly improbable that such a string could be caused by noise.

The current ANRO Baseband Reflectometer (ABR) receiver uses a single scanning range gate which is used to activate a tunnel diode threshold detector. The tunnel diode threshold detector is biased, via a closed loop CFAR technique, close to the negative resistance switching point; in the absence of signal, thermal noise sets the bias level[10]. Using the concept of a binary integrator, a target is detected when it is determined that m out of n target hits are received (e.g., 26 out of a possible 32) in any sliding time window. This approach is very inexpensive to accomplish, but from a sensitivity viewpoint is not efficient enough for longer range application.

A study of receiver technology performed under the program indicated that an improvement of over 25 dB is possible by the use of a coherent processing receiver. However, this approach is complex and costly. It is shown that by a simple addition of a mixer, the tunnel diode binary integrator can achieve an increase in sensitivity approaching 20 dB for a minor cost. Here, the received signal is mixed with a local oscillator whose frequency is chosen to achieve a baseband pulse of precisely $1/2$ rf cycle (plus or minus). Essentially, a new superhetrodyne receiver is created with an increased sensitivity level of less than $10^{\circ} \mu\text{V}$. This concept was patented under another SBIR program and is used to achieve the maximum range of 1 mile on a human target.[11]

In considering how to produce a detection scheme for an array of short pulse radar transmitters for intrusion detection, we have a much more complex problem. The array allows beam forming, which allows us to distinguish the azimuth angle at which the intruder is located, and a range gated detector allows us to determine its range. As in Figure 5-1, there are thus a large number of azimuth-range cells, and we need to apply a separate CFAR adjustment to each cell. To be able to distinguish between fixed and moving targets, unlike the earlier scheme, we now have to make the CFAR adjustment with the transmitter on; thus we are setting the threshold not on random noise, but on noise plus the clutter caused by reflections of the transmitted signal. Digital computer techniques allow us to look for the unique signatures of a target moving slowly within a cell, and follow it from cell to cell. After the ability to point the array of transmitters to a given azimuth angle was accomplished, two essential new elements required development; namely,

1. A range-gated variable-threshold tunnel diode detector (RGVTTDD). The computer scanning algorithm must set the required range gate so that the detector is only sensitive for a few nanoseconds around the required range; it also sets the tunnel diode sensitivity (see Figure 5-2).
2. A CFAR algorithm to compute how the sensitivity must be set. It is the purpose of this section to describe an approach to this algorithm.

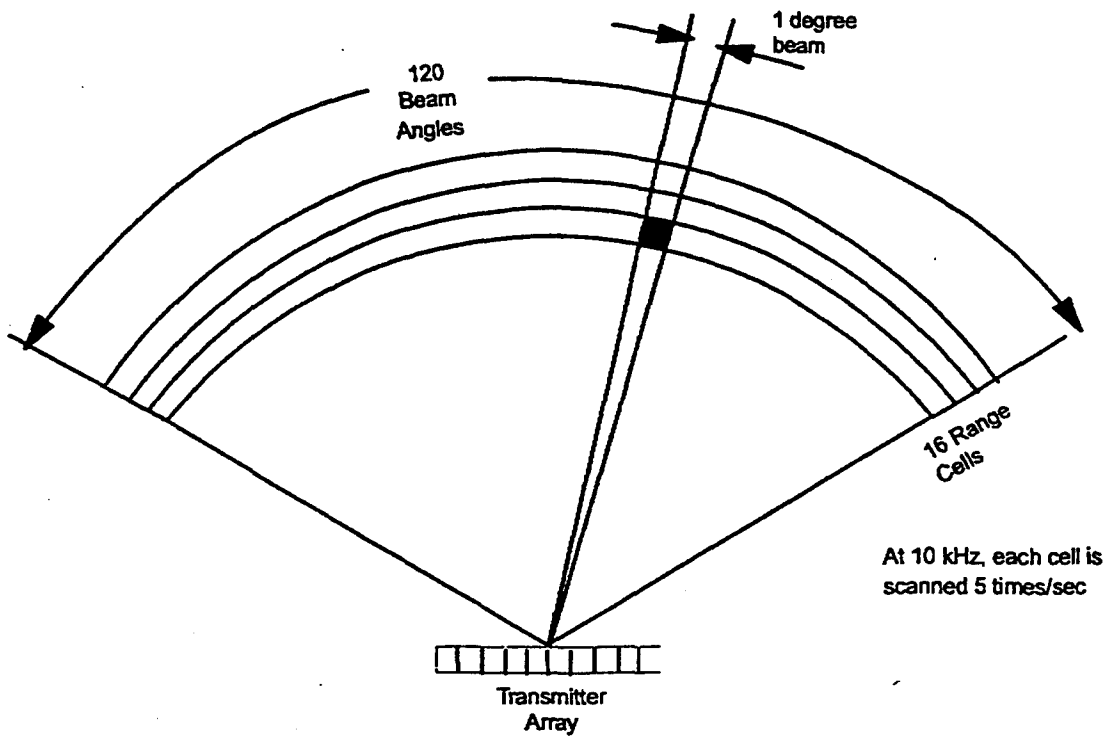


Figure 5-1. Range azimuth cells.

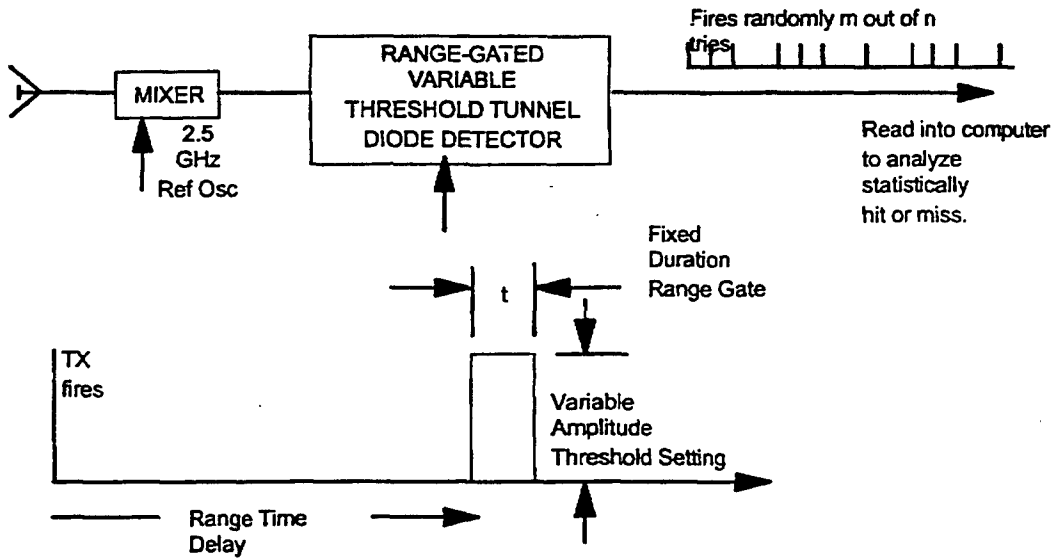


Figure 5-2. Range gated variable threshold tunnel diode detector receiver.

First, it is necessary to understand the nature of the signal applied to the detector. If the received signal were simply to be applied directly, one would see a multitude of replicas of the transmitted signal superimposed on each other, with most of the spectral content centered at around 2.5 GHz. The detection problem is simplified if we first apply the received signal to a simple mixer, as in Figure 5-3 forming an "envelope" detector.

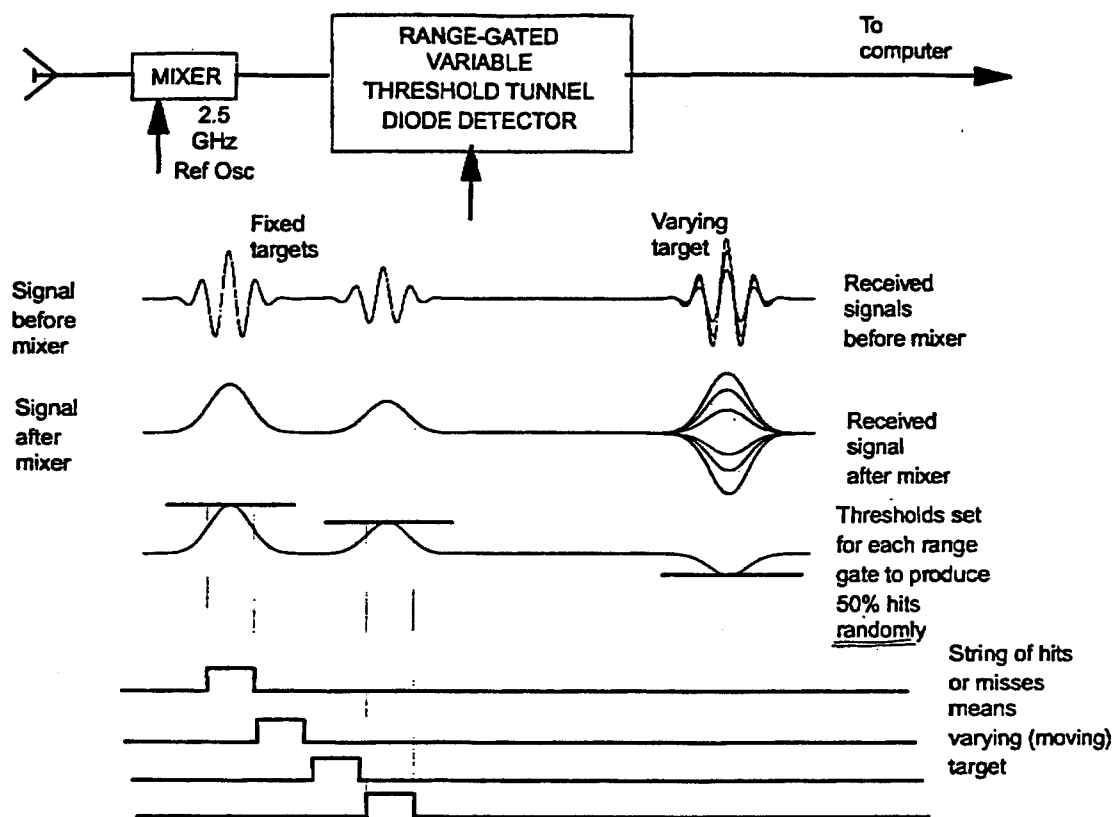


Figure 5-3. Envelope detector concept.

The reference signal for this mixer is the same 2.5 GHz source which is counted down and used to trigger the transmitter, ensuring that there is a constant phase relationship between the reference signal and the radiated short pulse signals. The output of the mixer is thus a superposition of the envelopes of the reflected pulses. The output from any one fixed target will be a unipolar pulse of an amplitude and polarity which depends on the phase relationship between the reflected signal and the reference, but the main point is that it will be constant. However, a moving target will produce a scintillating pulse whose amplitude will vary as the target moves closer or further away. The period of such fluctuations is a characteristic of the nature of the target; for a moving person, it has a period of a few Hertz. It is necessary to attempt velocity processing because of

ground clutter, which is a very large return. This then yields the basis of the CFAR algorithm: we set the threshold for any azimuth/range cell so that it fires about 50% of the time, randomly, when averaged over several seconds. We then examine the train of hits from the detector for that cell, looking for a sudden train of zeroes or ones that signify that the cell content is changing due to scintillation, caused by a target moving within the cell. If such a decision is made, the next process is to examine adjacent cells in range and azimuth to see if a similar effect occurs there, as the target moves into it. Note that this is a simple digital form of moving target identification, applied to short pulse radars. Requiring movement into adjacent cells helps us to reject scintillation due to within target motion, such as the waving branches of a tree. It then becomes an exercise in pattern recognition, looking for variations from a learned background pattern.

In summary, the problem here is no longer that of discriminating a signal from baseband noise, but instead to discriminate between a moving and a fixed target. There are two tools we will use:

1. Even with a simple tunnel diode threshold detector generating only 1's and 0's (hits and misses), there should be a difference in signature between noise, a fluctuating target with a moving center of mass, and a fluctuating target with a fixed center of mass (such as a tree). We need to acquire typical data on these signatures and develop the discrimination algorithms (which we can program into a computer).
2. Cell to cell movement, both in range and azimuth. Suspected activity in any one cell can prompt closer attention to all the surrounding cells, to see if a target is moving from one cell to an adjacent cell, and at what rate. This takes advantage of the azimuthal discrimination permitted by the multi-element transmitter array, as well as the narrow range gates.

5.2 THE RECEIVER SEARCH STRATEGY.

This section describes the strategy for the detector in the multi-transmitter beam-steering array radar. There is a single detector element based on a tunnel diode. Each time the transmitter array fires, it is steered at one beam angle and the detector is only sensitized for 20 nanoseconds at a determined time delay after the array fires. This determines a single range "cell" in the region being scanned.

For a given radar configuration, there are n azimuth angles and m range cells, which creates $n \times m$ cells within the area of coverage. If the pulse repetition frequency (PRF) is 10 kHz and the cells are scanned sequentially, each cell is revisited every $n \times m \times 100 \mu\text{secs}$.

VOLTAGE TO TD
DETECTOR

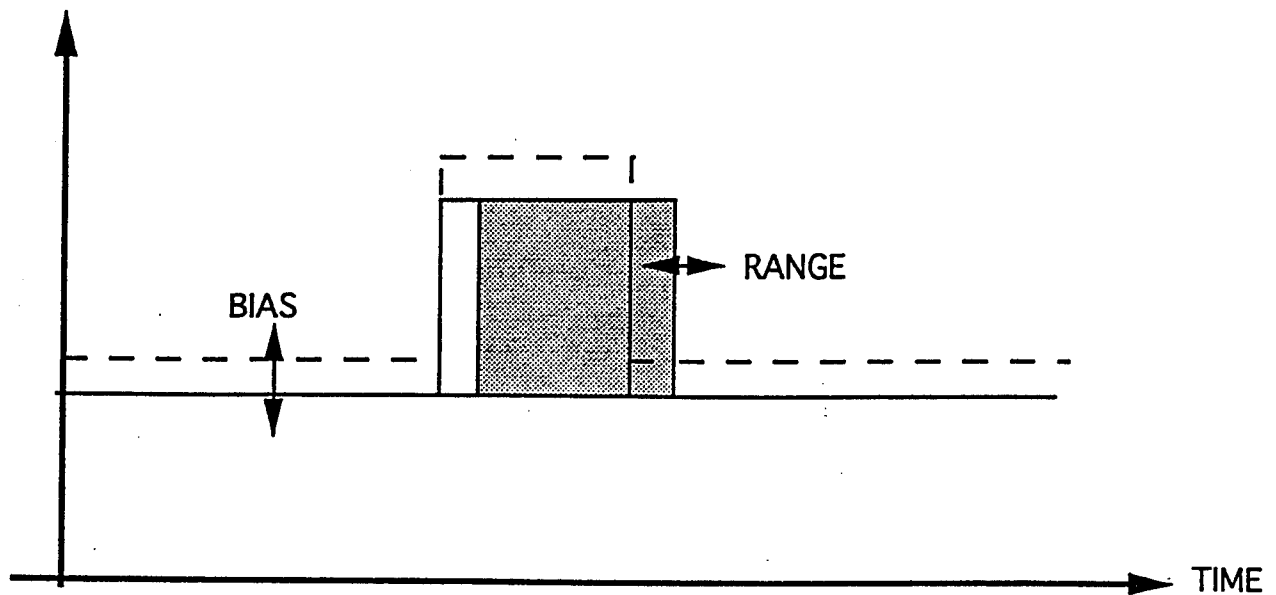


Figure 5-4. Range and bias adjustments.

5.2.2 Threshold Criterion.

The decision as to whether a target is present or not is based on the assumption that the distributions of 1's or 0's in H_{ij} is random, and thus a sequence of continuous 1's or 0's is unlikely. If perfectly random, the probability of a sequence of length l is 2 parts in 2^l .

e.g., probability of 16 1's or 0's is 2 in 65536.

However, experimental data shows that sudden insertion of a target into a cell causes either a string of hits (1's) or misses (0's): the target gives an enhanced signal above the clutter, or suppresses it. The search criterion is thus to look for a sequence of 1's or 0's, long enough to make the probability of this occurring due to noise suitably low.

Detection of such a string, however, is not a sufficiently unlikely occurrence due to noise that we can cause an alarm simply based on one cell. If such an alarm threshold is tripped, we set a flag to show that this cell *and each of its adjacent cells is on "alert"*, and maintain this alert for about 10-15 seconds.

Within this alert interval, if any of the adjacent cells also trips the threshold for a target, then an alarm can be given. This procedure of using adjacent cells enormously reduces the false alarm probability and looks for motion of the target from cell to cell.

5.2.3 Activity Required each 100 μ secs., i.e., PRF Interval.

1. Ensure at least 1 μ sec has elapsed since Tx fired.
2. Read TD detector status for current cell.
3. Based on the scan algorithm in use, for the next cell to be visited, send out a new value for the beam angle to the transmitter, and new range and bias data to the receiver. This allows about 100 μ secs for the new bias voltage to settle before the transmitter fires.
4. For the current cell, update to H_{ij} register, and count the number of 1's. Adjust the bias voltage register B_{ij} for this cell up or down as need to maintain a CFAR. These bias adjustments are done slowly to avoid backing off the tunnel diode sensitivity when a true target appears.
5. For the current cell, examine the H_{ij} register for a string of 0's or 1's of a required length such as 16 or 32. If a string of required length has occurred:
 - (a) If this cell is not on "alert", set it to alert, and set the alert bit in all contiguous cells, together with the time when the alert condition was set.
 - (b) If this cell is already on "alert", set an *alarm* condition to indicate the suspected cells on the computer display, and record the time when the alarm occurred.
6. For the current cell, by comparing current time with the *alert* time, if it has been on *alert* for > 15 seconds, reset the *alert* condition to off.
7. For the current cell, if it has been on *alarm* for > 1 minute, reset the *alarm* condition to off.
8. Wait for the next Tx firing.

SECTION 6

THE DNA UWB INTRUSION DETECTION ARRAY RADAR SYSTEM OPERATIONS AND TESTING

6.1 INTRODUCTION.

This section of the final report addresses the general concept of the application of the DNA UWB intrusion detection array radar real-world situations, and presents a description of the laboratory and field testing accomplished in the Lexington, MA, area.

6.2 THE EFFECT OF WEATHER CONDITIONS ON UWB TRANSMISSIONS.

Propagation of UWB signals has been tested in rain and fog conditions and appears to behave as described in conventional radar texts.[12] Because of the short range of interest, there is, virtually, no discernable attenuation of the 2.5 GHz signal either under heavy rain (e.g., 16 mm/hr) or heavy fog (e.g., visibility of 100 feet) conditions. The two-way attenuation for both heavy rain and fog is only 0.02 dB/km for two-way travel for the upper spectral content of the UWB transmission; namely, 3 GHz. Thus, at a 1 mile range, we can expect less than 0.1 dB attenuation.

The sophisticated UWB receiver whose threshold detector CFAR's on clutter and noise, as described in Section 5 and the LEF (see Section 4), depends on changes in signal strength in a given range cell for operation. The signal strength is a function of the direct waves from the transmitter which reflect from the specific target centers (the intruder) which include the head, the arms, the torso, etc. and the ground bounce signal. The ground bounce signal should be enhanced by the presence of rain and ice. It may be decreased somewhat by snow conditions and this remains to be tested. We have found, however, that when the sun returns after a snow storm, there is a melting and then a freezing which again results in a very good ice reflecting surface just below the snow, causing constructive and destructive cancellation of target returns.

6.3 UWB SIGNALS AND INTERFERENCE.

UWB signals are defined as having a fractional bandwidth (FB) of 25 percent or greater. For the nanosecond duration, 2.5 GHz signals radiated by this radar, the FB is given by:

$$FB = \frac{\text{Signal Bandwidth}}{\text{Nominal Center Frequency}} \times 100 \quad (6.1)$$

$$= \frac{1 \times 10^9}{2.5 \times 10^9} \times 10^2 = 40 \text{ percent,}$$

where the 1 ns duration transmitted signal has a signal bandwidth which is, approximately, the reciprocal of the pulse width. This means that signal spectral energy is spread over the band of many conventional receivers located in the 2-3 GHz region of the spectrum. There are several important questions that are often asked regarding these signals. For example:

(1) Does this type of signal interfere with existing systems, especially in the vicinity of an airfield where there is sensitive instrumentation?

(2) Do other systems operating in the 2-3 GHz band interfere with the radar's sensitive UWB receiver which is also capable of responding to signals in this range of frequencies?

and

(3) Given the wide spectrum of these UWB signals, does the FCC permit their use in the already crowded S-band, or, for that matter, other regions of the spectrum?

First, we address the questions of "jamming" other signals. We radiate a high peak power signal; namely, 100 kW, but only for a very short time, 1×10^{-9} seconds. From Parseval's Theorem, if the transmitted pulse is represented by $f(t)$ and its Fourier Transform as $F(\omega) \leftrightarrow f(t)$, then

$$\int_0^{\infty} f^2(t) dt = \frac{1}{2\pi} \int_{-\infty}^{+\infty} |F(\omega)|^2 d\omega. \quad (6.2)$$

This means that the radiated energy is spread over the entire frequency band. Since the PRF of the intrusion detection radar is 10 kHz, the period is 100 μ sec. The average radiated power *in the direction of the peak of the beam* is given by:

$$P_{av} = P_{peak} \times \frac{1 \text{ ns}}{100 \mu\text{s}} = 100 \times 10^3 \times \frac{10^{-9}}{10^{-4}} \quad (6.3)$$

= 1 watt.

And only a fraction of this power is intercepted by a conventional radar receiver having a bandwidth of 1 MHz; namely, from 6.2 and 6.3.

$$P_{\text{in-band}} = \frac{1\text{MHz}}{1\text{GHz}} \times 1 \text{ watt} \quad (6.4)$$

= 10^{-3} watts average power.

If the UWB radar is located distal to the receiver, the power intercepted by other equipment is further reduced by a factor of $\frac{1}{R^2}$, where R is the distance between the source and the receiver.

Typically, if this distance is thousands of feet, the in-band power is reduced by a further factor of 10^{-6} , resulting in only nanowatts of potential interference.

For about a 6-month period during the mid-1970's, we operated a 40 W peak source at Logan airport, Boston, MA, for runway and taxiway intersection control. In spite of initial apprehension by Massport operators, they admitted that no one complained of interference with sensitive airport surveillance equipment. For one week in June 1995, we operated the 100 kW array, developed under this program, several thousand feet from the airport surveillance radar at Hanscom Field, Bedford, MA, without any complaints; the Massport airport manager was notified of our transmission times in advance.

The second question is one of interference from other conventional sources. Other pulsed sources do not constitute a problem because our receiver is range gated; the receiver is only open for 20 ns every 100 μ s. And to indicate the presence of a target, we require a series of at least 6 hits out of 32 possible pulses to achieve a threshold: a binary integration. The result is that the probability of an outside pulsed source interfering with the UWB radar is remote. A strong CW source (for example, a cable TV station), however, can reduce system sensitivity because the CFAR tunnel diode receiver detection threshold would be caused to back-off in the presence of this type of interference. There is a known technique, however, to modify the receiver to prevent this from occurring. ANRO patented such a scheme earlier, but the present equipment does not include this modification.[13] Tests at Hanscom Field did not indicate the presence of any interfering sources at S-band.

Finally, the question of FCC licensing for UWB radar and communication systems should be addressed. We were granted an experimental license to operate the present intrusion radar by the FCC; namely, license #KK2XFH. This experimental license expires at the end of this year. We

believe that in spite of granting ANRO an experimental license, and that we have shown that we do not interfere with other receivers, the FCC will be reluctant to grant us a commercial license. A license for government operations, however, is likely.

We believe that to obtain a commercial license, an FCC rule change is required. Rule changes, typically, take years to process, and involve considerable legal expense. The particular rule in question concerns allowance for the actual PRF of the system. The FCC allows only a 20 dB compensation or derating factor for a pulsed system based on duty cycle. Even though our duty cycle, as indicated by 6.3 is 10^{-5} , to determine the average in-band receiver power, we can only use a factor of 10^{-2} for FCC licensing purposes. This correction factor was limited to 20 dB by the FCC to prevent a high energy pulse source from interfering with sensitive receivers even though they were activated only, for example, several seconds/year. The rule change that we would advocate is one to permit the use of the actual transmission duty cycle for radiated signals of 10 ns or less in duration.

6.4 POSSIBLE DELETERIOUS EFFECTS OF UWB RADIATION ON HUMANS.

It is well known that microwave signals can cause damage to human tissue. The heating effects, for example, of microwave ovens are well known. It is generally accepted that average power densities at microwave frequencies should be less than 10 mw/cm^2 , and some have suggested this power density should be as low as 1 mw/cm^2 . [14] The major concern is heating to the brain and the eyes.

With UWB transmissions much less work has been done regarding the deleterious effects to the body of short pulse high peak power radiation. ANRO prepared a white paper on this subject. [15] In this paper, it was shown that a study conducted by an independent researcher [16] found that field strengths in the order of 200 kV/meter revealed certain changes in human red blood cell membrane permeability in blood solutions in the laboratory.

In the DNA array just developed, the focussed beam at 10 feet yields about a 100 volt peak signal into 50 ohms. At S-band, this calculates to 10 kV/meter at 10 feet. At 5 feet, this is still an order of magnitude below the field strength resulting in blood changes. We recommend that when the transmitter is activated, no one should stand in front of the array: *certainly, no closer than 5 feet in front of the array*. The field is reduced by 20-30 dB behind the array so that there is no danger associated with operating *behind* the reflector surface.

6.5 TESTING OF THE UWB RADAR.

With the cooperation of Mr. James Mattieu, Massport Manager, Hanscom Field, Bedford, MA, ANRO was able to assemble the 10-element linear array at a remote part of the airport for evaluation. The site that we were offered was situated at the edge of an active taxiway with an, essentially, unobstructive view of the air field. We were loaned one of the small hanger areas with a source of electric power and a work bench which we found invaluable. The site was also located a short distance from ANRO's Lexington, MA, laboratory which made the ferrying of equipment to and from the site very convenient. Unfortunately, the site was only available for two weeks. When the equipment was finally ready for test after the usual search for broken cables and failed componentry, there was an Air Force air show in planning and progress which reduced the actual test time in half. Nevertheless, valuable qualitative experimental data was taken.

Another problem that we encountered was that although we had a view of thousands of feet across the runway and taxiways as we requested, test targets could only be placed out to about 250-300 feet from the array radar without interfering with the active taxiway; we were not permitted to walk or place equipment beyond this distance.

6.5.1 The Transmitter.

We showed that the beam, indeed, electronically scanned as it was designed by first placing a flat plate target on boresight about 60 feet from the array and observing the output of the four element receive array directly on a Tektronix Model #7854 sampling oscilloscope equipped with a 7S12 plug-in sampling head; this head has a 25 ps rise time. The beam was then steered by the computer to its maximum angle off boresight; namely, 30 degrees and the focussing range was set to 60 feet. A beam was formed at this angle but was reduced in amplitude by a factor of 0.8 and was dispersed in time by a nanosecond. These tests can only be considered qualitative, because there was insufficient time for a series of tests at different angles and ranges.

Another test which we performed was to focus the beam off-angle (at about 30 degrees) and to place a receive antenna at boresight. The purpose of the test was to examine the time domain residues as shown in Figure 3-30. The residues appeared several dB greater than expected. We believe that this is because the computerized calculations were based on the idealized waveform shown in Figure 3-17. Also, the responses from the individual elements are very similar during the first several cycles, but at times corresponding to 2 to 3 times the pulse width, the time domain side lobes are different. Thus, it is difficult to calculate the actual lobe levels unless the

time history of each individual transmitter is known. This is not surprising. It is concluded that more time should be expended in improving the match condition at each element; the techniques to do this are known.[17]

6.5.2 The Receiver and Display.

The receiver and the display were first tested in the laboratory. A summary of the scanning program is shown in Table 6-1. The present system is limited to a scan range of ± 30 degrees because of the limitation of the base-to-emitter voltage range of the avalanche transistor transducer (see Figure 3-3). For the next generation system, a breadboard, using a separate step recovery diode (used as a voltage vs. time delay transducer), has already been designed and tested. This transducer can extend the scanning range to ± 45 degrees, which is the desired design objective of the program.

Table 6-1. Scanning program summary.

<ul style="list-style-type: none"> • 10 Beam positions at 3° intervals on each side of boresight plus boresight provides coverage ± 30 degrees off boresight for breadboard system (± 45 degrees on next generation system).
<ul style="list-style-type: none"> • Three guard band fences established (near, mid, and far): near = 300 ft.; mid = 1000 ft.; far = 4000 ft.
<ul style="list-style-type: none"> • Each fence is comprised of 12 contiguous 10-foot range gates; each fence area is 120 feet wide.
<ul style="list-style-type: none"> • Dwell time in each range gate is 32 pulses or 3.2 ms for a PRF of 10 kHz.
<ul style="list-style-type: none"> • Minimum scan time is given by 12 gates x 3.2 ms time/gate x 21 beam positions x 3 range bands = 2.4 seconds.
<ul style="list-style-type: none"> • Calibration, processing, and display time.
<ul style="list-style-type: none"> • For the breadboard, the total time per complete scan is ~10 seconds.

The near, mid, and far radar fences are manually adjusted for the breadboard system. We have a voltage controlled delay designed so that the near (300 ft), mid (1000 feet) or far (4000 feet) fences are readily adjustable. The initial delay was set at 270 feet in the field which was the maximum distance we were permitted to reach just short of the taxiway.

The display was designed using a 386-based, 40 MHz, MS DOS/Windows, computer with a TMS 320 processor. The 21 beam positions, as shown in Figure 6-1, were programmed on the screen as a two-dimensional display, as seen in Figure 6-2. The x-axis represents the beam number and the y-axis the range gate cluster as indicated in Table 6-1. $R = 0$ in the display represents the start of the near, mid, or far radar fence; each of the 12 gates along the y-axis represents a 10-foot viewing gate. For test purposes, the electronic scanning was stopped and the beam positioned in the boresight direction.

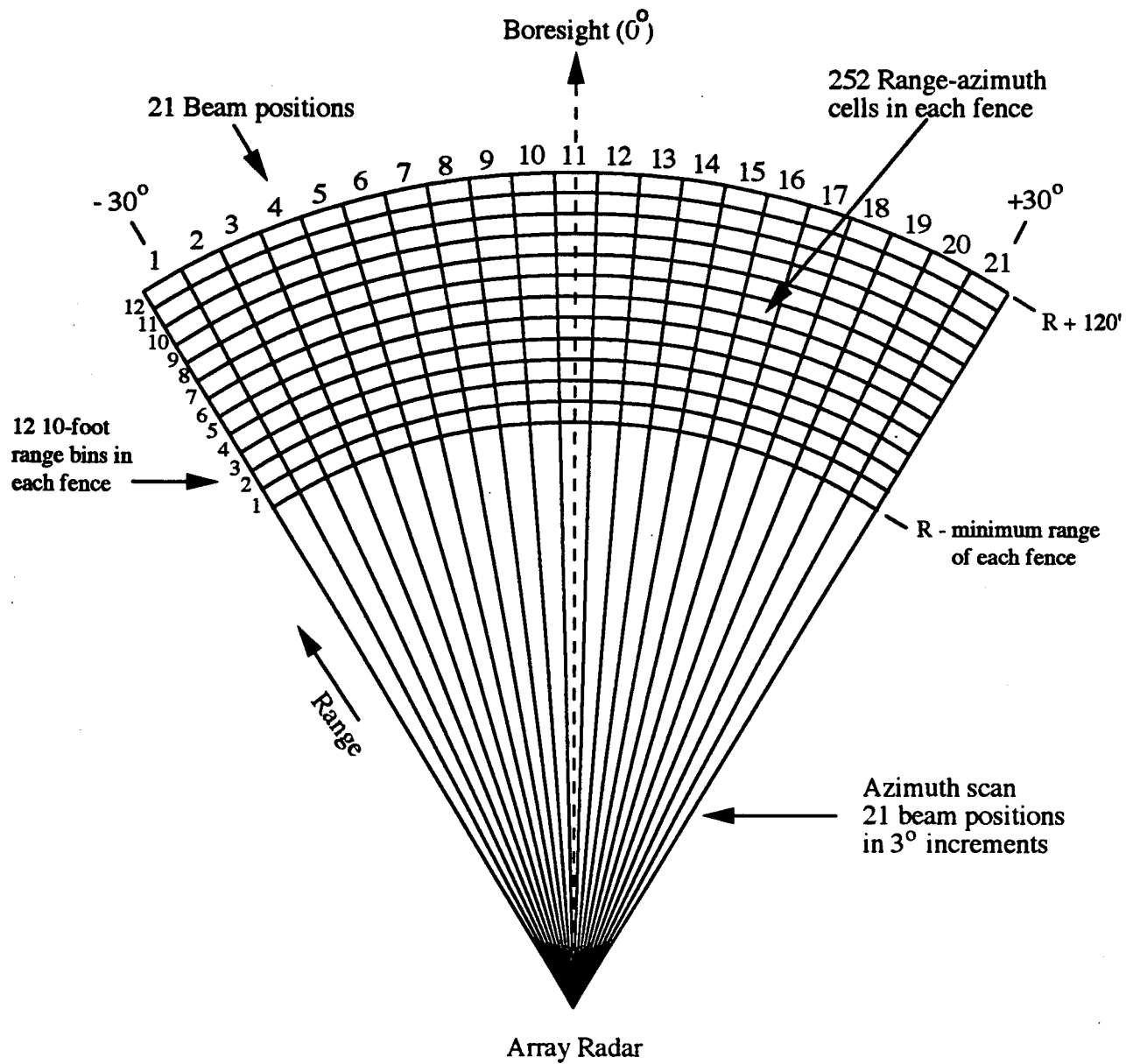


Figure 6-1. Beam scan positions in field of view and range cells.

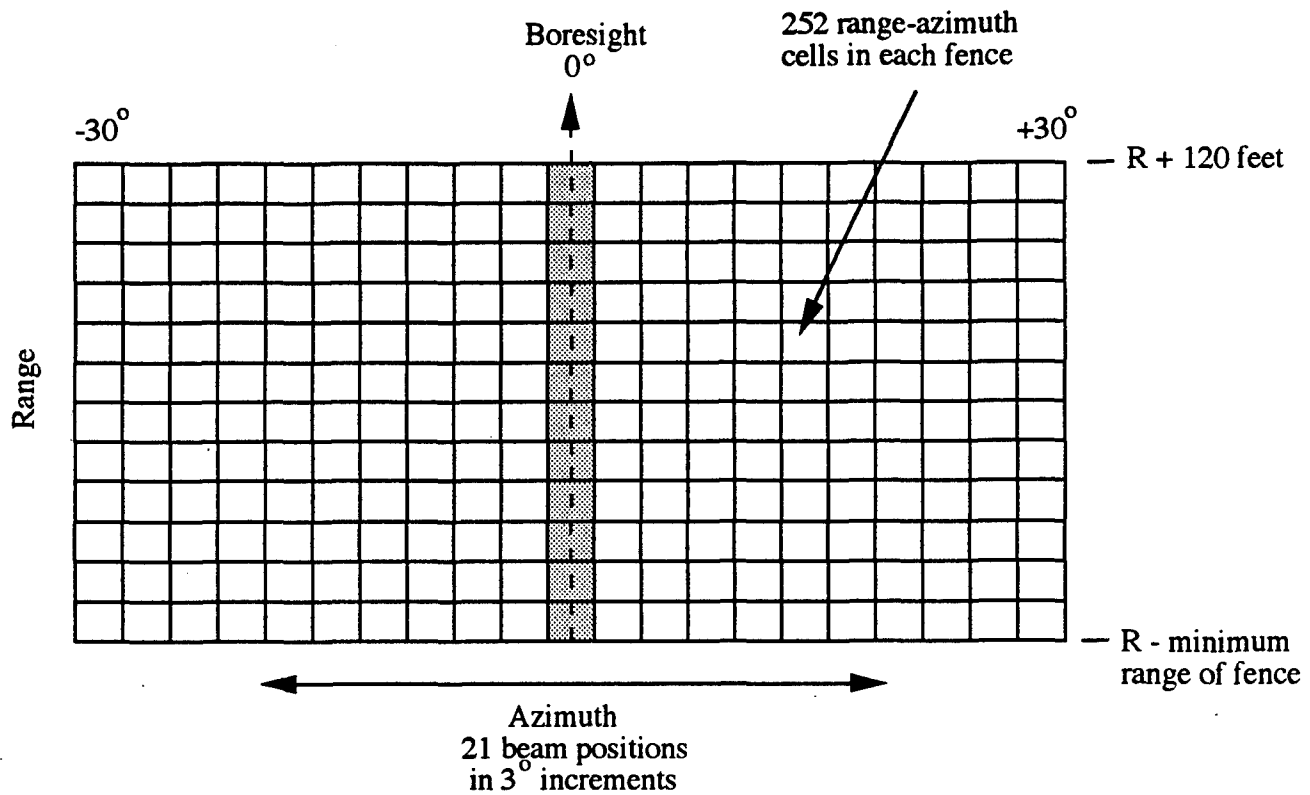


Figure 6-2. Beam and range cell display.

The testing of the receiver was more difficult than earlier versions of either the ABR or IDAS systems developed for DNA because of the new CFAR threshold scheme employed. It was necessary to use this scheme because of ground clutter. In the shorter range versions of the UWB sensor, the tunnel diode detector indicated the presence of a target when 27/32 hits exceeded a prescribed threshold. In this system, the threshold is established by the ground clutter itself. When an intruder moves into the 10-foot range gate the 1, 0 hit pattern in a 32 pulse period changes in the presence of an intruder and a hit is indicated. But, if the target enters a gate and stops, it becomes part of the clutter and the bias simply (dynamically) readjusts. So to demonstrate that the receiver is operating properly, it is necessary to move a target through the range gates at a prescribed rate. If the nearest neighbor cell, as shown in Figure 6-3, also detects a moving target, then the LEF analyzes the signal and a final determination is made (See Section 4).

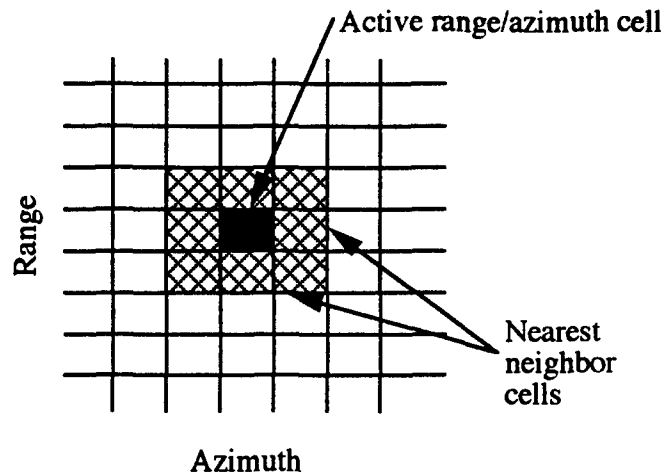


Figure 6-3. Nearest neighbor cell confirmation of target activity in next scan.

In the breadboard system, a moving target is indicated by a "red" square in the display shown in Figure 6-1. This changes to blue to indicate some possible hits, then green (all clear) when the movement stops. We look for two contiguous red cells (angle and/or range) before sending the signal to the LEF.

Although the individual parts of the system were demonstrated both in the field and the laboratory, there was insufficient time to evaluate the radar as a completed system. Also the test facilities were limited for anything but "targets-of-opportunity"; for example, taxiing aircraft. One of the strong recommendations of this report, is that additional funding be allocated to complete the integration and test of this unique intrusion detection sensor and to develop a preproduction model.

Finally, receiver sensitivity was enhanced on this program and evaluated in the laboratory by adding a superheterodyne front-end and as described in a recent U.S. Patent.[11] The receiver threshold was reduced to about 100 μ volts peak at S-band using this approach. This improvement in sensitivity is necessary to achieve the 1 mile design objective on intruder targets over mildly cluttered terrain (e.g., an air field). Further improvements to the receiving system include the development of a receive array which can also be electronically scanned by the application of a dc voltage. The receive array elements can be combined with the transmit elements by interleaving rather than duplexing.

SECTION 7

REFERENCES

- 1 G. F. Ross, L. Susman, "Array Antenna Signal Processing System (U)," U.S. Patent #3,714,655 (January 1973). (UNCLASSIFIED)
- 2 G. F. Ross, R. M. Mara, K. W. Robbins, "Short Pulse Microwave Source with a High PRF and Low Power Drain (U)," U.S. Patent #5,216,695. (UNCLASSIFIED)
- 3 G. F. Ross, "The Far Field Synchronization of UWB Sources by Closed Loop Techniques (U)," pp. 167-176, UWB Short Pulse Electromagnetics, Plenum Press, N.Y. (1993). (UNCLASSIFIED)
- 4 D. K. Barton, "Modern Radar System Analysis (U)," Artech House, 1988, eq. 4.2.4, p. 150. (UNCLASSIFIED)
- 5 E. A. Wolff, "Antenna Analysis (U)," John Wiley & Sons, 1966, eq. 7-106, p. 312. (UNCLASSIFIED)
- 6 J. E. Hill, "Antenna Designers Guide (U)," Watkins-Johnson Company, Catalog Number 200, 1990, p. 109. (UNCLASSIFIED)
- 7 ANDREW Antenna System Computer (U), Bulletin 8525V (9/89). (UNCLASSIFIED)
- 8 Rockwell Collins Space Systems Calculator (U), Perrygraf Division, Nashua Corp., 1974. (UNCLASSIFIED)
- 9 J. D. DeLorenzo, Final Report (U), Contract #N00024-90-C-4535, June 18, 1993, p. 31. (UNCLASSIFIED)
- 10 A. M. Nicolson, R. Brophy, "Detector Having a Constant False Alarm Rate and Method for Providing Same (U)," U.S. Patent #3,755,696. (UNCLASSIFIED)
- 11 G. F. Ross, R. M. Mara, "Coherent Processing Tunnel Diode UWB Receiver (U)," U.S. Patent #5,337,054, issued August 9, 1994. (UNCLASSIFIED)
- 12 M. Sholnik, "Introduction to Radar Systems (U)," p. 544, McGraw-Hill Book Company, N.Y., 1962. (UNCLASSIFIED)

- 13 H. M. Cronson, G. F. Ross, "Baseband Detector with Anti-Jam Capability (U)," U.S. Patent #4,688,041, issued August 18, 1987. (UNCLASSIFIED)
- 14 M. Skolnik, "Introduction to Radar Systems (U)," pp 518-519, McGraw Hill Book Company, 1962. (UNCLASSIFIED)
- 15 G. F. Ross, "A Program to Determine the Effect of High Level UWB Energy on Humans (U)," April 1993. (UNCLASSIFIED)
- 16 S. Cleary, et al., "Studies of Exposure of Rabbits to EM Pulse Fields (U)," Bioelectromagnetics, Vol. 1, 1980, pp 345-352. (UNCLASSIFIED)
- 17 G. F. Ross, "A Time Domain Criterion for the Design of Wideband Radiating Elements (U)," IEEE Trans. on Antennas and Propagation, Vol. AP-16, No. 3, pp 355-356, (May 1968). (UNCLASSIFIED)

APPENDIX A

GLOSSARY OF TERMS

ARTIFICIAL NEURAL NETWORKS. Networks that are trained to identify discriminants in applied waveforms.

AVALANCHE DIODE. A diode that breaks down in the reverse direction in tens of picoseconds.

AVALANCHE TRANSISTOR. A form of nanosecond duration one-shot multivibrator.

BALUN. A balanced line to unbalanced line transformer.

BEAMWIDTH. When the peak of the impulse response drops in half as a function of angle off the steered beam direction.

BINARY INTEGRATOR. A device that builds up a voltage by adding 1's and 0's only.

BORESIGHT. Beam looks straight ahead (normal to the array surface).

BPF. A bandpass filter.

CFAR. Constant False Alarm Rate - the threshold is set by permitting a prescribed number of hits regardless of whether the hits are due to noise, signal, or both.

COHERENCE. When two signals in the time domain coalesce.

ERP. Effective Radiated Power - the peak power generated, multiplied by the antenna gain.

ESR. Electronic Scanning Radar - beam scanned electronically as opposed to a mechanical platform movement.

GRATING LOBES. Multiple beam peaks within the space in front of the array.

IDAS. Intrusion Detection and Alert System.

LED. Light Emitting Diode (or gate) - provides an output with one signal *or* the other is present.

LEF. Leading Edge Filter - an active electronic network that translates the apparent distance to a target to a slowly changing voltage.

LINEAR ARRAY. All transmitter and or receive elements are located on a straight line.

LPD. Low Probability of Detection - signals that are difficult to find or determine their presence.

LPF. Low Pass Filter.

LPI. Low Probability of Intercept - signals that are difficult to collect or decipher.

MARX GENERATOR. A form of high voltage pulse generation where capacitors are charged in parallel and discharged in series.

NANOSECOND. 10^{-9} seconds.

NEURAL NETWORKS. See Artificial Neural Network.

NEURONS. Summing nodes in neural networks.

PAM. Pulse Amplitude Modulation.

PARABOLIC CYLINDER. A reflecting surface which is parabolic in a side view and whose front view is rectangular.

PICOSECOND. 10^{-12} seconds.

RANGE GATE. The time window for which the receiver is "ON".

RGVTTDD. A Range Gated Variable Threshold Tunnel Diode Detector.

SNIFFER. A distortionless probe located at each transmitter element.

SRD. Step Recovery Diode - a diode that changes state rapidly as a function of an applied current.

SSE. Sum Squared Error - used to evaluate the effectiveness of neural networks.

STAR POWER DIVIDER. A power divider having a single port in and n ports out where all n ports emanate from a single node.

TIME DOMAIN RESIDUES. The equivalent of side lobes in the conventional antenna pattern.

TUNNEL DIODE. A threshold detector that changes state with only small incident energies; has a negative resistance characteristic at threshold.

UWB. Ultra-wideband - these signals have a fractional bandwidth of $> 25\%$.

APPENDIX B

TESTING AND TRAINING A NEURAL NET FOR INTRUSION DETECTION

Step 1. Collect returns from the LEF.

The output of the UWB radar goes through the LEF to a data acquisition board. The Snap Master program saves the data in a *filename.SMA* file.

Step 2. Remove header information from the .SMA file.

In order to read the .SMA into MATLAB, the header at the beginning of the file must be removed. This may be done by:

- A) Using the DOS editor and deleting the lines by hand.
- or
- B) Using the program snap2mat.exe. To use snap2mat:
 - 1) The program must be placed in the directory with the files to be converted.
 - 2) The program assumes that the data files are of the form RADTSSxx.SMA. Where the xx represents numbers of the type 01, 02, 03,...23, etc., and that they are numbered consecutively.
 - 3a) From Windows -> Double-click on the snap2mat.exe icon from the file-manager.
- or
- 3b) From DOS -> Change into the directory and type snap2mat.exe.
 - 4) Type in the number of the first RADTSSxx.SMA file, ex 01.
 - 5) Type in the number of the last RADTSSxx.SMA file, ex. 50.
 - 6) The program puts out the files of the form RADxx.MAT.

Step 3. Load and process the files into MATLAB.

The converted data files were loaded with the MATLAB m-files MKNWINxx.M. This represents Make New Inputs xx. The xx corresponds to the number of the file. Every set of inputs was generated with one of these files and they are numbered consecutively in the order that they were used. The method of processing the data has improved with each new version of MKNWINxx.M. There are five types of MKNWINxx.M.

Type 1. Loads the ASCII files and saves the data in a MATLAB file.

Type 2. Loads & Processes the Walking Data.

Type 3. Loads & Processes the Running Data.

Type 4. Loads & Processes the Crawling Data.

Type 5. Combines the data from Types 1,2,&3 into data to train the neural net.

FOR FUTURE USE THESE HAVE BEEN RENAMED AS FOLLOWS:

Type 1. MKNWINxx.M -> LOADxx.M

Type 2. MKNWINxx.M -> WALKxx.M

Type 3. MKNWINxx.M -> RUNxx.M

Type 4. MKNWINxx.M -> CRAWLxx.M

Type 5. MKNWINxx.M -> PATRNxx.M.

LOADxx.M performs the following steps:

- A) Loads the data from the ./dwo directory and saves the workspace.
- B) Loads the data from the ./dro directory and saves the workspace.
- C) Loads the data from the ./dco directory and saves the workspace.

Note: Saving the data as a MATLAB file speeds the loading process.

WALKxx.M performs the following steps:

- A) Loads the data for walking.
- B) Prompts the user to input a Sample Frequency, Cutoff Frequency, Threshold, Step Size, Backstep, and Length.
- C) Performs a processing routine which:
 - 1) Filters the data.
 - 2) Scans the data until it crosses the specified threshold.
 - 3) Backs up Backstep points before the threshold.
 - 4) Extracts the data from this point in steps of stepsize to length. If the data ends it puts on zeros instead. If it backsteps past the beginning of the data it tacks on zeros at the front as well.
 - 5) Saves the results into a matrix where each column represents a pattern with increasing samples down the rows. The matrix has the naming convention of wo, ro, or co. These represent walking out, running out, or crawling out.
 - 6) Saves the results into a MATLAB file SETyxx. The y represents the number of the data set and the xx represents the number of the data file in that set. The y corresponds to the consecutive order of the groups of data.

RUNxx.M does a similar routine but saves the data in a matrix called ro for running out.

CRAWLxx.M does a similar routine but saves the data in a matrix called co for crawling out.

PATRNxx.M loads the data files which contain the matrices of the first three types and combines them into two matrices, P and PT. The P and PT matrices are such that the sample points in one pattern are in one column so the points in a pattern are down the rows and the separate patterns are across the columns. It also creates the T matrix. The T matrix is such that it has the same number of columns as the P matrix. In other words the P and T matrix must have the same number of patterns. The rows of the T matrix contain the target outputs. So if the output of a net has three nodes, or classes, then the T matrix should have three rows. Column one of the T matrix

should contain the outputs for the pattern in column one of the P input matrix. Typically only one T matrix was used for both P and PT. Therefore, these matrices must be the same size. So if fewer patterns were used to test the net than were used to train, some of the test patterns needed to be repeated in the PT matrix to get them to be same size. PATRNxx.M has an example of this repetition step.

Step 4. Train the net.

Once the inputs have been created, the next thing to do is to train the net with the data. All the nets are trained with the latest back-propagation routine called the Marquart-Levenburg method. To actually train a net you need to set up P, T, some initial weights and biases, and a training parameter vector. The biases mentioned are just like weights, but MATLAB multiplies these times a fixed input of 1. This provides the net with the ability to shift the threshold point of the squashing function. The actual MATLAB function to train a net is called *trainml*. One may see the help file on this routine by typing *help trainml* in the command window in MATLAB.

All the LEF outputs were trained with an m-file CLASSxx.M. These haven't changed much since the first one was created. Therefore the number xx is much smaller than those of MKNWINxx.M. The latest of these is CLASS22.M which loads the data set, creates some initial small random weights and biases for each layer of the net, makes a call to *trainml*, and then tests the nets performance with the PT matrix. The CLASSxx.M files also display bar graphs of the output errors for each pattern of the training and test data sets. This is done with a call to the MATLAB function *barerr*. Some of the CLASSxx.M files have a loop in them which allows them to do classify several times.

DISTRIBUTION LIST

DNA-TR-94-184

DEPARTMENT OF DEFENSE

DEFENSE INTELLIGENCE AGENCY
ATTN: DIW-4

DEFENSE NUCLEAR AGENCY
2 CY ATTN: ISST
ATTN: OPO
ATTN: OPS
3 CY ATTN: OPSSPS

DEFENSE TECHNICAL INFORMATION CENTER
2 CY ATTN: DTIC/OCF

OASD (C3I)
ATTN: ODASD I&S

OFFICE OF THE SECRETARY OF DEFENSE
ATTN: DNA OATSD LIASON OFFICE

U S CENTRAL COMMAND
ATTN: CCJ3
ATTN: CCPM

U S EUROPEAN COMMAND
ATTN: ECJ5N

UNDER SECRETARY OF DEFENSE (ACQ)
ATTN: ODDR&E/TS/LS

US NUCLEAR COMMAND & CONTROL
ATTN: LT COL AL RIGGLE

DEPARTMENT OF THE ARMY

ADVANCED RESEARCH PROJECT AGENCY
ATTN: EAO
ATTN: STO S FLANK

ARMY RESEARCH INSTITUTE
ATTN: PERI-ZT

DEPARTMENT OF THE ARMY
2 CY ATTN: DAMO-ODL-S

NIGHT VISION & ELECTRONIC SENSORS DIRECTORATE
ATTN: AMSAT-D-WCP

OFFICE OF THE CHIEF OF ENGINEER
ATTN: CEMP-ET

U S ARMY ELECTRONIC WARFARE LAB
ATTN: DELEW-I-S

U S ARMY MILITARY POLICE SCHOOL
ATTN: ATZN-MP-CD
ATTN: ATZN-MP-DE
ATTN: ATZN-MP-TB
ATTN: ATZN-MP-TS

U S ARMY NUCLEAR & CHEMICAL AGENCY
ATTN: MONA-SU

U S ARMY RESEARCH LABORATORY
ATTN: AMSRL-HR

ATTN: DR D HODGE
ATTN: SLCHE-CC-LHD HARRAH

U S ARMY TRAINING AND DOCTRINE COMD
ATTN: ATCD-N

USAS4A
ATTN: AMXSY-CA

DEPARTMENT OF THE NAVY

CNO (NO9N3)
ATTN: CODE 24B

DAVID TAYLOR RESEARCH CENTER
ATTN: CODE 1203

NAVAL FACILITIES ENG SERV CTR
ATTN: ESC66

NSWC
ATTN: CODE 2064 L D HEMBREE

OFFICE OF CHIEF NAVAL OPERATIONS
ATTN: NO9N

SPACE & NAVAL WARFARE SYSTEMS CMD
ATTN: PME-121-3

U S ATLANTIC COMMAND
ATTN: J324

US MARINE CORPS
ATTN: POS-16
ATTN: POS-20
ATTN: POS-30

DEPARTMENT OF THE AIR FORCE

AIR FORCE MATERIEL COMMAND
ATTN: AFMC/SP

DEPARTMENT OF THE AIR FORCE
ATTN: AF/RDST

ELECTRONIC SYSTEMS DIV
ATTN: AVJR

HQ ACC/SP
ATTN: HQ ACC/SP

MILITARY AIRLIFT COMMAND AMC/SP
ATTN: SP

PACAF/LGWSN
ATTN: SP

TECHNICAL DIRECTOR (NWI)
ATTN: NTSMS

USAF/SP
ATTN: USAF/SP
ATTN: USAF/SPO

USAFE/SP
ATTN: ATTN USAFE/SPO
ATTN: USAFE/SPP

DEPARTMENT OF ENERGY

ASSOCIATED UNIVERSITIES, INC
ATTN: DOCUMENT CUSTODIAN

DEPARTMENT OF ENERGY
ATTN: DASMA DP-20
ATTN: NN-513.4

SANDIA NATIONAL LABORATORIES
ATTN: J W KANE

OTHER GOVERNMENT

NATIONAL INSTITUTE OF STANDARDS & TECHNOLOGY
ATTN: L ELAISON

U S SECRET SERVICE
ATTN: LIBRARY

DEPARTMENT OF DEFENSE CONTRACTORS

ANRO ENGINEERING INC
2 CY ATTN: G F ROSS
2 CY ATTN: J D DELORENZO
2 CY ATTN: L R CAIN
2 CY ATTN: P MITCHELL

COMPUTER SCIENCE CORPORATION
ATTN: RICHARD A SWANSON

JAYCOR
ATTN: CYRUS P KNOWLES

KAMAN SCIENCES CORPORATION
ATTN: DASIAC

VITRO CORPORATION
ATTN: THOMAS J WHITTLE